Ion Mobility-Mass Spectrometry Studies of Organic and Organometallic Complexes and Reaction Monitoring

Victoria Elizabeth Wright

A thesis submitted in partial fulfilment of the requirements

for the award of Doctor of Philosophy (PhD) of Loughborough University

September 2013

To my Grandma (Sylvia Mavis Wright) for always loving, always believing and always being there for me. I miss you.

ACKNOWLEDGEMENTS

I offer thanks to my supervisors, Colin Creaser and Steve Christie, for their continued knowledge and guidance during my PhD. I'd also like to thank Andrew Poulton, Jim Reynolds and Paul Thomas, for their support and advice. In addition, I'd like to acknowledge the collaborating partners, Perdita Barran and her group for advice and allowing access to DTIMS instrumentation at the University of Edinburgh, Carles Bo and Fernando Castro-Gómez from the Institute of Chemical Research of Catalonia (ICIQ), for providing modelled structures and MOBCAL data. I am also grateful to Nick Tomkinson and his group for providing the catalyst and knowledge on the iminium reaction. I thank Loughborough University for the award of a studentship and AstraZeneca for financial support.

It has been an amazing experience working at the centre for analytical science at Loughborough University and to be able to call all my colleagues my friends. I thank you all, with special thanks to Rob for help with FAIMS, and Neil, Helen, Matt, Aadi and Lauren who were there through it all to put up with my rants and temper tantrums and keep me from going insane!

I would like to say a huge thank you to all my family and friends who have been there for me over the last few years. A special thanks to my parents who have always been there to pick me up when I'm down and support me along the way. Finally I couldn't have made the final hurdle had it not been for Ian Sherwood. Thank you for your love, support and encouragement. I know it hasn't been easy.

ABSTRACT

Ion mobility (IM) spectrometry is a gas-phase electrophoretic technique in which ions are separated on the basis of their relative mobility in the presence of a weak electric field gradient and a buffer gas. Ion mobility-mass spectrometry (IM-MS) has the capability of separating ions based on *m/z*, size and shape, providing additional structural information compared to using mass spectrometry on its own. In this thesis, IM-MS has been used to investigate organic and organometallic complexes and identify reactants, intermediates and products in reaction mixtures.

Collision cross sections (CCS) have been measured for three salen ligands, and their complexes with copper and zinc using travelling-wave ion mobility-mass spectrometry (TWIMS) and drift tube ion mobility-mass spectrometry (DTIMS), allowing a comparative size evaluation of the ligands and complexes. CCS measurements using TWIMS were determined using peptide and TAAH calibration standards with good intra-day and inter-day reproducibility. TWIMS measurements gave significantly larger CCS than DTIMS derived data in helium, indicating that the choice of calibration standards is important in ensuring the accuracy of TWIMS derived CCS measurements. The CCS data obtained from IM-MS measurements have been compared to CCS values obtained from X-ray coordinates and modelled structures.

The analysis of small organic and organometallic molecules has been extended to investigations of the potential of IM-MS for reaction monitoring and structural studies of the components of catalytic cycles. Reaction mixtures of an organocatalysed Diels-Alder cycloaddition reaction have been monitored using IM-MS and high-field asymmetric waveform ion mobility-mass spectrometry (FAIMS-MS). Reactant,

product, catalyst and reaction intermediates, including an intermediate not previously detected, were identified and the catalyst and intermediates monitored over time.

An organometallic catalytic cycle using a palladium catalyst has been analysed using IM-MS and the CCS of reactants, intermediates and products have been measured and compared to theoretical CCS calculations. Good agreement was observed between measured and calculated data. Species not amenable to electrospray ionisation were covalently bound to an ionisable tag containing a quaternary ammonium ion allowing the tagged molecules to be detected by IM-MS.

CONTENTS

LIST OF ABBREVIATIONS

IMS	Ion mobility spectrometry
IM-MS	Ion mobility-mass spectrometry
TWIMS	Triwave ion mobility-mass spectrometry
TAAH	Tetraalkyl ammonium halides
CCS	Collision cross section
DTIMS	Drift tube ion mobility spectrometry
FAIMS	High-field asymmetric waveform ion mobility spectrometry
FAIM-MS	High-field asymmetric waveform ion mobility-mass spectrometry
MS	Mass spectrometry
m/z	Mass-to-charge ratio
ESI	Electrospray ionisation
IEM	Ion evaporation model
CRM	Charge residue model
NSI	Nanospray ionisation
DC	Direct current
RF	Radio frequency
ToF	Time-of-flight
RToF	Reflectron time-of-flight
MCP	Microchannel plate
DMS	Differential mobility spectrometry

MALDI	Matrix assisted laser desorption ionisation
APCI	Atmospheric pressure chemical ionisation
SRIG	Stacked ring ion guide
LC	Liquid chromatography
GC	Gas chromatography
MSA	Mine safety appliance
DV	Dispersion voltage
CV	Compensation voltage
Q-ToF	Quadrupole time-of-flight
TIC	Total ion chromatogram
TWIG	Travelling wave ion guide
PA	Projection approximation
EHSS	Exact hard sphere scattering
TM	Trajectory method
IR	Infrared spectroscopy
NIR	Near infrared spectroscopy
NMR	Nuclear magnetic resonance
ESI-MS	Electrospray ionisation mass spectrometry
VOC	Volatile organic carbon

LIST OF FIGURES AND TABLES

CHAPTER ONE

INTRODUCTION

1.1 MASS SPECTROMETRY

Mass spectrometry (MS) was first introduced by J. J. Thompson in 1912. There have been numerous developments in mass spectrometry instrumentation over the last 100 years resulting in the technique being an invaluable tool in many analytical laboratories. Mass spectrometry has found applications in environmental, chemical and biological studies and has been coupled to a number of analytical techniques including gas chromatography, liquid chromatography and ion mobility spectrometry. This section describes the mass spectrometry instrumentation and methods based on the research presented in this thesis.

Mass spectrometry is a technique in which molecules in the condensed or vapour phase are transferred into the gas phase as ions and separated and detected depending on their mass-to-charge ratio (*m/z*). A mass spectrum shows peaks at the *m/z* of the ions present and their relative abundances. There are four main components which make up a mass spectrometer: sample introduction system, ionisation source, mass analyzer and detector (**Figure 1.1**). Each component will be described in more detail in this chapter.

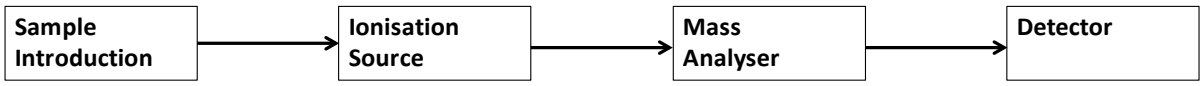

Figure 1. 1 Schematic of a mass spectrometer

1.1.1 Ionisation

An important part of mass spectrometry is the process of transferring an analyte from a matrix into the gas phase as an ion. There are many ionisation techniques available to ionise analytes from liquids, gases and solids at atmospheric pressure and under vacuum. However, for the purpose of this chapter only the techniques employed in the investigations described in this thesis will be discussed.

1.1.1.1 Electrospray Ionisation

The initial development of electrospray ionisation (ESI) was by Malcom Dole[1] in 1968. However, it wasn't until John Fenn developed the method further that it became a recognised technique for the ionisation of a wide range of analytes including small ions,[2, 3] peptides and proteins in the megadalton range[4]. ESI is a 'soft' ionisation technique in which ions are transferred into the gas-phase as intact protonated or metalated molecules. A schematic of an ESI source is shown in (**Figure 1.2**).

There are three main processes in ESI which are involved in the formation of gas-phase ions from solution: a) production of charged droplets, b) evaporation of solvent from the droplets and c) creation of gas-phase ions from the droplets.[5] The ESI source operates at atmospheric pressure where a solution containing analytes is passed through a capillary with an applied electric field voltage, typically 2-4 kV. In positive ion mode, negative ions are attracted to the inside of the capillary causing collation of positive ions at the surface of the liquid. The coulometric repulsion of positive ions at the surface overcomes the surface tension creating a cone (Taylor cone) with the tip being the most unstable part (**Figure 1.2**).[6]

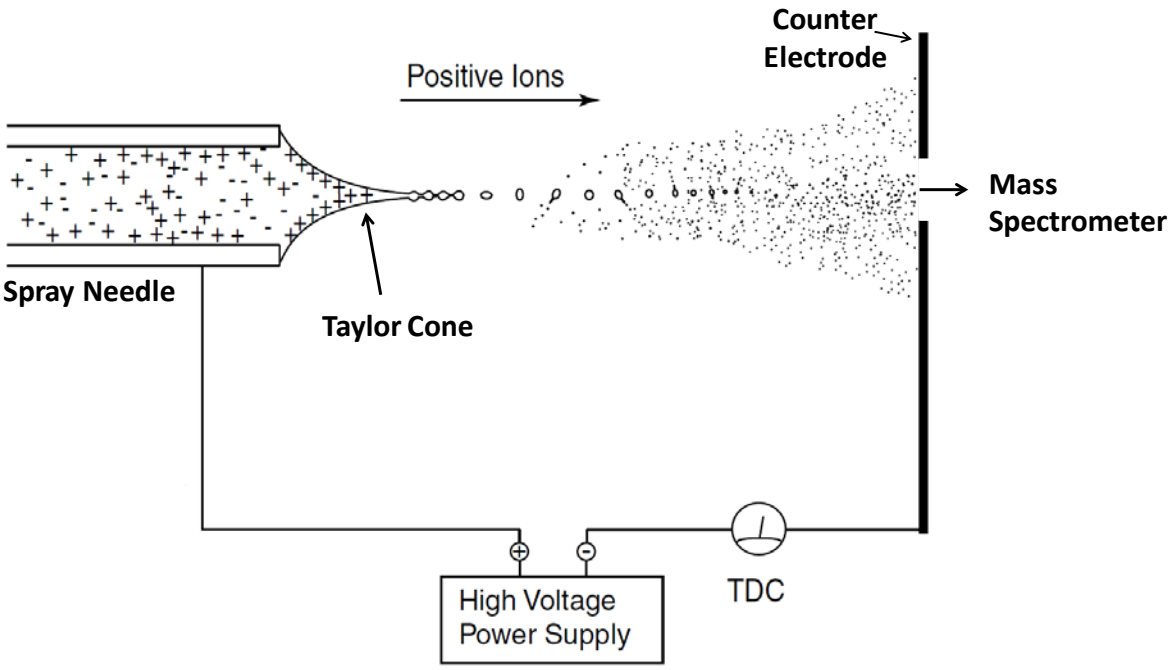

Figure 1. 2 Schematic of an electrospray ionisation source. Adapted from[5].

The sample solution eventually breaks up into a fine aerosol of charged droplets. A desolvation gas, usually nitrogen, aids evaporation of the solvent reducing the size of the droplets until the Rayleigh limit is reached. At this point coulombic repulsion of the ions in solution is equal to the surface tension. Further evaporation of the solvent causes the droplet to break up into smaller droplets. This process may be repeated until a single cation or anion is present in a droplet. The mechanism for desolvation has been extensively debated and has still not been fully resolved. The two main theories are: the ion evaporation model (IEM) and the charge residue model (CRM) (**Figure 1.3**).[6]

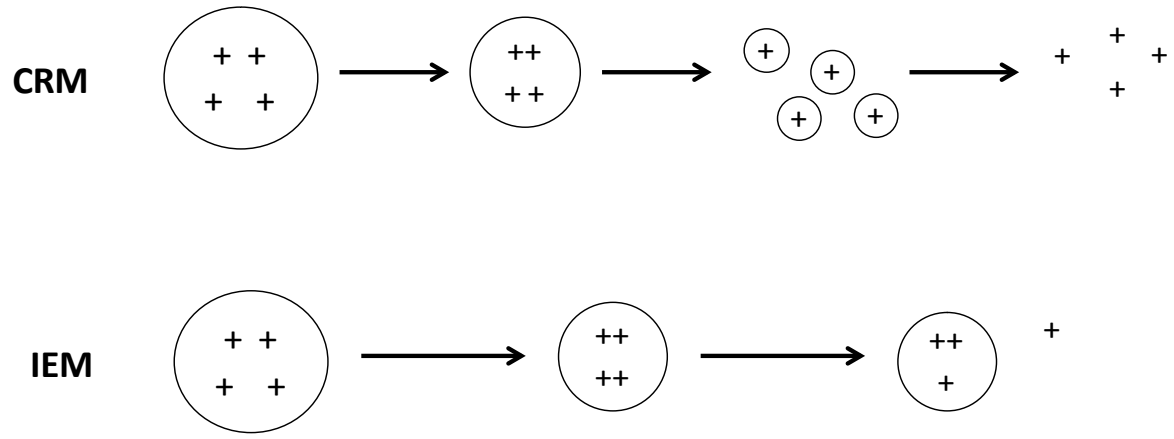

Figure 1. 3 A schematic of the charge residue and ion evaporation models in ESI.[7]

In the IEM, an ion on the surface of a droplet, that has undergone desolvation reducing its radius, may experience a field strong enough to overcome solvation forces and is ejected from solvent. In the CRM a gas-phase ion is produced when no more fissions or solvent evaporation can occur from the droplet, leaving a single solvated molecular ion.

1.1.1.2 Nanospray Ionisation (NSI)

NSI was developed by Wilm and Mann[8,9] in the 1990s as a variation of ESI. NSI involves the use of capillaries which have much smaller diameters than conventional ESI emitters, obtained with a microcapillary puller. The sample is loaded into the tip rather than forced through via pumps and the capillary is left open creating a 'self-flow' due to the applied electric field (2 kV) at the tip. Typical tip diameters and flow rates are 1-2 μm and 20-40 nL/min, respectively. ESI is a concentration sensitive ionisation technique, so sensitivity is not compromised by the solvents flow rate.

The benefits of using NSI are due to the efficiency of the technique. The volume of sample required is typically 1 μL and the diameter of the capillary results in smaller droplets containing less solvent molecules improving desolvation and ionisation. The tip can be placed much closer to the orifice of the mass spectrometer causing a larger percentage of the ions generated to be transferred into the mass spectrometer and be

detected. NSI has many applications where the analyte is in low quantities or is very expensive due to the small amount of sample required and the low flow rates.

1.1.2 Mass Analysers

The second component of a mass spectrometer is the mass analyser. Once an analyte has been ionised it is transferred through the mass analyser under the influence of magnetic or electric fields, under a vacuum and separated based on its *m/z*. There are many types of mass analyser, however, only quadrupole and time-of-flight MS were used in this work and are described here.

1.1.2.1 Quadrupole

Quadrupole mass analysers are one of the cheaper mass analysers commercially available.[7] They are capable of a resolution up to ~2000 and can analyse masses up to 4000 Th.[10] The analyser was first introduced by Wolfgang Paul in the 1950s.[11] A dynamic electric field is applied allowing ions with a certain *m/z* to pass through, whilst the other ions are neutralised, a quadrupole can be used as a trap or an ion filter. Quadrupoles are ideal for coupling with ESI due to the fact that they require a continuous beam of ions.

A quadrupole consists of four circular or hyperbolic shaped, parallel rods with an applied electric field. The opposing rods have a direct (DC) and radio frequency (RF) potential (≈ 1 MHz) superimposed (**Figure 1.4**).[12] The opposite pairs of rods alternate from positive to negative potential, meaning that if an ion enters the device it will be influenced by the alternating polarity of the electrodes, with the RF applied to the opposite pair of rods 180 degrees out of phase.

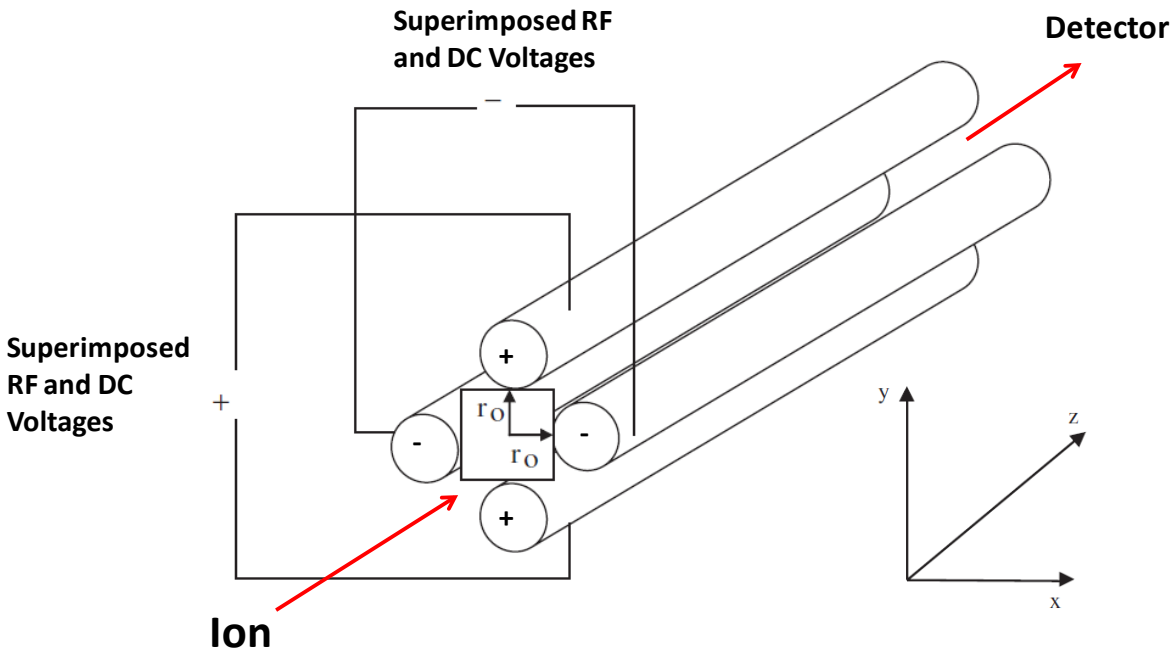

Figure 1. 4 Quadrupole schematic. Adapted from[7].

The ion motion within a quadrupolar field along any axis can be calculated separately. For the *x*-direction the force (F_x) on the ion is defined as follows[13]:

$$F_x = ma = m\frac{d^2x}{dt^2} = -e\frac{d\Phi}{dx} \qquad \textbf{Equation 1. 1}$$

where m is the mass of the ion, a is the acceleration in the *x*-direction, e is the electronic charge of the ion and Φ is the potential at any point (*x*, *y*, *z*) within the field. Therefore the ion motion in the x-direction can be determined by the Mathieu equation[14]:

$$\frac{d^2x}{d\xi^2} + (a_x - 2q_x cos2\xi)x = 0 \qquad \textbf{Equation 1. 2}$$

where a, q and ξ are defined as:

$$a_x = \frac{-8eU}{mr_0^2\omega^2} \quad \text{and} \quad q_x = \frac{4eV}{mr_0^2\omega^2} \quad \text{and} \quad \xi = \frac{\omega t}{2} \qquad \textbf{Equation 1. 3}$$

where U is the DC voltage, V is the RF voltage, ω is the angular frequency, r_0 is the quadrupole radius and t is time. The calculation can be modified to determine the motion for any direction (u):

$$\frac{d^2u}{d\xi^2} + (a_u - 2q_u cos2\xi)u = 0 \qquad \textbf{Equation 1. 4}$$

where

$$a_u = \frac{-8eU}{mr_0^2\omega^2} \quad \text{and} \quad q_u = \frac{4eV}{mr_0^2\omega^2} \qquad \textbf{Equation 1. 5}$$

To allow an ion at a particular *m/z* to traverse the quadrupole it must have a stable trajectory. The a_u and q_u parameters determine the regions in which the working point of an ion has a stable trajectory. Changing these values discriminates against certain *m/z* meaning quadrupoles act as mass filters. The *a* and *q* values can be varied by changing *V* and *U*. A stability diagram is shown in **Figure 1.5**.

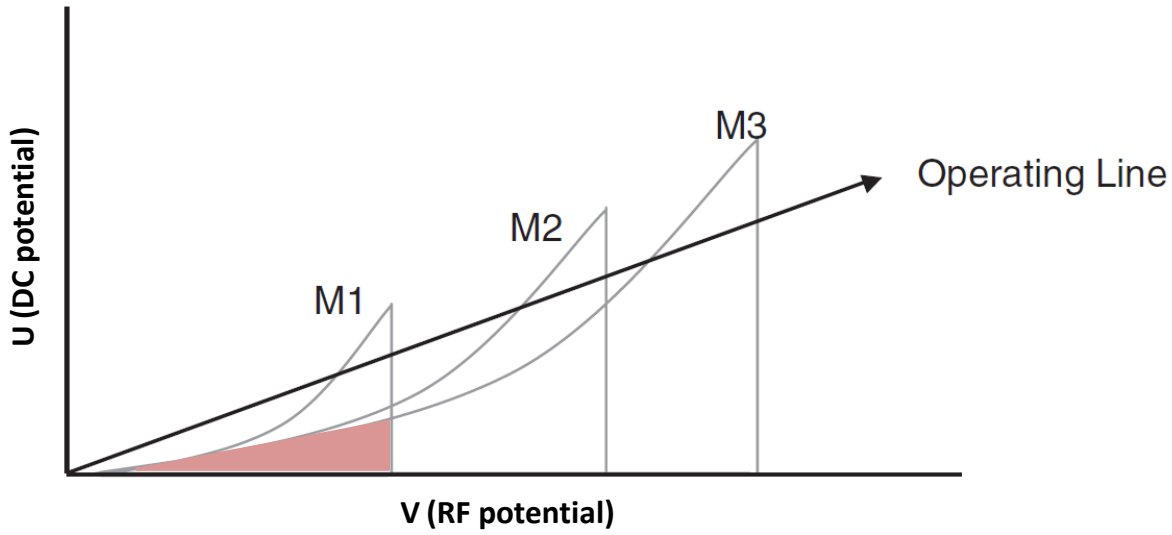

Figure 1. 5 Stability regions of three *m/z* and the 'operating line'. Adapted from[7].

If a constant ratio between *U* and *V* is maintained a line of operation is obtained (**Figure 1.5**). Altering the *U* and *V* voltages changes the position of an ions working point in and around the stability region, therefore, the lower *m/z*, ions become unstable and the higher *m/z* ions become stable. The shaded area of the diagram is the region in which all three *m/z* ratios have a stable oscillation and will traverse the quadrupole without colliding with the rods. Although all ions are transmitted there will be no discrimination and therefore no resolution between them. Optimum resolution is obtained when the line of operation passes through the apex of the stability region for each *m/z*. This mass 'filtering' capability means that an ion can be mass selected. This allows specific information such as fragmentation patterns to be obtained.

1.1.2.2 Time-of-Flight

Time-of-flight (ToF) is the other type of mass analyser used in this work. The concept of ToF was introduced by Stephens[15] in 1946, however, the first commercial instrument was developed by Wiley and McLaren[16] in 1955. The advantages of a ToF are its high sensitivity and high upper mass range. Linear ToF analysers in theory have an unlimited mass range, however, practically they are generally limited to approximately 300 kDa. In ToF MS (**Figure 1.6**) ions are accelerated out of the source region by an acceleration voltage (*E*) pulse. This electrical field accelerates bunches of ions into a field free drift region (*D*). All ions are exposed to the same acceleration voltage and therefore have the same kinetic energy (*KE*)[17]:

$$KE = zeE \qquad \textbf{Equation 1. 6}$$

where *e* is the charge on an electron and *z* is the charge number. If all the ions have the same kinetic energy it means the velocity (*v*) of an ion is directly related to its mass (*m*):

$$v = \left(\frac{2zeE}{m}\right)^{1/2}$$ **Equation 1. 7**

Ions are therefore separated based on their *m/z*. The time (t) taken for an ion to traverse the length of drift region is calculated by:

$$t = \left(\frac{m}{2zeE}\right)^{1/2} D$$ **Equation 1. 8**

This can be rearranged in terms of *m/z* to show how the time taken for ions to travel through the drift region can be converted into the mass-to-charge ratios of an ion:

$$\frac{m}{z} = 2zeE\left(\frac{t}{D}\right)^2$$ **Equation 1. 9**

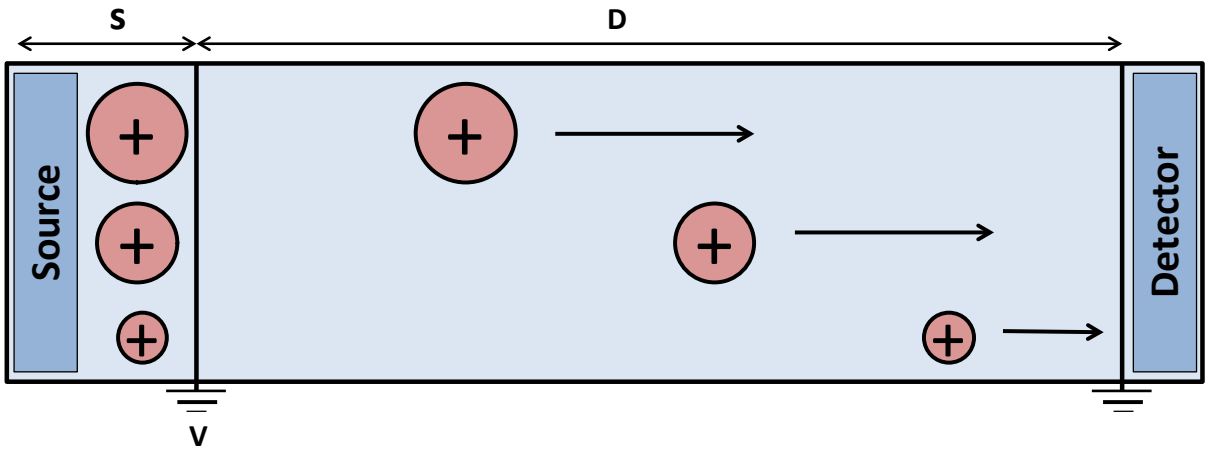

Figure 1. 6 Schematic of a linear ToF.

Ideally all ions leaving the source region should have the same kinetic energy, but in reality this is not the case and ions with the same *m/z* may have a variety of kinetic energies and therefore arrive at the detector at different times. Spatial distribution effects are also observed due to the formation of ions at different points within the source. This leads to poor resolution but has been overcome by a variety of

methods.[10,16-17] One method was developed by Mamyrin[18] and is called reflectron time-of-flight (RToF) (**Figure 1.7**).

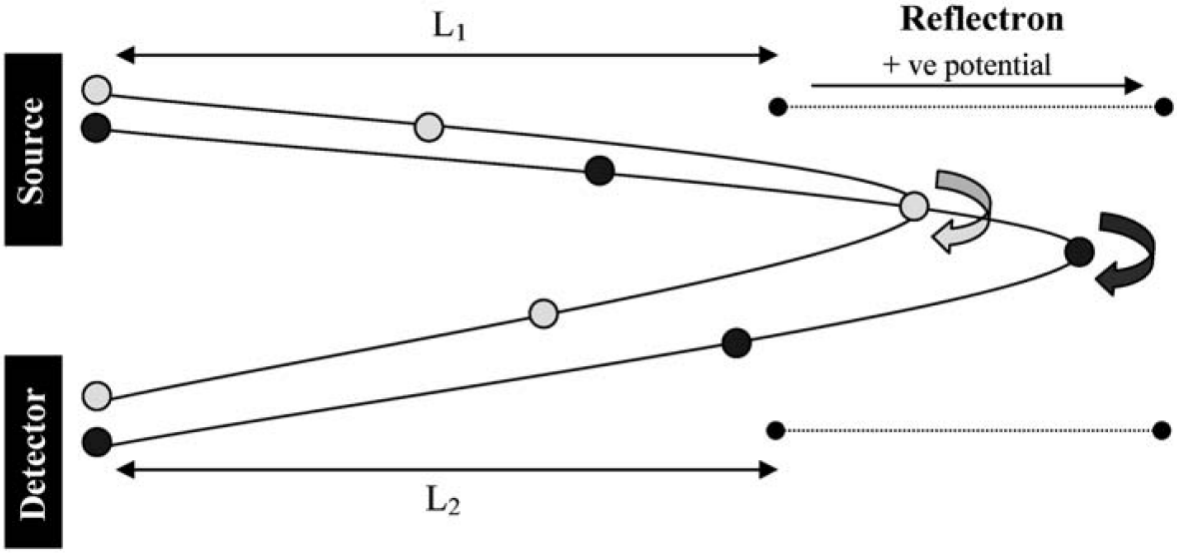

Figure 1. 7 Schematic of a reflectron time-of-flight mass spectrometer.[7]

RToF uses an electrostatic lens which acts as a reflector, deflecting ions back down the drift tube, which corrects for the difference in KEs, meaning ions with same *m/z* will arrive at the detector at the same time. The reflectron consists of a series of electrostatic grids or rings with an applied electrical potential that are positioned at the end of the drift region. Ions with higher KEs travel faster and will penetrate further into the electrostatic potential before being turned round whereas ions with lower KEs travel slower and do not penetrate the field as far before being reflected, therefore, travelling a shorter distance. This means ions with the same *m/z* but differing KEs will arrive at the detector simultaneously, improving resolution.

1.1.3 Detectors

The final component of a mass spectrometer is the detector. There are many different types of detector, however, the detection of an ion is always based on their frequency of

oscillation, mass, charge or velocity.[10] For the purpose of this work, only microchannel plate detectors (MCP) will be described briefly here.

1.1.3.1 Microchannel Plate detectors

A microchannel plate (MCP) is made from a lead glass and consists of an array of miniature electron multipliers situated parallel to one another.[19] The plates contain cylindrical channels coated with a semiconductor material which enhances secondary electron emission. Once an incident ion hits the surface of the cylinder, secondary electrons are produced which are collected at the end of the detector and measured as current. The production of secondary electrons can enhance the signal by a factor of 10^{2-4} for a single plate, or 10^8 if multiple plates are combined. MCPs are widely used for ToF and quadrupole-time-of-flight (Q-ToF) analysis as they are suited to the detection of large beams of ions due to their flat conversion surface with a large area.[20]

1.2 ION MOBILITY SPECTROMETRY

Ions suspended in a gas or liquid will diffuse spontaneously unless an external force is applied. In the presence of a force, such as the Coulombic force exerted by an electric field, an ion will move in the direction of the field lines. The velocity at which the ions move is dependent on the medium in which the ions are present and the characteristics of the ion. These characteristics are termed mobility.[21] The nature of ion diffusion and mobility allows for the separation of an ionic mixture. When an ion is in the gas-phase and in the presence of an electromagnetic field this is called ion mobility spectrometry (IMS).

The principle of ion mobility spectrometry was developed in the early 1900s; however, it was not until the 1970s that the first ion mobility spectrometer was commercially available.[22, 23] This technique has found many applications most commonly in areas of security, but also environmental, forensic and biological applications.[24]

1.2.1 Principles of Ion Mobility

Ion mobility is governed by gas diffusion laws. First Fick's law states:

$$J_M = -D\nabla_N \qquad \textbf{Equation 1. 10}$$

where J_M is the molecular flux which is the number of molecules flowing through a unit area per unit time, D is the diffusion coefficient and ∇_N is the concentration gradient. Molecules diffuse differently in each different medium and therefore D is a property of the diffusing molecules and the media molecules. D is proportional to the velocity of diffuse flow, v_D:

$$v_D = (D/N)\nabla_N \qquad \textbf{Equation 1. 11}$$

where *N* is the number density. In gases, *D* is determined by:

$$D = \frac{3}{16}\left(\frac{2\pi kT}{\mu}\right)^{1/2}\frac{1}{N\Omega} \qquad \textbf{Equation 1. 12}$$

where *k* is the boltzman constant (1.380×10^{-23} m^2 kg s^{-2} K^{-1}), *T* is the gas temperature (K), μ is the reduced mass (μ = mM / m+M) of the diffusing ions (M) and gas molecules (m) and Ω is the collision cross section ($Å^2$).

Ω is the collision integral for the diffusing ions and gas molecules and is an average over all orientations. This is the only variable in the equation dependent on the ion and the gas which is neither a constant nor a parameter that can be set.

Ions subjected to an electric field (E, V cm^{-1}) in the presence of a drift gas, usually helium or nitrogen will reach a terminal drift velocity (v_d) dependant on their mobility (K, **Eqn. 1.13**). Species with different K do not have the same v_d and therefore can be separated on the basis of their mobility (K):[25]

$$K = \frac{v_d}{E} \qquad \textbf{Equation 1. 13}$$

The time taken for an ion to traverse the length (d) of the drift tube is known as the drift time (t_d) and in terms of mobility is expressed as[26]:

$$K = \frac{d}{t_d E} \qquad \textbf{Equation 1. 14}$$

It is usual to report mobility in terms of reduced mobility (K_0), which is the mobility (K) normalised for temperature (T, k) and pressure (P, Torr) of the gas atmosphere through which the ions migrate.[23]

$$K_0 = \left(\frac{273}{T}\right)\left(\frac{P}{760}\right) \qquad \textbf{Equation 1. 15}$$

The mobility of an ion is dependent on its characteristics and the experimental conditions. The Mason-Schamp equation (**Eqn. 1.16**) relates the mobility of an ion to these parameters:

$$K = \left(\frac{3q}{16N}\right)\left(\frac{2\pi}{\mu kT}\right)^{1/2}\left(\frac{1}{\Omega}\right) \qquad \textbf{Equation 1. 16}$$

where q is the charge on the ion.

At a given temperature and pressure the mobility of an ion is dependent on the reduced mass, charge and collision cross section. The mobility of an ion is only independent of the electric field to pressure ratio (E/N, Td where 1 Td = 10^{-17} V cm^2) at low electric fields. Above ~2 Td the mobility of an ion becomes field dependant.[25] A modified version of the Mason-Schamp equation (**Eqn. 1.16**) has recently been derived by W. F. Seims *et al*.[27] however, the following chapters have only considered **Eqn. 1.16**)

Ions behave differently at low and high electric fields and this forms the basis of techniques such as differential mobility spectrometry (DMS) and high field asymmetric waveform ion mobility spectrometry (FAIMS). In these techniques, ions are separated by their differing behaviour in both high and low electric fields.

1.2.2 Instrumentation

A traditional IMS drift tube instrument is shown in **Figure 1.8**. The main components of an IMS are the ion source, reaction region, drift region and detector.[25]

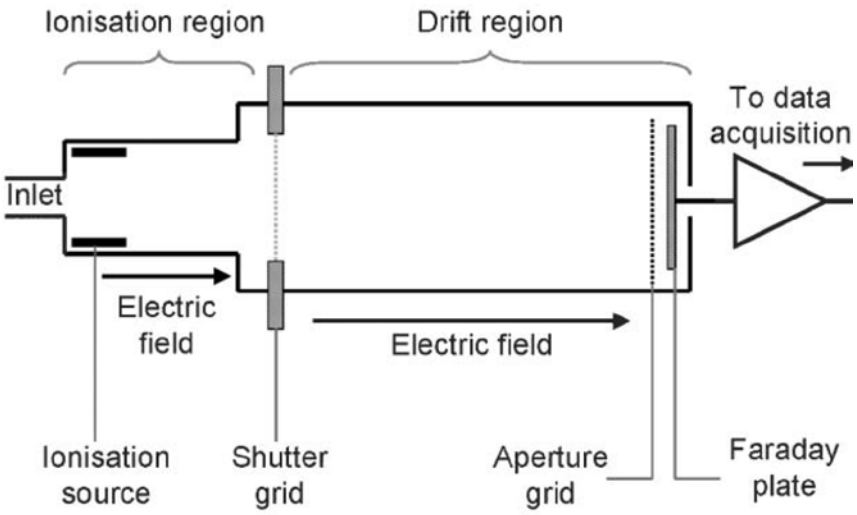

Figure 1. 8 Schematic of a traditional IMS.[26]

Ions are introduced into an ionisation region where they are ionised and then held at an electric ion shutter grid which opens for a short time pulsing the ions into the drift cell. The ions traverse the drift cell in the presence of an electric field gradient and a buffer gas before being detected.

1.2.2.1 Sample Introduction and Ionisation

Numerous techniques are available for the ionisation of samples for IMS including ESI[28], matrix assisted laser desorption ionisation (MALDI),[29] and atmospheric pressure chemical ionisation (APCI)[26,30]. The most common method utilises a 370 MBq Ni^{63} source which emits β particles, ionising the drift gas and forming thermalised electrons (**Eqn. 1.17**).[26]

$$N_2 + \beta \rightarrow N_2^+ + \beta' + e^- \qquad \textbf{Equation 1. 17}$$

A series of ion-molecule reactions occur with trace amounts of water forming ions such as, $(H_2O)_nH^+$ and $(H_2O)_nO_2^-$ which then react with molecules to create charged species including: MH^+, M_2H^+, $M(H_2O)H^+$ and MO_2^-.

There have been many sample introduction methods reported for IMS. These include diffusion tubes[31], permeation tubes[32], direct headspace injection[33] and absorption of sample vapour onto a nickel wire[34]. IMS has been coupled to other separation techniques such as liquid chromatography, (LC)[35,36] and gas chromatography, (GC)[37,38].

1.2.2.2 Drift tubes

The drift region in IMS is where separation occurs. There are four types of drift region: linear drift tube, aspiration, differential and travelling wave. In this work only linear drift tube and travelling wave IMS were used and therefore explanations will be limited to these two techniques.

Drift Tube Ion Mobility Spectrometry

There are a variety of drift tube designs for drift tube ion mobility spectrometry (DTIMS), however, the basic features are the same. After exiting the reaction region the ions are held at a shutter grid, which pulses swarms of ions (~50-250 μs) into the drift region. There are two main types of shutter grid: the Bradbury-Nielson[39] type and the Tyndall[40] type.

The Bradbury-Neilson shutter grid consists of multiple parallel thin wires that are coplanar to each other and under tension. The alternate wires are isolated electrically and mechanically and the shutter is only open when the alternating wires equal the same voltage. The Tyndall design consists of three parts; two parallel wire grids separated by 0.3 mm with a thin mica sheet. The two grids are held at different voltages when the shutter is closed and to open the shutter the voltage for grid one equals the voltage of grid two.

Once the grids are open the ions are accelerated into the drift cell, which may be a few cm to one m in length. The time it takes an ion to reach the detector is termed the drift time (t_d) and occurs on the msec timescale. This is calculated using **Eqn. 1.18**.

$$t_d = \frac{d}{v_d} \qquad \textbf{Equation 1. 18}$$

where *d* is the distance between the ion shutter and the detector. The ions traverse the drift tube in the presence of a constant electrical field gradient created by metal drift rings. The rings are electrically connected together by a series of resistors. The voltage gradient across the drift cell varies between instruments but is typically between 1-500 Vcm^{-1}.[26]

A buffer gas, typically He or N_2, enters the drift tube at the detector end and travels in an opposing direction to the analyte. The analyte ions collide with buffer gas molecules which slows the analyte down. Larger molecules undergo more collisions than smaller molecules and therefore take longer to reach the detector meaning they have a greater t_d and a lower k.

Travelling Wave Ion Mobility Spectrometry

One of the most recent developments in IMS is travelling wave ion mobility spectrometry (TWIMS), developed by Waters (Manchester, UK) for their Synapt.[41-43] In the place of a uniform electric field gradient used in traditional linear IMS, an RF field is applied to a stacked ring ion guide (SRIG)[41] (**Figure 1.9**) which confines the ions whilst a DC voltage is used to create a 'travelling wave' which moves the ions through the drift cell. Ions either, travel in front of, surf the top or fall behind the wave resulting in transport of the ions down the drift tube.

Ions are trapped in a SRIG prior to entering the mobility cell. Once ions have accumulated, the trap releases ions into the mobility cell for a set period of time. The SRIG mobility cell in TWIMS containing 61 electrode pairs with an applied RF voltage, radially confines the ions, suppressing diffusion and coulomb expansion, providing higher transmission efficiency.[42-44] A superimposed DC voltage is applied to electrode pairs to propel the ions through the cell. A DC pulse creates a series of potential hills which are repeated every 6 electrode pairs. The result of these pulses creates the 'travelling wave' sequence throughout the length (185 mm) of the cell.[42]

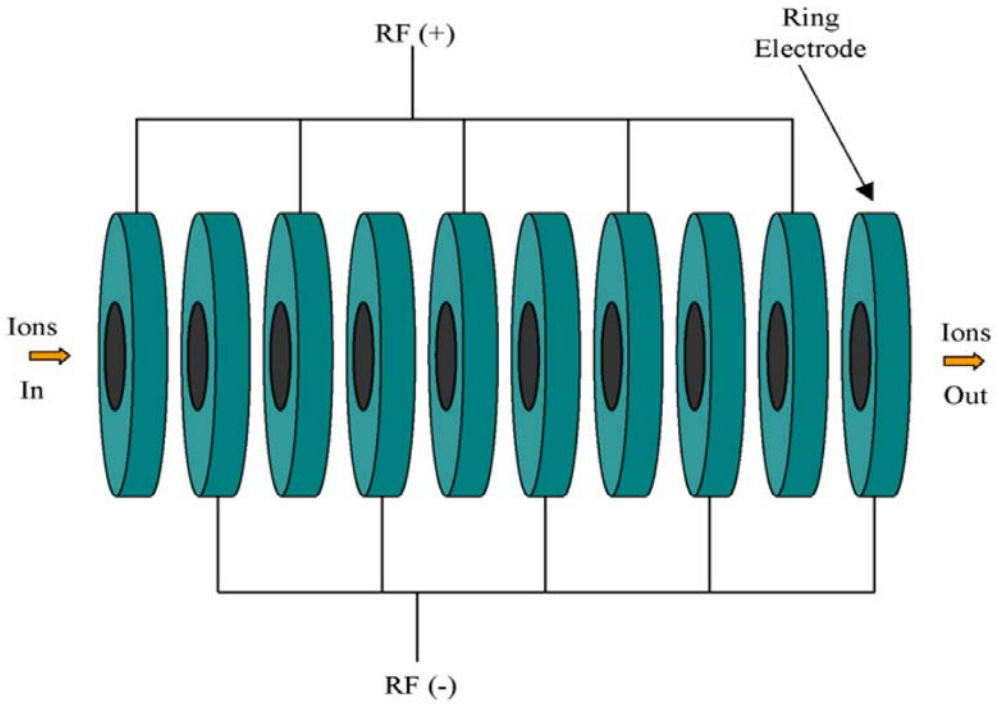

Figure 1. 9 A schematic of a stacked ring ion guide.[42]

The position of an ion with respect to the wave is dependent on the size of the ion. The important parameter in this process is the ratio (c) of ion drift velocity at the steepest wave slope (E_{max}) to wavespeed (s) (**Eqn. 1.19**).[44]

$$c = \frac{KE_{max}}{s} \qquad \textbf{Equation 1. 19}$$

If $c << 1$; waves will pass beneath the ions, if $c > 1$; the ions will be pushed ahead of the wave and if $c \approx 1$; the ions will 'surf' the wave, occasionally falling behind it. This results in separation between the ions (**Figure 1.10**).

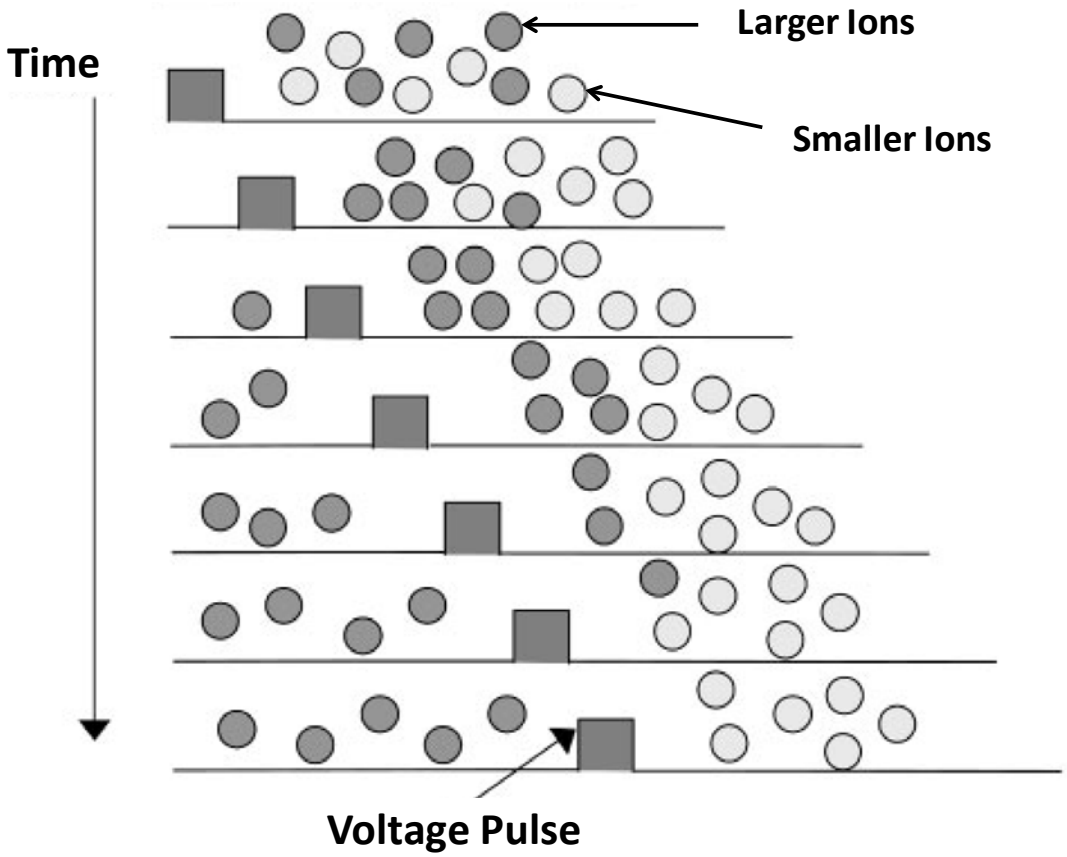

Figure 1. 10 Schematic of ion separation in TWIMS. Adapted from[41].

The relationship between v_d on K and E is linear in traditional IMS, however, in TWIMS the relationship is non linear meaning the Mason-Schamp equation (**Eqn. 1.16**) no longer applies and the determination of collision cross sections (CCS) much more complicated. The determination of CCS will be discussed in greater detail in Section 1.4.

1.2.3 High-Field Asymmetric Waveform Ion Mobility Spectrometry (FAIMS)

FAIMS was developed in Russia in the 1980's,[45] however, the first report describing the technique in English was by Buryakov *et. a.l*[46] in 1993. It was brought to the USA by the mine safety appliance (MSA) corporation for the potential use in detection of explosives. Many variations of FAIMS have since been developed including cylindrical, flat plate and miniaturised FAIMS.[47, 48] As is the case for DTIMS and TWIMS, FAIMS can also be coupled with MS as a detector for added orthogonal multidimensional analysis. For the purpose of this work only miniaturised FAIMS with MS will be described in detail. FAIMS has been used for the analysis of proteins and peptides[48, 49], metabolites[50], pharmaceuticals[50] and security[51].

1.2.3.1 Principles of FAIMS

In FAIMS, ions are separated based on the differences in their mobility in alternating high and low electric fields (**Figure 1.11**). Ions travel between two electrodes at atmospheric pressure under the influence of an asymmetric RF waveform. This waveform is known as the dispersion voltage (DV). The high field voltage is greater than the low field voltage, however, the ions are subjected to the low field region for a longer period than the high field region to ensure the ions have an equal influence from both fields.[50]

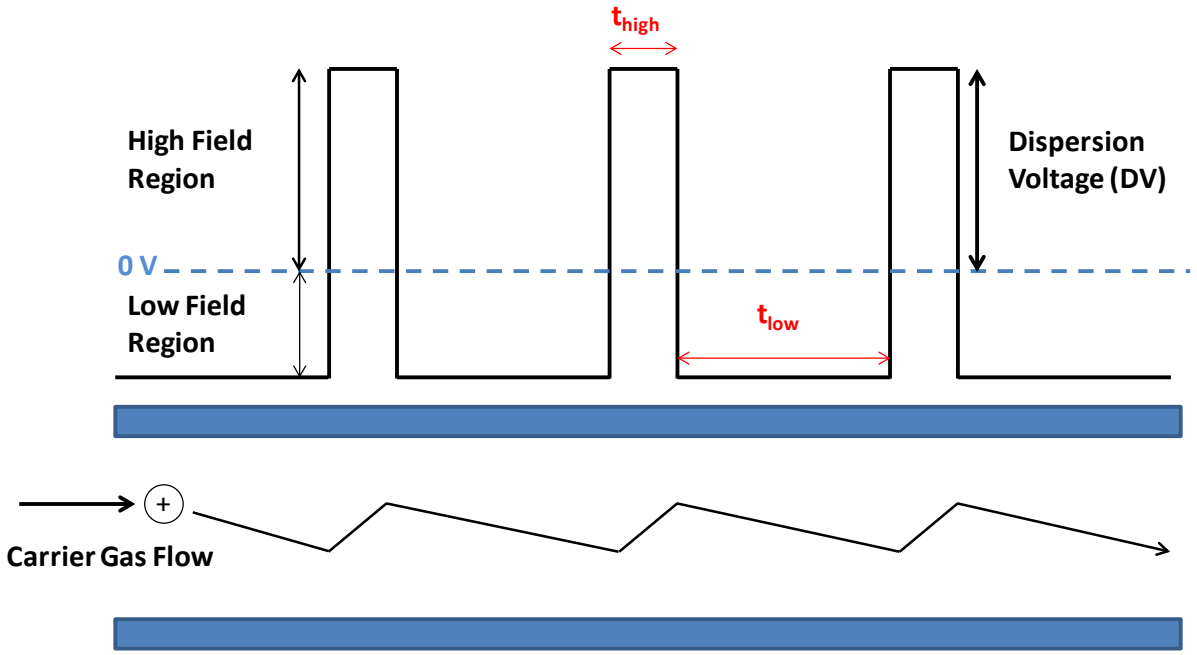

Figure 1. 11 A schematic showing the asymmetric waveform in FAIMS. Adapted from[50].

If the mobility of an ion in the low field is different to its mobility in a high field, the ion will drift towards an electrode where, on collision with the electrode it becomes neutralised. A compensation voltage (CV) is applied to one of the electrodes to correct the trajectory of the ion, allowing it to traverse the electrodes. The mobility of an ion in the high field electric waveform ($K_h(E)$) can be calculated using:

$$K_h(E) = K_0\big(1 + \alpha(E)\big) \qquad \textbf{Equation 1. 20}$$

where K_0 is the reduced mobility at low electric field, α is a coefficient for the dependence of mobility of an ion on the electric field strength and E is the high field component of the electric waveform.[48] The differential mobility of ion is dependent on the characteristics of an ion including mass, charge, functionality and conformation; the CV required for an ion to traverse the electrode is α and therefore compound specific. During an analysis the CV can be scanned to allow transmission of all ions, or the

device can act as an ion filter by using one CV which selects ions based on their differential mobility.

1.3 ION MOBILITY-MASS SPECTROMETRY

The normal detector for traditional IMS was a Faraday plate,[26] however, IMS coupled with MS has become a widely used configuration in recent years. McDaniel was the pioneer of IM-MS, first interfacing IMS to a magnetic sector instrument in 1968.[52] This was quickly followed by the hyphenation of ToF-MS[53-55] and quadrupole-MS[56, 57] to IMS. Today there are a large variety of IM-MS instruments available, however, only the three instruments used in this work will be discussed in detail.

1.3.1 Ion Mobility Quadrupole Time-of-Flight Mass Spectrometer (MoQToF)[58]

The MoQToF is a quadrupole-time-of-flight instrument developed at the University of Edinburgh, based on a Waters Q-ToF spectrometer (Micromass UK Ltd., Manchester, UK) which has been modified to house a linear ion mobility cell and ancillary optics. A schematic of the instrument is shown in **Figure 1.12**.

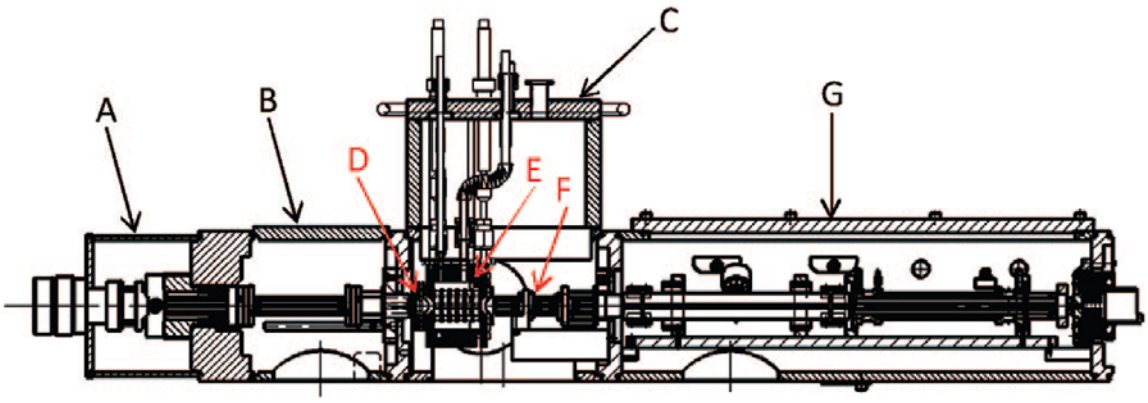

Figure 1. 12 Schematic diagram of the MoQToF showing a z-Spray ESI ion source (A), vacuum chamber 1 housing a pre-cell hexapole (B), vaccum chamber 2 housing a pre-cell Einzel lens (C), drift cell (D), post-cell hexapole (E), chamber containing gas and electric feedthroughs required for the drift cell (F), vacuum chamber 3 containing the quadrupole mass analyser and hexapole collision cell (G) leading to a ToF mass analyser.[58]

Analytes are ionised via a NSI source (A) and transferred into region B where they can be stored for mobility experiments. Ions are focussed into the mobility cell using a three-element lens stack. After exiting the drift cell ions are transferred to the quadrupole via a post-cell hexapole. The quadrupole can act as a mass filter or set to allow all ions to be transmitted. Another hexapole is located post-quadrupole transferring ions to the ToF analyser. In quadrupole-only mode the ions are detected on a point detector and in ToF mode they are detected using an MCP detector.

Cross sectional and sectional diagrams of the drift cell are shown in **Figure 1.13**. The drift cell is 5.1 cm long and made from a copper block and end cap separated by a ceramic ring. The cell and end cap can be heated via ceramic heaters and cooled via liquid nitrogen. Temperature is monitored using a set of three thermocouples and the pressure of the cell monitored via a ½ in. exit port located at the top of the cell using a Baratron (MKS).

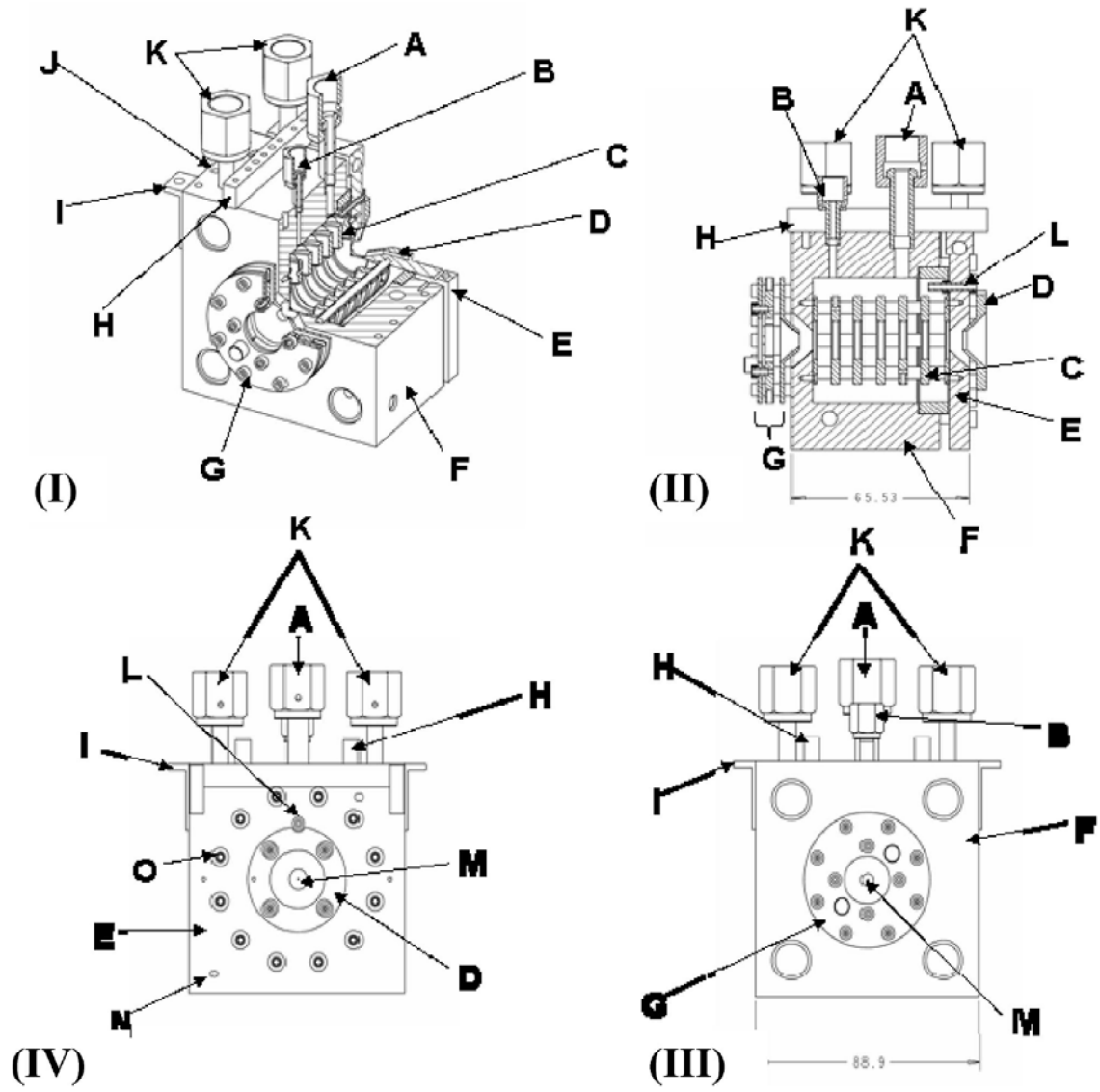

Figure 1. 13 **Cross sectional and sectional diagrams of the MoQToF drift cell. (I) 3D section through cell, (II) section from side view of cell, (III) front view, (IV) rear view. Part labels (A) Baratron connection, (B) gas in, (C) gas out, (D) exit lens, (E) end cap (C2), (F) cell body (C1), (G) Einzel lens (L1, L2 and L3), (H) heater terminal block, (I) mounting brackets, (J) heaters, (K) cooling line inlets, (L) feedthrough to drift rings, (M) molybdenum orifice, (N), thermocouple mounting and (O) cell screws.**[58]

The drift field is present between the cell body and end cap orifice. The linear field is maintained by 5 copper guard rings connected with resistors. The drift gas is typically, He, however, other gases can be used. Pressures with He are approximately 3-3.5 Torr and voltages are up to 65 V (12.7 V cm^{-1}) across the cell. The voltages to the modified parts of the instrument are controlled using an in-house power supply. Ions are pulsed

into the mobility cell which initiates the start of 200 ToF scans (bins), each being the length of one pusher period (30-85 μsec). The MassLynx software (Waters, Manchester, UK) displays the data as a total ion chromatogram (TIC), however, selected ion data can be extracted and drift times calculated by multiplying the scan number by the pusher time. The experimental determination of CCS will be discussed later in Section 1.4.

1.3.2 Travelling wave ion mobility quadrupole time-of-flight

The Synapt HDMS (Waters, Manchester, UK) was developed in 2007[42] as a new ion mobility-mass spectrometry technique and has since been used for the analysis of peptides and proteins,[59-63] metabolites,[64] pharmaceuticals[65] and organometallic complexes[66, 67]. A diagram of the instrument is shown in **Figure 1.14**.

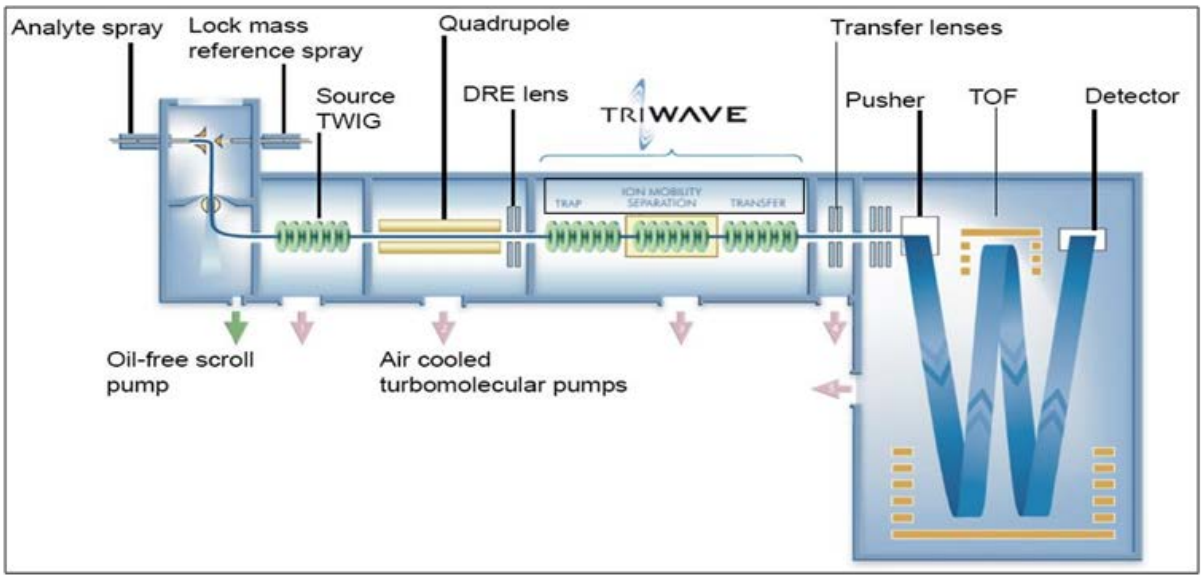

Figure 1. 14 A schematic of a Waters Synapt HDMS G1[68]

The analytes are ionised with an ESI source and transferred into a travelling wave ion guide (TWIG) consisting of a series of planar electrodes with an applied alternating RF voltage with opposing phases on adjacent electrodes. TWIGs are operated with RF voltages at frequencies of 2.7 MHz and variable amplitudes up 400 V pk-pk. The ions

are propelled through the guide via a travelling wave as is described in Section 1.2. The ions enter the quadrupole where all ions can be transmitted or they can be selected according to their *m/z*.

Prior to entering the TWIMS mobility cell the ions are trapped by a stacked ring ion guide (SRIG)[41] containing 33 electrode pairs with an applied RF voltage with the exception of the last electrode which is dc only.[42] The ions are pulsed from the trap as ion packets into the mobility cell before entering the transfer region where the ions are transferred to the ToF for mass analysis via an Einzel lens and transfer lenses.[42]

Ions pulsed into the mobility cell initiates the start of 200 ToF scans (bins), each being the length of one pusher period (typically, 45 or 64 μsec). The MassLynx software (Waters, Manchester, UK) displays the data as a total ion chromatogram (TIC), however, selected ion data can be extracted and drift times calculated by multiplying the scan number by the pusher time.

1.3.3 FAIMS-MS Instrumentation

The instrument used for this work was carried out on a prototype miniaturised FAIMS device (Owlstone, Cambridge, UK), interfaced with an Agilent 6230 orthogonal ToF mass spectrometer (Agilent Technologies, Santa Clara, CA, USA).

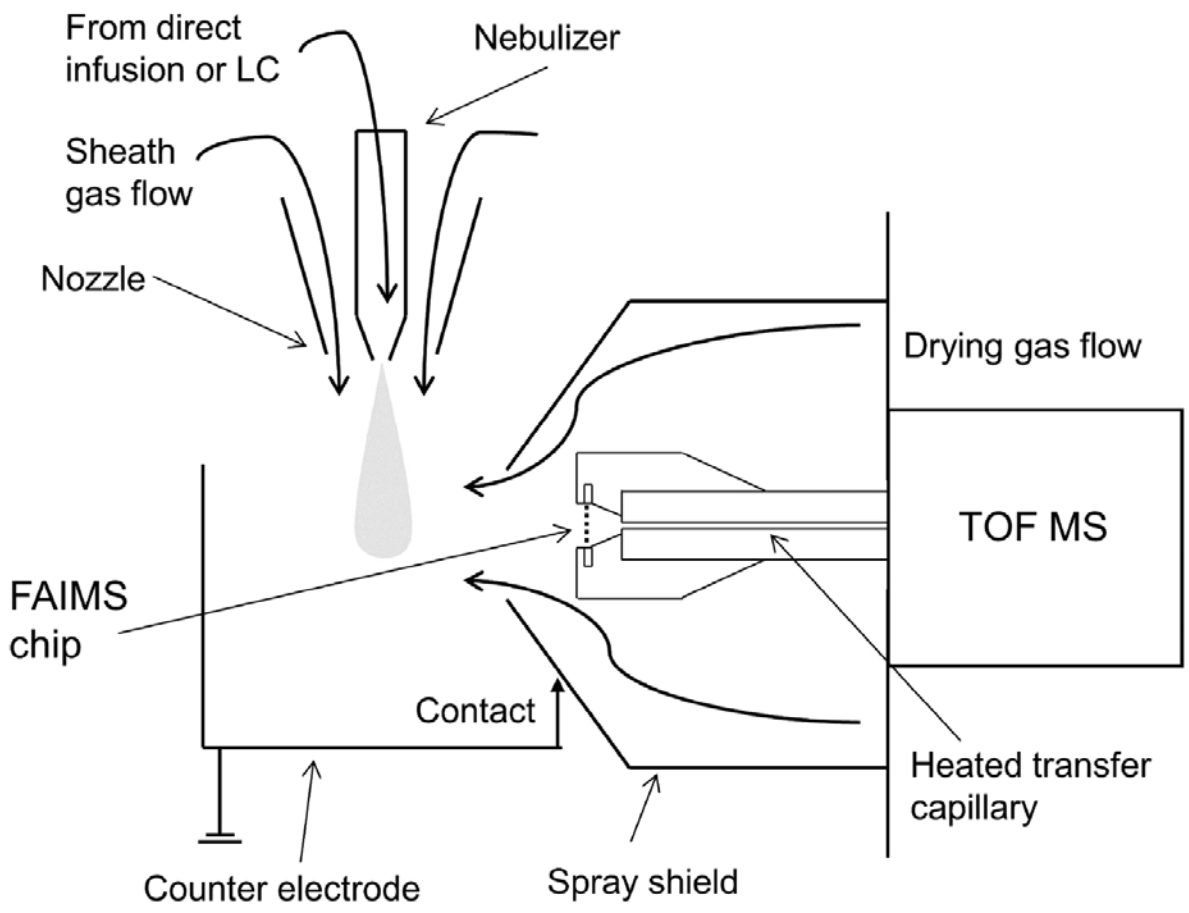

Figure 1. 15 A schematic of the interfacing for a FAIMS chip and ToF.[69]

The ESI source of the ToF spectrometer has been modified to include a FAIMS chip (**Figure 1.15**). The chip is a planar FAIMS device and contains 16 electrode pairs. Each channel has a width of 100 μm and a length of 700 μm. Due to the smaller electrode channels, higher electric field intensities can be applied across the gap compared to that of other devices which have channels an order of magnitude larger.[69] To generate the field asymmetric waveforms, DV, the chip is connected to a generator module. Once ions have passed through the chip and they can be detected by the ToF.

1.4 THE DETERMINATION OF COLLISION CROSS SECTIONS

The collision cross section (CCS or Ω) of an ion describes its shape and size.[70] The determination of CCS, either by measurement or calculation is therefore essential to structural studies by IMS.[71,72]

1.4.1 Experimental Calculations

In the early days of IMS when measurements were made using DTIMS with a fixed electric field gradient, the CCS measurements were simple and well understood. CCS can be calculated from the measured drift time (t_d) by rearranging the Mason-Schamp equation (**Eqn. 1.16**)[73].

$$\Omega = \frac{(18\pi)^{\frac{1}{2}}}{16} \frac{ze}{(kT)^{\frac{1}{2}}} \left[\frac{1}{m_I} + \frac{1}{m_N}\right]^{\frac{1}{2}} \frac{760}{P} \frac{T}{273.2} \frac{1}{N} \frac{t_d E}{L} \qquad \textbf{Equation 1. 21}$$

where N is the gas density number (proportional to pressure), k is the Boltzmann's constant, T is temperature (k) P is pressure (Torr) of the gas atmosphere through which the ions migrate z is the nominal charge on the analyte, e is the charge on an electron (1.6022×10^{-19} C), (m_I) is the mass of the analyte ion, (m_N) is the molecular mass of the buffer gas, E is the electric field and L is the length of the drift cell.

The DTIMS CCS measured in this work were determined using an in-house modified commercial Q-ToF instrument (Micromass UK Ltd., Manchester, UK) described previously.[58] To calculate the CCS, the drift time of an analyte ion is measured multiple times over a range of drift voltages (V_D). The pressure is taken before and after each run. The average pressure is then divided by V_D and plotted against t_d (the arrival time distribution). The intercept of the resulting graph is the time ions spend in the instrument without being retarded in the drift cell (dead time). The slope ($t_a(P/V_D)$) can

be inserted into **Eqn. 1.22** to obtain mobility which is inserted into **Eqn. 1.16** to calculate the CCS (Ω).

$$K^\circ = \frac{z_D^2 T^\circ}{P^\circ T \left(\frac{dt_a}{d\left({}^{p}/_{V_D}\right)} \right)} \qquad \textbf{Equation 1. 22}$$

where z_D is the longitudal drift distance and t_a is the arrival time calculated by:

$$t_a = \frac{z_D^2 T^\circ}{K^\circ T P^\circ V_D} \frac{P}{V_D} + t_0 \qquad \textbf{Equation 1. 23}$$

where t_0 is the time the ions spend outside the drift cell. The linear relationship between t_d and K means the DTIMS CCS calculations are relatively simple. In cases where this relationship is no longer linear, for example, in TWIMS; the determination of CCS is much more complex.[73, 74]

In order to determine the CCS in a TWIMS instrument, standards are needed which have a known CCS previously determined via conventional DTIMS. The standards are used to plot a calibration curve of corrected CCS (*CCS'*) against effective drift time t_d''. *CCS'* is the CCS which has been corrected to account for the non-linear relationship of the travelling wave using the CCS of the known values from DTIMS ($CCS_{(Drift\ Tube)}$) (**Eqn. 1.24**).

$$CCS' = \frac{CCS_{(Drift\ Tube)}}{e \times \left(\frac{1}{M_{ion}} + \frac{1}{M_{gas}} \right)^{1/2}} \qquad \textbf{Equation 1. 24}$$

The t_d of the analytes has to be corrected to account for the Triwave which is achieved in two stages, first to correct for the offset in the drift cell:

$$t_d' = t_d - 920 \qquad \textbf{Equation 1. 25}$$

where t_d is the drift time (μs) and 920 is the travelling wave offset time (μs). This value is specific to the Synapt G1. At a wave velocity of 300 m/s each pair of ring electrodes in the drift cell has an offset of 10 μs (t_m) and each pair of ring electrodes in the transfer region has an offset of 10 μs (t_t). There are 61 pairs of electrodes in the drift cell and 31 in the transfer region. Therefore, the total offset is 920 μs.

In the second stage t_d" is the t_d' after it has been corrected for the time the ions take to leave the drift cell and reach the detector (44 μs ToF flight time and 41 μs to reach the ToF) and is mass dependent. It is calculated by:

$$t_d" = t_d' - \sqrt{\left(\frac{m/z}{1000}\right)} \times 85 \qquad \textbf{Equation 1. 26}$$

The t_d" values can now be substituted into the calibration graph and from this CCS can be determined using **Eqn. 1.27**:

$$CCS'_{(T-wave)} = t_d"^{B} \times A \times e \times \left(\frac{1}{M_{ion}} \times \frac{1}{M_{gas}}\right)^{1/2} \qquad \textbf{Equation 1. 27}$$

for power calibration plots and

$$CCS'_{(T-wave)} = [(t_d" \times A) + B] \times e \times \left(\frac{1}{M_{ion}} \times \frac{1}{M_{gas}}\right)^{1/2} \qquad \textbf{Equation 1. 28}$$

for linear calibration plots where parameter B compensates for the non-linear effect of the TWIMS system and parameter A for the temperature, pressure and electric field conditions, *e* is the charge and *M* is the mass.

Clemmer has compiled a database[75] of CCS for peptides and proteins which have been widely used as standards to determine CCS by TWIMS. This was due to a need to calculate CCS for biological molecules, however, due to the increase of analyses on small molecules,[71] there have been ongoing investigations into other standards to give accurate CCS for non biological small molecules including tetraalkyl ammoinium halides[65] and drug-like molecules[65].

1.4.2 Theoretical Calculations

Theoretical CCS may also be calculated and compared with measured CCS in structural studies. There are various programs which have been developed to calculate CCS from a set of coordinates obtained from x-ray or modelled structures. The most widely used CCS calculator is MOBCAL[76].

MOBCAL consists of three algorithms: the projection approximation, (PA),[77] the exact hard sphere scattering, (EHSS)[78] and the trajectory method, (TM)[79]. The PA calculates CCS based on a hard sphere model with radii equal to hard sphere collision distances. The analyte is a 'projection' in which the buffer gas either collides with the ion or misses. The analyte is then rotated and the procedure is repeated. This continues until all angles and rotations have been analysed and the final reported value is an average of all projections. The exact hard sphere scattering is a hard sphere model where the angles of scattering are taken into consideration upon collision of the buffer gas and analyte. The trajectory method represents the ion as a collection of atoms each with a 12-6-4 potential.

MOBCAL[76] has become the most widely used program, however, there have been other reported modifications to the PA method to create new calculators such as the Waters[67] calculator and the Leeds[80] calculator.

1.5 EFFECTS OF DRIFT GAS IN IM-MS

The effects of drift gas on mobility have been well studied. The most common drift gases are air, helium (He) and nitrogen (N_2). However, argon (Ar) and carbon dioxide (CO_2) have also been investigated.[81,82] The mobility was shown to be the greatest in the smallest and least polarisable gas, He, and the lowest in the most polarisable and largest gas, CO_2.This has been demonstrated in both conventional IMS and TWIMS.[81,82]

The drift gas can have a significant effect on the separation factor (α) calculated by:

$$\alpha = K_1/K_2 \qquad \textbf{Equation 1. 29}$$

where K_1 is the mobility constant of the fastest drifting compound and K_2 is the mobility constant for the slower drifting compound. Aniline was compared against 9 other compounds in each of the drift gases. The results showed a different α value for each drift gas. **Figure 1.16** demonstrates the mobility results for iodoaniline and chloroaniline in the four drift gases.

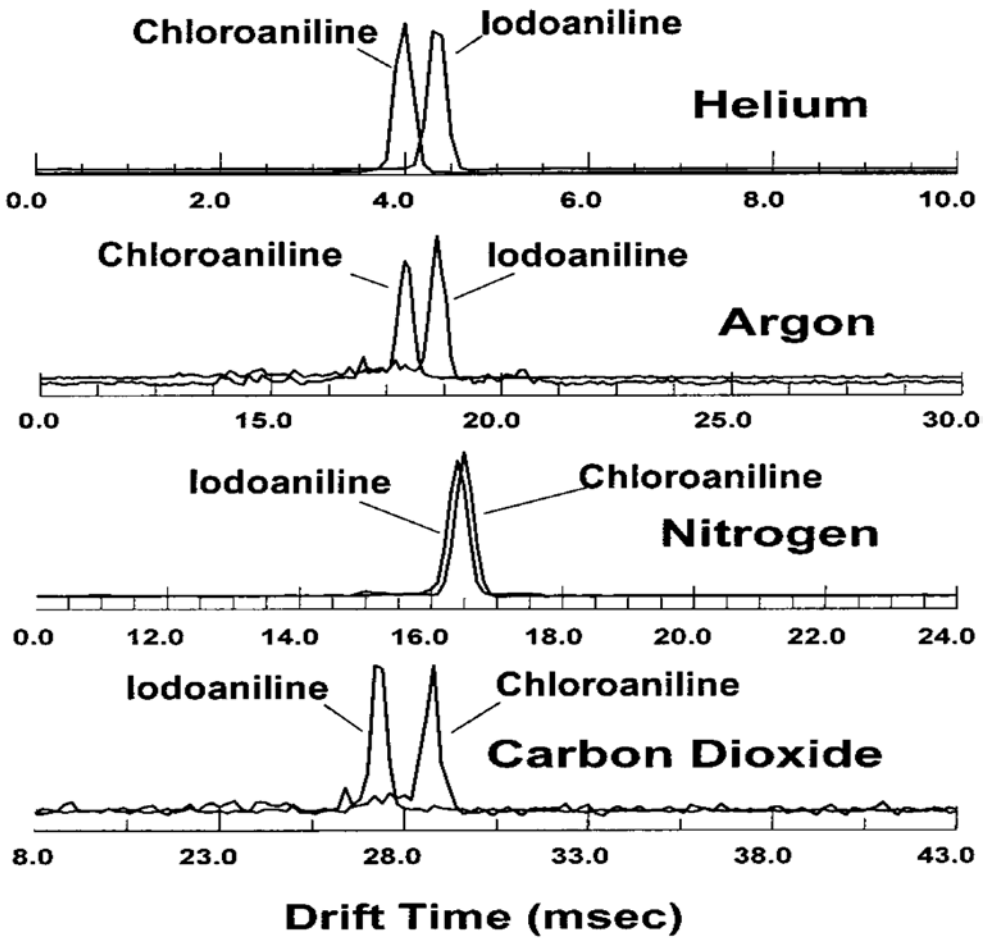

Figure 1. 16 Mobility spectra for iodoaniline and chloroaniline in helium, nitrogen, argon and carbon dioxide.

In He chloroaniline drifts faster than iodoaniline, in Ar the drift times are similar to that of He, in N_2 the peaks overlap and in CO_2 the peaks are resolved again, but are the opposite way round to He and Ar. If the drift time was simply a function of polarisability it would be expected that Ar would have a similar spectrum to N_2, rather than He. The reason for the unexpected results is due to the reduced mass (μ) which is greater for Ar/iodoaniline than Ar/chloroaniline which when substituted into **Eqn. 1.30** has a significant effect on t_d.

$$t_d = \frac{16N}{3}\left(\frac{\mu kT}{2\pi}\right)^{1/2}\frac{L^2\Omega}{V_q} \qquad \textbf{Equation 1. 30}^{[79]}$$

where V is the total voltage drop an ion experiences. If an ion is ≤ the mass of the drift gas then the mass of the ion has an influence on t_d. However, if the mass of the analyte is much greater than the mass of the drift gas then the μ effectively equals the mass of the drift gas and would, therefore, not contribute to the separation of two large ions. If ions have an equal charge, large ions are separated based solely on CCS whereas smaller ions are separated on mass and CCS.[81]

Another important factor which is highly relevant to the work published in this thesis that can be affected by drift gas is the effective size of the ions.[81] The radii of 10 compounds were measured in the four drift gases mentioned previously. The radii increased in the order He < Ar < N_2 < CO_2. The reason for this relationship is due to the polarisability of the gases which also increase in the order He < Ar < N_2 < CO_2. When radius is plotted against drift gas polarisability, the small ions demonstrated a linear relationship, therefore, the more polarisable the drift gas, the larger the ion radius. However, this effect does not affect all ions equally. A similar experiment was carried out using cocaine and metabolites which showed the relationship between drift gas polarisability and CCS to be linear.[83]

The effects that drift gases have on the size and mobility of an ion are important when considering the use of standards to determine CCS using TWIMS, particularly where the standards have a known CCS in He, but the measurements are made in N_2. He is small with low polarisability whereas N_2 is much larger and is highly polarisable, so it is expected that analysis in N_2 will produce larger CCS. The use of standards is considered to correct for the polarisability effects of N_2. However, it has been shown that an average 2% difference occurs between TWIMS data that has been measured in N_2 and corrected to He and DTIMS CCS data measured in He for a variety of peptide ions.[84] Campuzano *et al*.[65] reported a similar observation for CCS of betamethasone and

dexamethasone measured in nitrogen using TWIMS and calibrated with a drug-like calibration mix. This suggests that the conditions in the TWIMS drift cell may generate larger CCS than in DTIMS and that the calibration procedure does not fully correct for polarisability effects which are expected to be greater for smaller compounds due to the high charge densities.

1.6 TEMPERATURE EFFECTS IN TWIMS

Heating effects in DTIMS are easy to incorporate into CCS measurements as the drift cell temperature is monitored and taken into account when carrying out the calculations using **Eqn. 1.16**. In TWIMS, the temperatures are not monitored and therefore it is assumed that the calibration procedure will remove any differences due to ion heating. However, this may not be the case due to the different effects ion heating will have on non identical ions.

Morsa *et al.*[85] investigated the heating effects of experimental Triwave parameters on the effective temperature of an ion using a first generation Synapt (Waters, Manchester, UK) and *p*-methoxybenzyl pyridinium as a chemical thermometer. Merenbloom *et al.*[86] investigated the heating effects on a second generation Synapt (Waters, Manchester, UK) using a leucine enkephalin dimer as a chemical thermometer. Similar effects were observed for both instruments with dissociation occurring prior to the TWIMS drift cell and ion heating effects of ~555-774 K. The effect of ion temperatures on TWIMS CCS measurements is discussed in Chapter 2.

1.7 INTRODUCTION TO REACTION MONITORING

A variety of techniques such as infrared spectroscopy (IR),[87] near infrared spectroscopy (NIR),[88] nuclear magnetic resonance (NMR),[89] and liquid chromatography (LC)[90] have been used in reaction monitoring.

The development of ESI has opened up new possibilities and opportunities for MS, allowing in-tact analytes to be probed that otherwise would have been difficult to analyse using other ionisation methods. Reaction monitoring by ESI-MS has many advantages over techniques such as NMR. For example, ESI-MS is able to detect ions with NMR unsuitable nuclei and paramagnetic ions as well as labile components which would otherwise require low temperature experiments. Other advantages of the use of ESI-MS for reaction monitoring are; the ability to detect short-lived intermediates in real-time, high sensitivity enabling detection of trace intermediates, rapid analysis, isotope patterns and structural information for aided identification.[91]

The first analysis of an ionic transition metal complex was by Chait *et. al.*[92] in 1990, however, since then many organic and organometallic reactions have been studied including the Friedel-Crafts acylation,[93] the Diels-Alder cycloaddition,[94,95] the Wittig reaction,[96,97] the Olefin metathesis reaction,[98-101] the Heck reaction,[102] the Stille reaction[103] and the Suzuki reaction[104].

A particular area of interest in reaction understanding is the investigation of catalytic cycles. Catalytic cycles are reactions involving a catalyst where numerous intermediates are formed before the final product. These intermediates are often transient species which have very short lifetimes. Often when a new cycle is developed the exact mechanistic pathways are unknown and sometimes lead to by-products and dead end products lowering yields. It is therefore desirable for reaction pathways to be

determined and understood. Reaction monitoring is an important process in determining these pathways.

Reaction monitoring using MS can be either on-line or off-line. Off-line involves mixing the reactants in an external vessel and then taking aliquots of the reaction mixture at various time intervals, diluting the mixture and infusing the diluted sample into the MS.[91] This works if the intermediates are sufficiently stable but, transient species will go undetected. The simplest way to perform on-line reaction monitoring is to use a syringe for direct infusion. Multiple syringes can be used to pump two reactants into a microreactor before entering the ionisation source of the MS. This allows two reactants to mix and the reaction to occur during infusion preventing air stable or transient components breaking down before ionisation and detection. A PEEK mixing tee has been used as microreactor allowing the two reactants to be mixed prior to infusion into the MS. To change the reaction time the capillary into the MS can be lengthened or shortened.[105-107] Alternatively, a capillary mixer adjustable reaction chamber[108] may be utilised, which consists of two capillaries, an inner capillary and an outer capillary each attached to a syringe. Mixing occurs at the end of the inner capillary and the reaction time can be varied by moving the inner capillary closer or further from the ionisation source or by changing the syringe flow.

MS is an extremely useful tool for investigating mechanistic pathways and detecting components within catalytic cycles. However, if transient species are isomeric it may be difficult to distinguish between them by MS. IMS separates ions based on their shape and therefore has the potential to distinguish between isomeric species. IMS has been used in the online monitoring of trihalomethane and haloacetic acid concentrations in drinking water,[109] ammonia in water and waste water,[110] volatile organic carbons (VOCs) in laboratory air,[110] monomer concentrations in (semi-) batch emulsion

polymerisation reactors,[111] VOCs in air during yeast fermentation,[112] and nicotine in air during the manufacture of transdermal systems.

The hyphenation of IMS and MS allows the acquisition of both accurate mass data and also structural CCS data on reactants, intermediates and products in reaction mixtures. IM-MS has been used previously in the real-time monitoring of pharmaceutical reactions[113] and 7-Fluoro-6-hydroxy-2-methlindole to 4-[(4-fluoro-2-methyl-1*H*-indol-5-yl)oxy]-2-metyl-1*H*-indol-ol.[114] The use of IMS enhanced the clarity of the data for the components of the reaction mixtures.

1.8 OVERVIEW OF THESIS

Ion mobility-mass spectrometry (IM-MS) has been used to investigate small organic molecules and organometallic complexes. The travelling wave drift cell has been calibrated using peptide and tetraalkylammonium halide (TAAH) calibrants to enable the calculation of collision cross sections (CCS) via TWIMS. Organic and organometallic compounds have been studied using TWIMS and drift tube ion mobility spectrometry (DTIMS) and their CCS obtained. The experimentally determined CCS were compared to CCS values calculated using MOBCAL from x-ray and Gaussian modelled data.

This method has been applied to the study of reactions which have been monitored using on-line and off-line techniques. Reactants, products and intermediates (including a never before seen intermediate) have been observed and their CCS obtained. In cases where species are neutral and therefore not visible using mass spectrometry, charge bearing groups have been tagged onto a reactant resulting in charged intermediates and product within a catalytic cycle. High-field asymmetric waveform ion mobility-mass spectrometry (FAIM-MS) has been used to analyse intermediates, which showed the separation of the catalyst and intermediates. This work has demonstrated the potential of IM-MS, in combination with molecular modelling, to provide structural information on small molecules and insights into transient species in catalytic cycles.

1.9 CHAPTER ONE REFERENCES

1. Dole, M., Mack, L.L., Hines, R.L., *J. Chem. Phys*, 1968, **49**, 5.
2. Yamashita, M., Fenn, J.B., *Phys. Chem.*, 1984, **88**, 4451.
3. Yamashita, M. and Fenn, J.b., *Phys Chem*, 1984, **88**, 4672.
4. Whithouse, C.M., Dreyer, R. N., Yasashita, M., and Fenn, J.B., *Anal. Chem*., 1985, **57**, 675.
5. Santos L.S, *Reactive Intermediates: MS Investigations in Solution*, Wiley-VCH, 2010.
6. Kebarle, P., *J. Mass Spectrom.*, 2000, **35**, 804.
7. Rodrigues J.A., Taylor A.M., Sumpton, D.P., Reynolds , J.C., Pickford, R., Thomas-Oates, J., Adv Carbohydr Chem Biochem., 2007, **61**, 9.
8. Wilm, M.S., Mann, M., *Int. J. Mass Spectrom. and Ion Proc.*, 1994, **136**, 167.
9. Wilm M, Mann M., *Anal. Chem.*, 1996, **68**, 1.
10. Hoffmann, E., Stroobant, V., Mass Spectrometry: Principles and Applications, Third Ed., Wiley, 2007.
11. Paul, W., Steinwedel, H., *Z. Naturforsh*, 1953, **8a,** 488.
12. March, R.E., Hughes, R.J., *Quadrupole storage mass spectrometry*, Chemical Analysis Series, Vol. 102, John Wiley, New York, 1989.
13. March, R.E., *J. Mass Spec.*, 1997, **32**, 351.
14. Mathieu, E., *J. Math. Pures. Appl.*, 1868, **13**, 137.
15. Stephens, W., *Phys. Review*, 1946, **69**, 691.
16. Wiley, W.C., McLaren, J.B., *Rev. Sci. Instrum*., 1955, **26**, 1150.
17. Cotter, R.J., *Anal. Chem*., 1992, **64**, 1027.
18. Mamyrin, B.A., Karataev, V.I., Schmikk, D.V., Zagulin, V.A., *Sov. Phys. JETP*, 1973, **37**, 4.

19. Wiza, J.L., *Nucl. Instr. and Meth*, 1979, **162**, 587.

20. Chernusheevich, I.V., Loboda, A.V., Thompson, B.A, *J. Mass Spectrom.*, 2001, **36**, 849.

21. Differential Ion mobility Spectrometry, Nonlinear Ion Transport and Fundamentals of FAIMS, A. A. Shvartsburg, 2009 CRC Press, Taylor & Francis Group.

22. H. Borsdorf and G. Eiceman, *App. Spec. Rev.*, 2006, **41**, 323.

23. Cohen, M.J., Karasek, F.W., *J. Chromatogr. Sci.*, 1970, **8**, 330.

24. Guharay, S.K., Dwivedi, P., Hill, H.H.Jr., *IEEE Transactions on Plasma Science*, 2008, **36**, 1458.

25. Eiceman, G. A. and Karpas, Z., *Ion Mobility Spectrometry*, CRC Press Taylor & Francis Group, Second., 2005.

26. Creaser, C. S., Bramwell, C. J., Noreen, S., Hill, C. A., Thomas, C. L. P., *Analyst*, 2004, **129**, 984.

27. Seims, W. F., Viehland, L. A., Hill, H. H. Jr., *Anal. Chem*., 2012, **84**, 9782.

28. Shumate, C.B., Hill, H.H.Jr., *Anal. Chem.*, 1989, **61**, 601.

29. Gilig, K.J., Ruotolo, B., Stone, E.G., Russell D.H., Fuhrer, K., Gonin, M., Schultz, A.J., *Anal. Chem.*, 2000, **72**, 3965.

30. Revercomb, H.E., Mason, E.A., *Anal. Chem.*, 1975, **47**, 971.

31. Grob, R.L., *Modern Practise of Gas Chromatography*, John Wiley and Sons, New York, 1977.

32. O'Keefe, A.E., Ortman, G.C., *Anal. Chem.*, 1966, **38**, 760.

33. Karpas, Z., *Anal. Chem.*, 1989, **61**, 684.

34. Metro, M.M., Keller, R.A., *J. Chromatogr. Sci.*, 1973, **11**, 520.

35. McMinn, D.G., Kinzer, J.A., Shumate, C.B., Siems, W.F., Hill, H.H. Jr., *J. Micro. Sep.*, 1990, **2,** 188.

36. Hill, H.H.Jr., Siems, W.F., St. Louis, R.H., McMinn, D.G., *Anal. Chem.*, 1990, **62,** 1201.

37. Baim, M.A., Eatherton, R.L., Hill, H.H.Jr., *Anal. Chem.*, 1983, **55**, 1761.

38. Kanu, A.B., Hill, H.H.Jr, *J. of Chromatogr. A*, 2008, **1177,** 12.

39. Bradbury, N.E., Neilson, R.A., *Phys. Rev.*, 1936, **49**, 388.

40. Tyndall, A.M., *The mobility of positive ions in gases,* 2003, Cambridge University Press, Cambridge.

41. Giles, K., Pringle, S.D., Worthington, K.R., Little, D., Wildgoose, J.L., Bateman, R.H., *Rapid Commun. Mass Spectrom.*, 2004, **18**, 2401.

42. Pringle, S.D., Giles, K., Wildgoose, J.L., Williams, J.P., Slade, S.E., Thalassinos, K., Bateman, R.H., Bowers, M.T., Scrivens, J.H., *Int. J. Mass Spectrom.*, 2007, **261**, 1.

43. Giles, K., Wildgoose, J.L., Langridge, D.J., Campuzano, I., *Int. J. Mass Spectrom.*, 2010, **298**, 10.

44. Shvartsburg, A.A., Smith, R.D., *Anal. Chem.*, 2008, **80**, 9689.

45. Gorshkov, M.P., USSR Inventers Certificate No. 966583, 1982.

46. Buryakov, I.A., Krylov, E.V., Nazarov, E.G., Rasulev, U.K., *Int. J. Mass Spectrom. Ion Proc.*, 1993, **128**, 143.

47. Gruevremont, R., *J. Chromatogr. A.*, 2004, **1058,** 3.

48. Brown, L.J., Toutoungi, D.E., Devenport, N.A., Reynolds, J.C., Kaur-Atwal, G., Boyle, P., Creaser, C.S., *Anal. Chem.*, 2010, **82,** 9827.

49. Brown, L.J., Creaser, C.S., *Current Analytical Chemistry*, 2012, **8**, No.4.

50. Reynolds, J.C., Brown, L.J., Smith, R., Harry, E.L., Creaser, C.S., Focus on MS and spectroscopy.

51. Staubs, A.E., Matyjaszczyk, M.S., *IEEE Conference on Technologies for Homeland Security*, 2008, **1, 2,** 199.

52. McDaniel, E.W., Martin, D.W., Barnes, W.S., *Rev. Sci. Instrum,* 1962, **33**, 2.

53. McAfee, K.B.Jr, Sipler, D.P., Edelson, D., *Phys. Rev.,* 1967, **160,** 130.

54. Edelson, D., Morrison, J.A., McKnight, L.G., Sipler, D.P., *Phys. Rev.,* 1967, **164**, 71.

55. Young, C.E., Edelson, D., Falconer, W.E., *J. Chem. Phys.,* 1970, **53**, 4295.

56. Albritton, D.L., Miller, T.M., Martin, D.W., McDaniel, E.W., *Phys. Rev.,* 1968, **171**, 94.

57. McDaniel. E.W., *J. Chem. Phys.*, 1970, **52**, 3931.

58. McCullough B J, Kalapothakis J, Eastwood H, Kemper P, MacMillan D, Taylor K, Dorin J, Barran PE, *Anal Chem*., 2008, **80**, 6336.

59. Scarff, C.A., Thalassinos, K., Hilton G.R., and Scrivens, J.H., *Rapid Comm. Mass Spectrom*., 2008, **22**, 3297-3304.

60. Thalassinos, K., Grabenaur, M., Slade, S.E., Hilton, G.R., Bowers, M.T., Scrivens, J.H., *Anal. Chem.,* 2009, **81**, 248.

61. Salbo, R., Bush, M.F., Naver, H., Campuzano, I.,Robinson, C.V., Pettersson, I., Jørgensen, T.J.D., Haselmann, K. F., *Rapid Comm. Mass Spectrom.,* 2012, **26**, 1181.

62. Michaelevski, I., Eisenstein, M., Sharon, M., *Anal. Chem.*, 2010, **82**, 9484.

63. Atmanene, C., Petiot-Bécard, S., Zeyer, D., Dorsselaer, A.V., Hannah, V.V., Sanlier-Cianférani, S., *Anal. Chem*, 2012, **84**, 4703.

64. Cuyckens, F., Wassvik, C., Mortishire-Smith, R.J., Tresadern, G., Campuzano, I., Claereboudt, J., *Rapid Commun. Mass Spectrom.*, 2011, **25**, 3497.

65. Campuzano I, Bush MF, Robinson CV, Beumont C, Richardson K, Kim H, Kim HI, *Anal. Chem.*, 2012, **84**, 1026.

66. Williams JP, Bugarcic T, Habtemariam A, Giles K, Campuzano I, Rodger PM and Sadler PJ, *J. Am. Chem. Soc. Mass Spectrom.* 2009, **20**, 1119.

67. Williams JP, Lough JA, Campuzano I, Richardson K and Sadler PJ, *Rapid Comm. Mass Spectrom.*, 2009, **23**, 3563.

68. Waters Synapt G1 Instrument manual.

69. Brown, L.J., Smith R.W., Toutoungi, D.E., Reynolds, J.C., Bristow, A.W.T., Ray, A., Sage, A., Wilson, I.D., Weston, D.J., Boyle, P., Creaser, C.S., *Anal. Chem.*, 2012, **84,** 4095.

70. Berant, Z., Karpas, Z., *J. Am. Chem. Soc.*, 1989, **111**, 3819.

71. Laphorn, C., Pullen F., Chowdhry, B. Z., *Mass Spectrom. Rev*., 2013, **32**, 43.

72. Covey, T., Douglas, D.J., *J. Am. Soc. Mass Spectrom.*, 1993, **4**, 616.

73. Smith, D.P., Knapman, T.W., Campuzano, I., Malham, R.W., Berryman, J.T., Radford, S.E., Ashcroft, A.E., *Eur. J. Mass. Spectrom*., 2009, **15**, 113.

74. http://www2.warwick.ac.uk/fac/sci/lifesci/research/jscrivens/people/konstantinos_thalassinos/t-wave/synapt_calibration-_january_2008.pdf, Date accessed March 2013.

75. Valentine, S.J., Conterman, A.E., Clemmer, D.E., *J. Am. Chem. Soc. Mass Spectrom.*, 1999, **10**, 1188.

76. www.indiana.edu/~nano/Software/mobcal.txt, Date accessed November 2012.

77. Von Helden G, Hsu MT, Gotts N, Bowers MT, *J. Phys. Chem.*, 1993, **97**, 8182.

78. Shvartsburg AA, Jarrold MF, *Chem Phys Lett*., 1996, **261**, 86.

79. Mesleh MF, Hunter JM, Shvartsburg AA, Schatz GC, Jarrold M F, *J. Phys. Chem.*, 1996, **100**, 16082.

80. Knapman TW, Berryman JT, Campuzano I, Harris SA and Ashcroft AE, *Int. J. Mass Spectrom.*, 2010, **298**, 17.

81. Reid Asbury, G., Hill, H.H.Jr., *Anal. Chem.*, 2000, **72,** 580.

82. Howdle, M.D., Eckers, C., Laures, A.M.-F., Creaser, C.S., *Int. J. Mass Spectrom.*, 2010, **298**, 72.

83. Matz, L.M., Hill, H.H.Jr., Beegle, L.W., Kanik, I., *J. Am. Chem. Soc. Mass Spectrom.*, 2002, **13**, 300.

84. Bush, M.F., Campuzano, I.D.G., Robinson, C.V., *Anal. Chem.*, 2012, **84**, 7124.

85. Morsa, D., Gabelica, V., De Pauw, E., *Anal. Chem.*, 2011, **83**, 5775.

86. Merenbloom, S.I., Flick, T.G., Williams, E.R., *J. Am. Soc. Mass Spectrom.*, 2012, **23**, 553.

87. Tewari, J., Dixit, V., Malik, K., *Sensors and Actuators B: Chemical*, 2010, **144**, 104.

88. Hammond, J., Moffat, A.C., Jee, R.D., Kellam, B., *Anal. Commun.*, 1999, **36**, 127.

89. Gibson, S.E., Hardwick, D.J., Haycock, P.R., Kaufman, K.A.C., Miyazaki, A., Tozer, M.J., White, A.J.P., *Chem. Eur. J.*, 2007, **13**, 7099.

90. Radhakrishna, T., Screenivas Rao, D., Om Reddy, G., *J. Pharm. Biomed. Anal.*, 2001, **26**, 617.

91. Reactive Intermediates MS Investigations in Solution, 2010 WILEY-VCH Verlag GmbH & Co. KGaA, Ed. L. S. Santos.

92. Katta, V., Chowdhury, S.K., Chait, B.T., *J. Am. Chem. Soc.*, 1990, **112,** 5348.

93. Speranza, M., Sparapani, C., *Radiochim. Acta*, 1981, **28**, 87.

94. Eberlin, M.N., Cooks, R.G., *J. Am. Chem. Soc.*, 1993, **115**, 9226.

95. Eberlin, M.N., *Int. J. Mass Spectrom.*, 2004, **235**, 263.

96. Johlman, C.L., Ijames, C.F., Wolkins, C.L., Morton, T.H., *J. Org. Chem.*, 1983, **48**, 2628.

97. Lum, R.C., Grabowski, J.J., *J. Am. Chem. Soc.*, 1993, **115**, 7823.

98. Hinderling, C., Adlhart, C., Chen, P., *Angew. Chem. Int. Ed.*, 1998, **37**, 2685.

99. Adlhart, C., Hinderling, C., Baumann, H., Chen, P., *J. Am. Chem. Soc.*, 2000, **122,** 8204.

100. Adlhart, C., Chen, P., *Helv. Chim. Acta*, 2003, **86,** 941.

101. Adlhart, C., Volland, M.A.O., Hofmann, P., Chen, P., *Helv. Chim. Acta*, 2000, **83,** 3306.

102. Sabino, A.A., Machado, A.H.L., Correia, C.R.D., Eberlin, M.N., *Angew. Chem. Int. Ed.*, 2004, **43,** 2514.

103. Santos, L.S., Rosso, G.B., Pilli, R.A., Eberlin, M.N., *J. Org. Chem.*, 2007, **72,** 5809.

104. Aliprantis, A.O., Canary, J.W., *J. Am. Chem. Soc.*, 1994, **116,** 6985.

105. Fümier, S., Griep-Raming, J., Hayen, A., Metzger, J.O., *Chem. Eur. J.*, 2005, **11**, 5545.

106. Meyer, S., Koch, R., Metzger, J.O., *Angew. Chem. Int. Ed.*, 2003, **42**, 4700.

107. Meyer, S., Metzger, J.O., *Analytical and bioanalytical Chemistry*, 2003, **377**, 1108.

108. Wilson, D., Konermann, L., *Anal. Chem.*, 2003, **75**, 6408.

109. Emmert, G.L., Geme, G., Brown, M.A., Simone, P.S., *Anal. Chim. Acta*, 2009, **656**, 1.

110. Eiceman, G.A., *Trend Anal. Chem.*, 2002, **21,** 259.

111. Vautz, W., Mauntz, W., Engell, S., Baumbach, J.I., *Macromol. React. Eng.*, 2009, **3**, 85.

112. Kolehmainen, M., *Anal. Chim. Acta*, 2003, **484**, 93.

113. Roscioli, K. M., Zhang, X., Li, S. X., Goetz, G. H., Cheng, G., Zhang, Z., Siems, W. F., Hill, H. H. Jr., *Int. J. Mass Spectrom*., 2013, **336** 27.

114. Harry, E.L., Bristow, A.W.T., Wilson, I.D., Creaser, C.S., *Analyst*, 2011, **136**, 1728.

CHAPTER 2

STRUCTURAL STUDIES OF METAL LIGAND COMPLEXES BY ION MOBILITY-MASS SPECTROMETRY

2.1 INTRODUCTION

The drift velocity (v_d) of an ion in the presence of an electric field (E) and a buffer gas is dependent on the mobility (K), of the ion as described in Chapter 1, Section 1.2. In a linear DTIMS drift cell with a static field, the collision cross section (CCS) of an ion can be determined directly from the ion mobility using the Mason-Schamp equation **(Eqn. 1.16**).

Ion mobility hyphenated with mass spectrometry (IM-MS) provides added specificity for analysis of target analytes using DTIMS. In recent years, travelling wave IM-MS (TWIMS)[2] has also been used to determine CCS.[3-11] The principles of TWIMS have been described in more detail in Section 1.2 However, in summary, the drift cell contains paired electrodes that create a pulsed voltage which carries the ions through the drift cell as a travelling wave.

In a TWIMS drift tube the relationship between drift time and mobility is non-linear and therefore standards with known CCS, that have been previously determined using a linear DTIMS drift cell, are needed to calibrate the system. A graph is plotted of known CCS modified to account for reduced mass and charge, against effective drift time and from this the CCS of an analyte can be determined. Calibrants have included peptides[11-13], tetraalkylammonium halides (TAAHs)[5], and pharmaceutical compounds[5] with structures that are usually different to that of the analyte ion under investigation. There have been several reports of this approach to TWIMS CCS measurements of metabolites,[4,5] proteins and peptides,[6-10] arenes and adamantanes, and other small molecules analysed in helium and nitrogen drift gases[11]. The experimentally determined CCS for the arenes were similar for both drift gases indicating low polarisability effects between the analytes and drift gas as a result of the rigidness and low functionality of

these molecules. However, this is not the case for most ions, including the salen ligands and complexes discussed in this chapter.

The study of metal containing ions by IM-MS has been reported using linear drift tubes and TWIMS. The CCS of biological molecules binding small metals such as the alkali metals[14-17] as well as transition metals,[18-23] have been widely studied. The CCS of cationised polystyrene with Li^+, Na^+, Cu^+ and Ag^+ have also been reported.[24] In contrast, little work has been carried out on small non-biological metal-ligand complexes containing transition metals. Ruthenium anti-cancer complexes have been studied and their CCS determined using TWIMS-MS.[12,13]

Experimentally measured CCS have been compared to theoretical values calculated from x-ray structures and molecular models using MOBCAL[25] projection approximation, (PA), exact hard sphere scattering, (EHSS) and trajectory, (TM) methods, and a Waters CCS calculator[13] described in Section 1.4. The measured CCS for the ruthenium complexes[12] showed good agreement with the PA and TM approximations, however, the EHSS method overestimated the CCS. The smallest of the ruthenium complex showed good correlation with the PA, TM and EHSS methods. The Waters algorithm was also used to calculate the CCS using x-ray coordinates producing results similar to those obtained using MOBCAL, modelled structures and the experimental data. This suggests that the CCS obtained from x-ray data may provide a good representation of the structures of metal complexes in the gas-phase present in the drift cell.

2.2 AIMS AND OBJECTIVES

In this chapter, the analysis of three salen ligands and their metal-ligand complexes of copper and zinc using IM-MS is reported. The aims were to:-

- Analyse a series of salen ligands and their metal-ligand complexes using ion-mobility mass spectrometry under optimised conditions.
- Develop and optimise experimental conditions to analyse a set of peptide and tetraalkyl ammonium halide calibrants for the measurement of CCS by TWIMS.
- Determine the CCS of the salen ligands and metal-ligand complexes using TWIMS and static field DTIMS.
- Compare TWIMS CCS measurements with DTIMS data.
- Compare the experimental CCS data to CCS determined from model structures and X-ray coordinates.

2.3 EXPERIMENTAL

2.3.1 Materials

HPLC grade methanol, water and the peptide standards; $(Glycine)_2$, $(Alanine)_3$, $(Alanine)_5$, $(Lysine)_4$, $(Phenylalanine)_4$, $(Phenylalanine)_5$ were purchased from Fisher Scientific (Loughborough, UK). Lutidine and the following (TAAHs): tetraethylammonium bromide, tetrapropylammonium iodide, tetrabutylammonium iodide, tetrahexylammonium iodide, tetraoctylammonium bromide, tetradodecylammonium bromide were obtained from Sigma-Aldrich (Gillingham, UK) and tetrapentylammonium bromide, tetraheptylammonium bromide were obtained from Fisher Scientific (Loughborough, UK).

2.3.2 Ligand synthesis

Ligand 1: trans-1,2-diaminecyclohexane (0.49 g, 0.0043 mol) was weighed in a 25 mL round-bottom flask and dissolved in methanol (2 mL). Salicylaldehyde (1 g, 0.0081 mol) was added. The mixture was stirred for 1 hr. The yellow precipitate formed was filtered and then weighed and placed in a vial. It was then recrystalised from hot methanol.

Ligand 2: phenylenediamine (0.51g, 0.0046 mol) was weighed in a 25 mL round-bottom flask and dissolved in methanol (5.5 mL). Salicylaldehyde (1 g, 0.0081 mol) in methanol (0.7 mL) was added to the solution. The mixture was stirred for 2 hr 15 min. The solution turned yellow after 3 min of stirring. The yellow precipitate formed was filtered and placed in a desiccator for 1 hr and then weighed and placed in a vial. It was then recrystalised from hot methanol.

Ligand 3: ethylenediamine (0.57 g, 0.0095 mol) was weighed in a 25 mL round-bottom flask and dissolved in methanol (15 mL). Salicylaldehyde (1.78 g, 0.0146 mol) was

added and the solution stirred for 1 hr 30 min. The yellow precipitate formed was filtered and recrystalised from hot methanol.

2.3.3 NMR and CHN Data

Ligand 1 - δ_H (400 MHz; $CDCl_3$) 1.43-1.99 (10H, m, ArH) 6.77-7.26 (8H, m, ArH), 8.26 (2H, s, 2 x NCH), 13.33 (2H, s, 2 x OH). $C_{20}H_{22}N_2O_2$ (322.4): calcd. C 74.51, H 6.88 N 8.69; found C 72.14, H 6.58, N 8.46.

Ligand 2 - δ_H (400 MHz; $CDCl_3$) 6.85-7.40 (12H, m, ArH), 8.65 (2H, s, 2 x NCH), 13.05 (2H, s, 2 x OH). $C_{20}H_{16}N_2O_2$ (316.4) calcd. C 75.93, H 5.10 N 8.86; found C 75.86, H 5.06, N 8.89.

Ligand 3 - δ_H (400 MHz; $CDCl_3$) 3.947 (4H, s, 2 x CH_2) 6.84-7.32 (8H, m, ArH), 8.36 (2H, s, 2 x NCH), 13.21 (2H, s, 2 x OH). $C_{16}H_{16}N_2O_2$ (268.3) calcd. C 71.62, H 6.01 N 10.44; found C 71.78, H 6.07, N 10.49.

2.3.4 Sample Preparation

The ligands and metal-ligand complexes were prepared as 1 nmol/μL solutions in 90:10 methanol:water. Ligands 1, 2 and 3 and their copper complexes were diluted (1:10) prior to analysis. The ligand:zinc complexes were diluted; L1:Zn (1:10), L2:Zn (1:20), L3:Zn (1:5) prior to analysis.

2.3.5 Ion mobility - Mass Spectrometry

TWIMS analyses were performed using a Waters Synapt HDMS spectrometer (Waters Corporation, Manchester, UK), with a hybrid quadrupole/ion mobility/orthogonal acceleration time-of-flight (oa-ToF) geometry controlled by Waters MassLynx operating sofware. Samples were introduced into the electrospray ionisation source via direct infusion methanol:water (90:10) at a flow rate of 5 μL/min. The source and

desolvation temperatures were set to 120°C and 250°C, respectively, gas flow (N_2) rates were set to 20 L/h and 600 L/h respectively. The tri-wave drift cell conditions were set at 30 mL/min drift gas (N_2) with a ramped travelling wave height of 8-18 V and a velocity of 300 m/s. The acquired IM-MS data were processed using DriftScope and MassLynx 4.1 (Waters, Manchester, UK). CCS were determined using peptide and TAAH standards of known CCS in helium. The calibration standards were analysed by IM-MS and used to produce a calibration curve after the data was corrected for the non-linear electric field in the TWIMS system. The CCS of the free ligands and metal complexes were then determined from the graph using **Eqn.2.1**[26] which is discussed in more detail in Section 1.4.

$$\Omega'_{(\mathrm{T-wave})} = {t_d}''^{\mathrm{B}} \times \mathrm{A} \times \mathrm{q} \times \left(\frac{1}{\mathrm{M_{ion}}} \times \frac{1}{\mathrm{M_{gas}}}\right)^{1/2} \qquad \textbf{Equation 2. 1}$$

where Ω' is the determined collision cross section, q is the charge, M is the mass, parameter B compensates for the non-linear effect of the TWIMS system and parameter A for the temperature, pressure and electric field conditions and t_d" (μs) is the effective drift time corrected to account for instrument offsets calculated using **Eqn. 2.2**.

$$t_d'' = t_d' - \sqrt{\left(\frac{m/z}{1000}\right)} \times 85 \qquad \textbf{Equation 2. 2}$$

where t_d' (μs) corrects for the offset in the drift cell using **Eqn. 2.3**:

$$t_d' = t_d - 920 \qquad \textbf{Equation 2. 3}$$

DTIMS analyses were performed in helium using an in-house modified commercial quadrupole time-of-flight instrument (Micromass UK Ltd., Manchester, UK) in the Department of Chemistry at the University of Edinburgh (courtesy of Professor Perdita

Barran). The QTOF was modified by the addition of a chamber containing a linear, 5.1 cm copper drift cell and ancillary ion optics.[27] Ions were produced by positive nESI ionisation using a Z-spray source, within a spray voltage range of 1.2 - 1.8kV and a source temperature of 80^{o}C. Source pressure was optimized for signal transmission. nESI spray tips were prepared in-house at the University of Edinburgh with a micropipette puller (Fleming/Brown model P-97, Sutter Instruments Co., USA) using 4" 1.2 mm thin wall glass capillaries (World Precision Instruments, Inc., USA). The drift cell was filled with helium buffer gas (CP grade, 99.999% purity, BOC Specialty Gases Ltd, Guildford, UK) and the pressure was measured using a Baratron (MKS Instruments). The temperature of the drift cell was closely monitored and recorded. The electric field across the cell was varied from 12 - 3 V.cm^{-1}. Ion arrival time distributions were recorded by synchronisation of the release of ions into the drift cell with mass spectral acquisition. The arrival time of ions was measured at 8 different voltages from 60 V-15 V across the 5.1 cm long drift cell. The ratio of the electric field strength (E) to buffer gas density value (N) varies over this range from 9.96 – 2.50 × 10^{-17} V/cm^2 for singly charged ions drifting in helium at 300K. The plot of arrival time versus P/V (pressure/voltage) for each measurement, was fitted to a straight line with a linear regression R^2 coefficient of 1.00, indicating that all measurements were taking place under low field conditions where **Eqn. 1.16** is valid.

The mobility of the ion of interest was obtained from the plot of average arrival time versus pressure/temperature and from this the rotationally-averaged CCS for each resolvable species at a given charge state were obtained using **Eqn. 1.16.**

2.3.6 Theoretical determination of CCS

MOBCAL was used to calculate theoretical CCS by applying three algorithms: the projection approximation (PA),[28] the exact hard sphere scattering method (EHSS) [29] and the trajectory method (TM)[30] described in detail in Section 1.4. Molecular structures were taken either from X-ray crystallographic data (neutral ligands and complexes) from the CrystalWeb database[31] or optimized using a Density Functional Theory (DFT) based method for the protonated ligands and complexes. DFT optimisation was carried out by Carles Bo and Fernando Castro-Gómez from the Institute of Chemical Research of Catalonia (ICIQ), Tarragona, Spain. Helium parameters were assumed when carrying out MOBCAL calculations. For H, C, N, and O atoms, the 12-6 default parameters in MOBCAL[30] were considered as well as recently developed sets from Siu *et al.*[32] and from Campuzano *et al.*[5] For Cu and Zn atoms, the 12-6 parameters for silicon were used. For all the atoms, charge-induced dipole interactions were included from Mulliken atomic charges computed at the DFT level.

DFT calculations were performed using the GAUSSIAN09[33] package within B3LYP formalism. The standard 6-31G(d,p) basis set was used to describe the H, C, N and O atoms. The relativistic effective core pseudo potential LANL2DZ was used, together with its associated basis set, for Zn and Cu. Full geometry optimisations were performed. The nature of the stationary points encountered has been characterised by harmonic vibrational frequencies analysis. The Fortran77 MOBCAL code was compiled and optimised using the Portland PGFORTRAN Compiler. Some scripts were built for running calculations in batches.

2.4 RESULTS AND DISCUSSION

2.4.1 Analysis of Ligand and metal complexes

Drift tube ion mobility-mass spectrometry (DTIMS-MS) and TWIMS-MS have been used to determine CCS for three salen ligands, L1-L3 (**Figure 2.1**), and their metal complexes with copper (II) and zinc (II) under low field conditions. The ligands and metal complexes form singly charged ions of the type $[Metal^{2+}+L\text{-}H^{+})]^{+}$ in the electrospray (ESI) source, equivalent to a protonated version of the neutral metal complex with the proton located on a nitrogen or oxygen atom. Modelling studies revealed the most stable structure to be those with the proton on the most basic oxygen site.

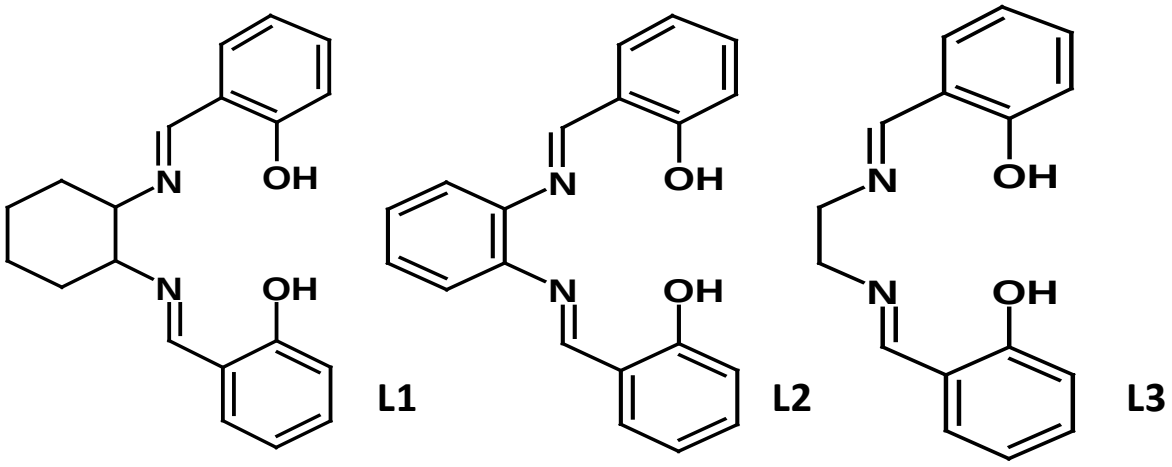

Figure 2. 1 Chemical structures of ligand 1, ligand 2 and ligand 3

Peptide or TAAH standards were used to calibrate the TWIMS drift tube data from which the analyte CCS were determined. The TWIMS ion mobility spectra for L1, L1Cu and L1Zn are shown in **Figure 2.2**.

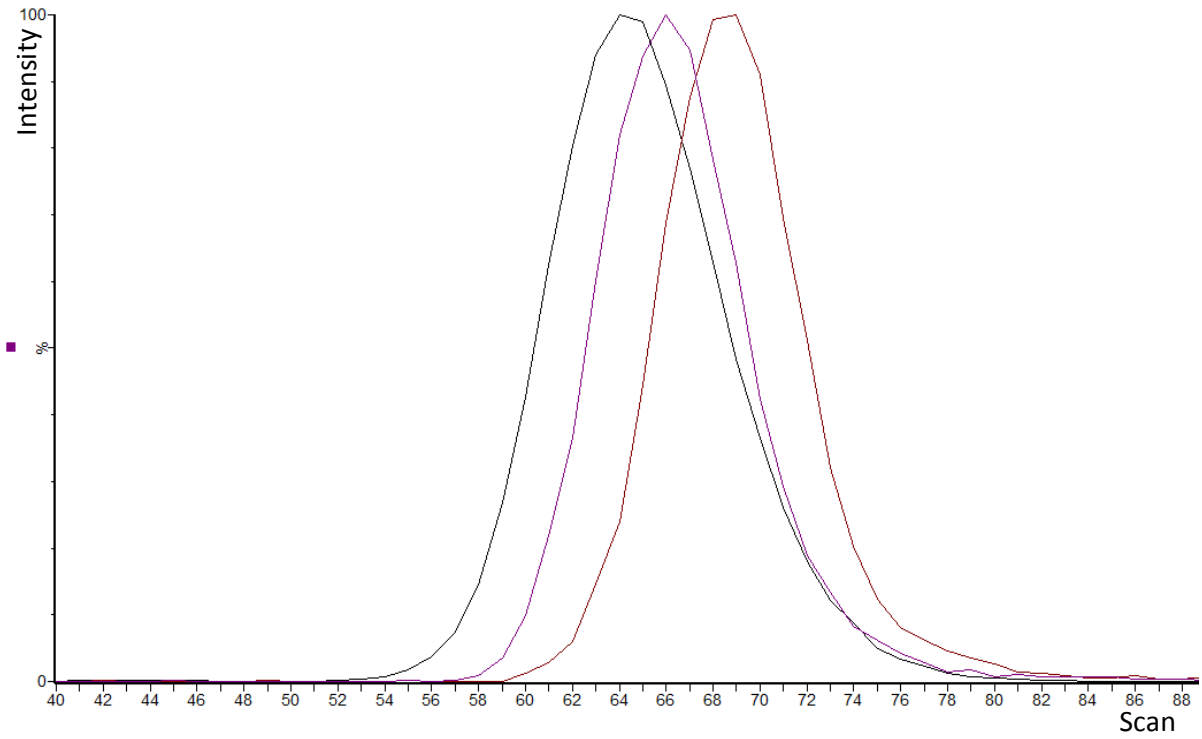

Figure 2. 2 TWIMS ion mobility spectra of ligand L1 (left, *m/z* 323.176) and the L1Cu (centre, *m/z* 384.089) and L1Zn (right, *m/z* 385.089) metal complexes.

The free ligand and metal complexes may be distinguished from each other with ligand 1 having the shortest drift time, followed by the copper complex and then the zinc complex.

Six peptide standards (**Table 2.1**) were chosen from the Clemmer database[34] and analysed by TWIMS-MS to create a calibration curve from which the CCS of target metal-ligand complexes could be determined. The ratio of the peptides was optimised to produce a spectrum where each peptide had a similar peak intensity, from which the ion mobility and CCS could be reproducibly determined.

Table 2. 1 **The six peptides used to calibrate the TWIMS drift cell.**

Charge State	Analyte	*m/z*	Published CCS in He[34]
1	$(Gly)_2$	133.06	62.0
1	$(Ala)_3$	232.13	89.0
1	$(Ala)_5$	374.20	115.0
1	$(Lys)_4$	531.40	157.8
1	$(Phe)_4$	607.29	168.6
1	$(Phe)_5$	754.36	200.0

The peptides were analysed in nitrogen under the experimental conditions described in Section 2.3.5. The selected ion responses (SIR) for the protonated peptides were extracted from the total ion response (TIR) (**Figure 2.3**). A sharp symmetric peak was observed for each peptide ion. The ion drift times (t_d) were calculated by multiplying the scan (bin) number at the peak apex for each peptide by the TOF scan time (45 μs/scan).

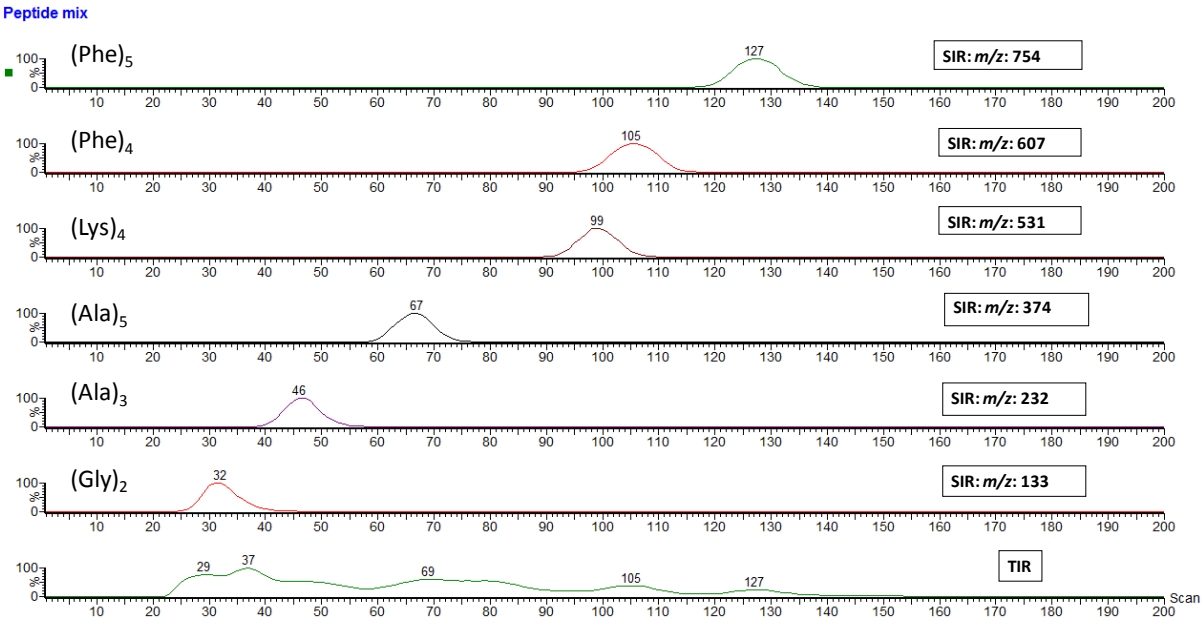

Figure 2. 3 TWIMS ion mobility spectra observed for the total ion response (TIR) and select ion responses (SIR) of the six peptides.

Calibration graphs were created for the peptide standards using power and linear trendlines. Examples are shown in **Figure 2.4**.

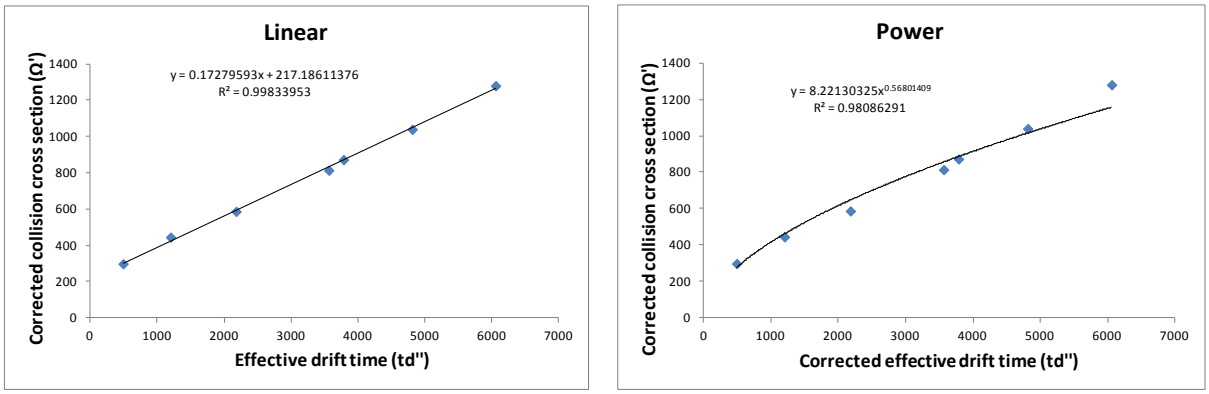

Figure 2. 4 Linear and power plots of corrected collision cross section (Ω'/Å^2) against effective drift time (td"/μs) for the peptide standards.

The linear trendline produces an R^2 value of 0.998 and the power trendline an R^2 of 0.980. The reason for this variability is that the power plot forces the intercept through zero resulting in a poor fit to the data points. The linear fitting is not affected by this and is viable for any analyte with a drift time and CCS falling within the range of the CCS of the standards analysed. CCS for ligand 1 and its copper and zinc complexes are

shown in **Table 2.2**. CCS were determined by correcting t_d for the offset in the drift cell (920 μs) and the time the ions spend outside the drift cell before reaching the detector (**Eqn. 2.2-2.3**). In all cases the power plot gave a larger CCS than the linear data because of the poor fit. It was concluded that the power fitting will only work under a very specific set of TWIMS cell conditions and therefore the data presented in this chapter was determined using only linear calibration data. This point will be discussed further in Chapter 3 where data was obtained at a variety of wave heights.

Table 2. 2 Experimental CCS determined using peptide standards using power and linear calibration graphs.

Compounds	CCS/ $Å^2$ (Linear)	CCS/ $Å^2$ (Power)
Ligand 1	112	121
L1Cu	114	123
L1Zn	115	124

The determination of CCS by TWIMS was also carried out using lutidine and tetraalkylammonium halide (TAAH) calibrants. TAAHs are ammonium ions with variable length alkyl chains (R_4N^+, $R=C_nH_{2n+1}$, n=2-8) (**Table 2.3**). They were analysed under similar conditions to the peptides and processed in the same way. The ion mobility spectra (TIR and SIRs) are shown in **Figure 2.5.**

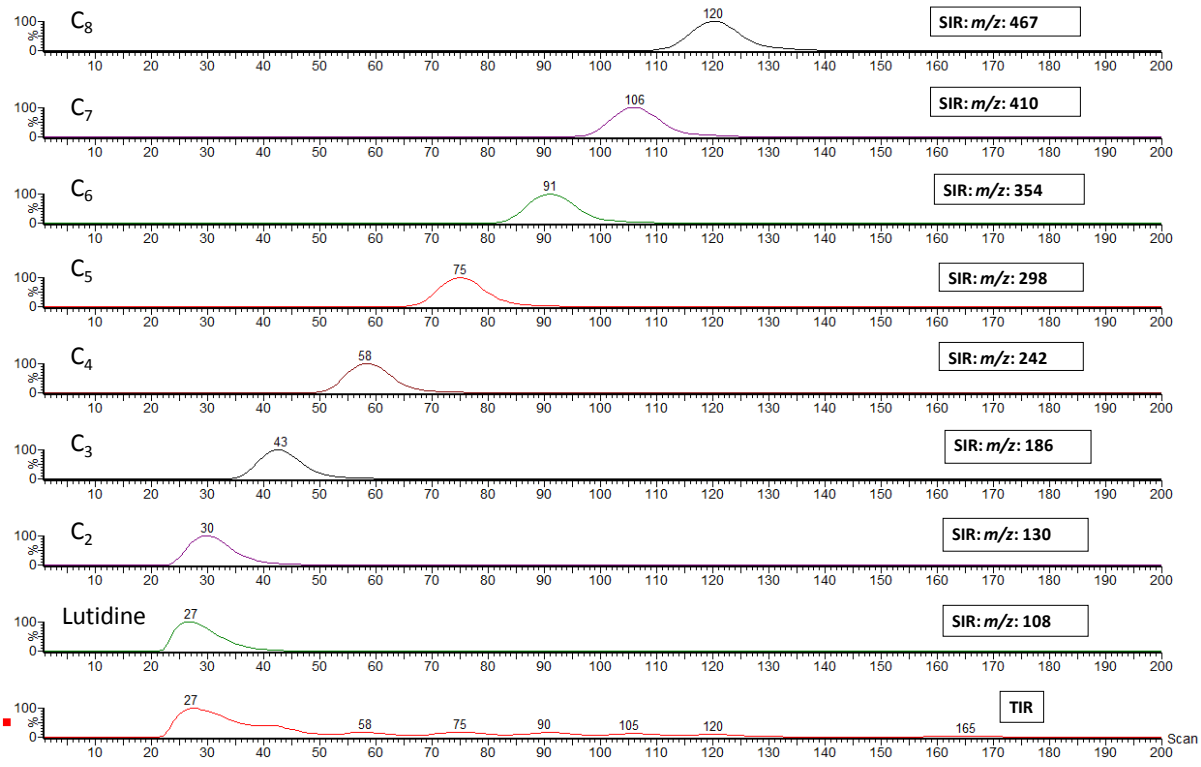

Figure 2. 5 TWIMS ion mobility spectra for the TIR and SIRs of the TAAH standards.

The CCS of lutidine and the TAAH standards (C_2-C_8) were first determined at the University of Edinburgh using the MOQTOF mass spectrometer to obtain the 'known' values which may then used to calibrate the TWIMS drift cell. The instrument and conditions are described in Section 2.3.5, however, the important point to note is that the instrument contains a linear drift cell. The results obtained were consistent with results reported in the literature[5,32] (**Table 2.3**).

Table 2. 3 TAAHs and Lutidine data taken from the literature and CCS measured in Edinburgh used for CCS calibrants in this study.

Compounds	Edinburgh CCS/Å^2		Iain C[5] CCS/Å^2		Chi-Kit S[32] CCS/Å^2
	He	**N2**	**He**	**N2**	**He**
Lutidine	55	112			
C_2	64	121	66	122	64
C_3	88	144	89	144	87
C_4	112	162	111	166	109
C_5	137	187	134	190	132
C_6	160	211	155	214	154
C_7	178	235	175	237	174
C_8	202	259	194	258	194

The CCS values for the TAAH determined in helium by DTIMS were then used to calibrate the TWIMS cell and determine the CCS of the ligand and metal-ligand complexes measured in nitrogen. The calibration graphs show the same trend as for the peptides with the linear trendline producing an R^2 of 0.997 and the power trendline an R^2 0.985 (**Figure 2.6**). The linear calibration data was therefore used to determine the CCS of the analytes.

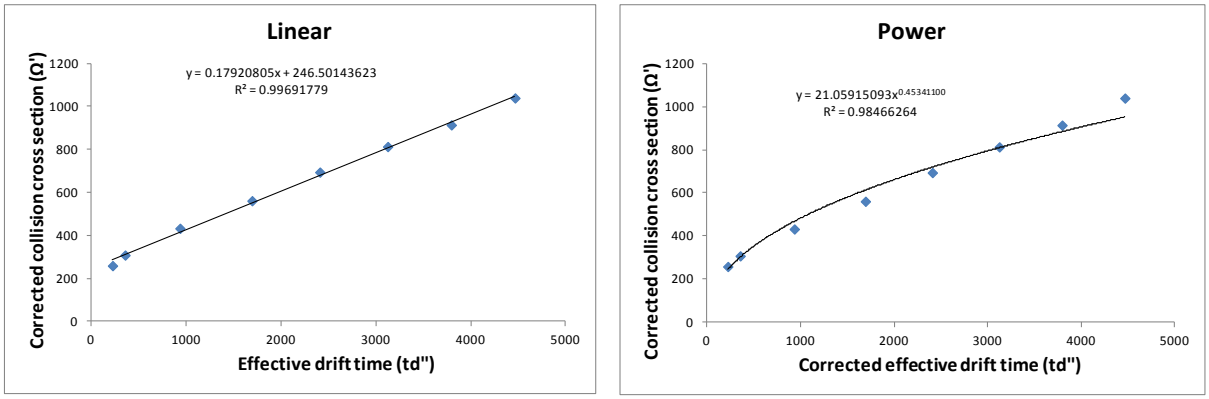

Figure 2. 6 Linear and power plots of corrected collision cross section (Ω'/Å^2) against effective drift time (td"/μs) for the TAAH standards.

2.4.2 CCS Data from DTIMS and TWIMS Measurements

The CCS for the ligands and complexes determined using DTIMS and TWIMS are given in **Table 2.4**. The inter- and intra-day reproducibility (%RSD) of the TWIMS measurements were 1.1% and 0.7%, respectively.

Table 2. 4 Collision cross sections determined by DTIMS and TWIMS using TAAH and peptide calibration standards.

Compound	*m/z*	Experimental CCS/Å^{2a}		
		TWIMS (TAAHs)	TWIMS (Peptides)	Drift tube
Ligand 1	323	119	112	109
Ligand 2	317	112	107	105
Ligand 3	269	103	97	94
L1Cu	384	120	114	109
L2Cu	378	115	108	104
L3Cu	330	102	97	94
L1Zn	385	122	115	110
L2Zn	379	118	110	106
L3Zn	331	104	98	97

[a] TWIMS data measured in nitrogen, DTIMS data measured in helium.

The CCS of the protonated ligands measured by TWIMS and DTIMS decrease in size in the order L1 > L2 > L3 (see **Table 2.4**). L1 has a trans conformation of the cyclohexane ring compared to the planar benzene ring giving it the largest CCS. Ligand 3 has a smaller CCS than ligands 1 and 2 due the absence of an aromatic or aliphatic ring. The CCS of the free ligands and the metal-ligand complexes increase in size in the order L, L:Cu < L:Zn, consistent with the slightly larger ionic radius of Zn(II) than Cu (II).

The CCS for the ligands and metal-ligand complexes from the TWIMS data, calibrated using the two sets of standards showed an average 6% difference. The CCS determined using the TAAH calibrants are systematically larger than the CCS obtained using peptide calibrants. The CCS measured by TWIMS were also larger than the DTIMS

CCS measurements; on average by 9% for the TAAH standards and 3% for the peptide standards. Campuzano *et al*.[5] reported a similar observation for CCS of betamethasone and dexamethasone measured in nitrogen using TWIMS and calibrated with a drug-like calibration mix. This suggests that the conditions in the TWIMS drift cell may generate larger CCS depending on the species being analysed and the calibration process.

The difference between the CCS measured by TWIMS, using TAAH and peptide calibrants, and DTIMS is most likely due to the use of standards with CCS determined in helium to calibrate measurements made in nitrogen in the TWIMS drift cell. This extrapolation provides an approximation of the CCS in helium, but does not fully correct for the compound dependent interaction of the polarisable nitrogen drift gas with the calibrants and the ligands and their metal complexes.[11-13,35] However, the TWIMS experimental CCS values closely reflect the DTIMS CCS measurements in helium. A further contributing factor may be ion heating in the TWIMS drift tube as a result of the RF ion confinement. Morsa *et al.*[36] used a TWIMS drift tube to investigate the effect of experimental TWIMS parameters on the effective temperature of an ion. They used *p*-methoxybenzyl pyridinium as a chemical thermometer and showed that the vibrational effective temperature ($T_{eff,vib}$) increases with increasing wave height and decreasing velocity and drift gas pressure. The heating effect is expected to be greater for smaller ions than larger ones as larger ions move slower. $T_{eff,vib}$ is also greater for ions in a nitrogen drift gas than a helium drift gas at lower ion velocities, although at higher velocities helium shows similar effects.[36] T_{eff} varies from ion to ion and therefore may be different for the ligands, their metal complexes, and the TAAH and peptide calibrants. If ion heating effects are not fully corrected by the calibration process, this may contribute to the variation between CCS determined using TWIMS with TAAH and peptide calibrants and the DTIMS data. T_{eff} may also affect ion structure and hence

CCS, although the significance of these changes are unknown.[36] The use of calibration standards clearly corrects partially, but not fully for all these factors. An additional effect that will have an influence on both forms of IMS is that of injection energy. Both apparatus, inject ions into a higher pressure region, this can cause conformational change which may be reflected in the measurements, and may be different for each set of calibrants. In this study, the peptide standards, which have very different functionality provide a better estimate of the CCS for the ligands and metal-ligand complexes determined by DTIMS than the TAAHs standards, which form a simple homologous series.

The X-ray structures of the ligands and their metal complexes were obtained from the Crystalweb crystal structure database, and the pdb files were input into the set of codes contained within MOBCAL in order to obtain theoretical CCS (**Table 2.5**) using all three MOBCAL methods (PA, EHSS and TM). There was generally good agreement between the PA and TM approximations, allowing for the reproducibility of the measurements. However, the EHSS method overestimates the CCS, which is consistent with previously reported data.[12,13] Experimental CCS determined by TWIMS using the peptide and TAAH standards show better correlation with both the PA and TM derived from the x-ray data, than with the DTIMS data, with the exception of the free ligands L2 and L3. It should be noted that the CCS derived from the x-ray data suggest that CCS L2 $\geqslant$ L1 > L3, which differs from the order observed experimentally. This may be due to protonation in the gas-phase restricting out of plane rotation of the phenol rings, which does not occur in the solid state. The DTIMS experimental data correlates poorly with both the PA and TM derived CCS from the x-ray structures, showing consistently smaller CCS radius. These observations suggest that CCS derived from x-ray

coordinates should be used with caution in structural studies of small ligands and metal-ligand complexes measured by IM-MS.

Table 2. 5 Theoretical collision cross sections calculated from X-ray and modelled structures using MOBCAL.

Compound	MOBCAL (He) X-ray CCS/Å^2			MOBCAL (He) Modelled CCS/Å^2		
	PA	EHSS	TM	PA	EHSS	TM
Ligand 1	115	123	116	120	128	117
Ligand 2	117	124	116	117	123	115
Ligand 3	110	115	106	106	112	105
L1Cu	116	122	114	121	128	118
L2Cu	113	117	110	118	123	115
L3Cu	105	108	101	107	112	105
L1Zn	118	124	118	122	129	119
L2Zn	113	117	114	119	124	115
L3Zn	103	107	101	108	113	106

The geometries of the ligands and their metal complexes were therefore modelled in their protonated gas-phase form at ICIQ, Tarragona, by computing the minimum energy isomer by DFT (**Appendix 2)**. MOBCAL was used to calculate the theoretical CCS from the modelled data (**Table 2.5**). The PA and TM CCS derived from the modelled data show reasonable agreement with those derived from the x-ray data. The modelled and x-ray results correlate better with the experimental data using the TAAH standards than the peptide standards and DTIMS data. This suggests that MOBCAL overestimates the CCS for these small ions.

MOBCAL was modified by optimising the parameters. Three sets of the 12-6 van der Waals potential parameters (epsilon and sigma) were considered: the default values included in MOBCAL[30] and the new sets developed by Siu et al.[32] and Campuzano et al.[5]. These new sets consider a larger diversity of ions (aminoacids and metal-ions) for optimising the van der Waals parameters. Theoretical CCS calculated using the modified parameter sets are shown in **Table 2.6**. The recalculated CCS showed good agreement between the PA and TM approximation for both sets of data. The TM and PA CCS data obtained using the Siu parameters on the x-ray coordinates are within 5 $Å^2$ of the DTIMS experimental data, which is at the upper end of the range for measurement uncertainty. The Campuzano TM optimised data set indicates a slight overestimation of the CCS with the calculated CCS displaying increased correlation with the peptide standard data.

Table 2. 6 **Theoretical collision cross sections calculated from X-ray and modelled structures using MOBCAL with Siu's and Campuzano's parameter sets.**

Compound	MOBCAL X-ray CCS/Å^2				MOBCAL Modelled CCS/Å^2			
	Siu			Campuzano	Siu			Campuzano
	PA	EHSS	TM	TM	PA	EHSS	TM	TM
Ligand 1	104	112	107	110	110	113	109	114
Ligand 2	107	112	107	112	107	111	106	113
Ligand 3	99	100	97	102	97	99	97	102
L1Cu	107	112	104	111	112	114	110	116
L2Cu	104	110	101	108	109	112	106	113
L3Cu	96	98	92	99	99	100	97	103
L1Zn	109	113	108	114	113	114	111	116
L2Zn	104	110	107	112	110	113	106	113
L3Zn	95	99	92	99	100	100	98	103

Figure 2.7 shows a comparison of the experimental data and the x-ray and modelled data using the Siu parameters, for the L1Cu complex. A comparison of the experimental CCS data against the modelled CCS data calculated using the new parameters displays excellent agreement between the DTIMS and the PA and TM data obtained using the Siu parameters, within on average ~3 Å^2. This illustrates the need for refinement of the methods used to calculate CCS from coordinate sets and highlights the sensitivity of this approach. The peptide data also correlates well with the Siu PA parameter data allowing for the slight (3%) overestimate for the TWIMS data using the peptide standards. There

is poorer correlation between the DTIMS and TWIMS experimental measurements and the TM results using the Campuzano parameters. The presented data demonstrates that the PA and TM calculations with the modified parameters for the modelled structures show better correlation with the experimental data for the ligands and complexes studied and that TWIMS CCS measurements using peptide standards may be correlated with calculated data for structural studies of low molecular weight metal complexes.

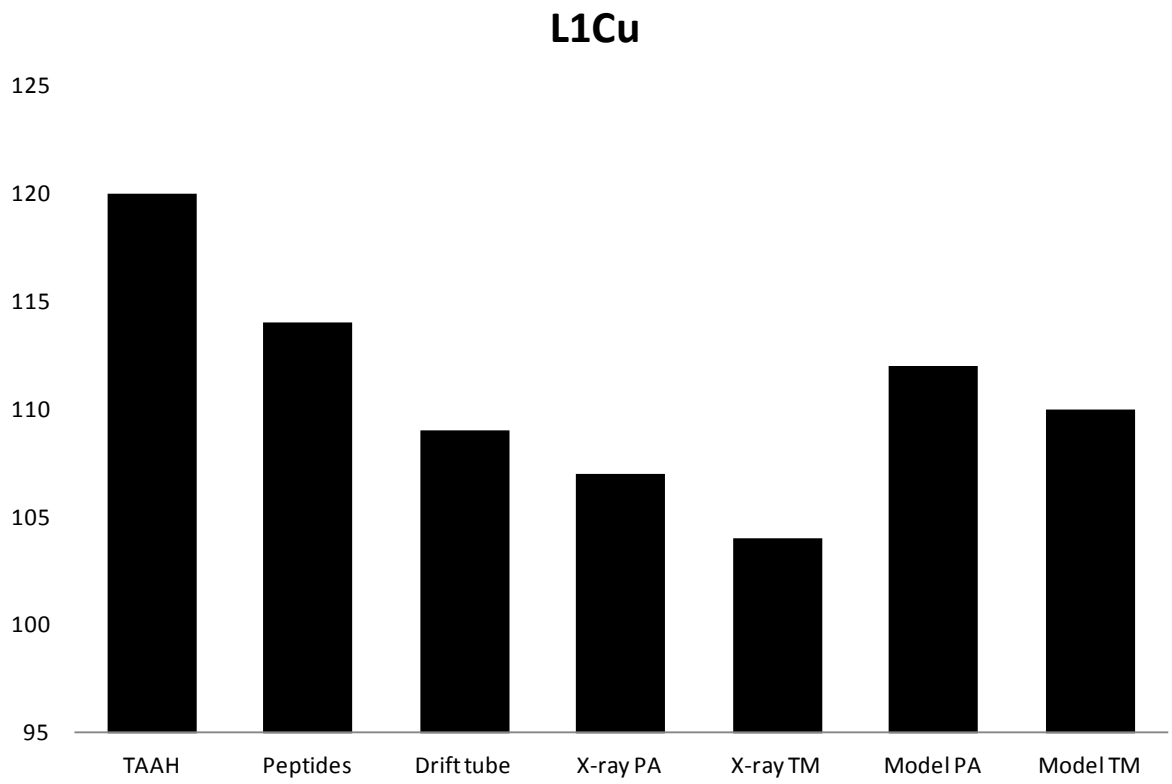

Table 2. 7 **A comparison between the experimental data from DTIMS and TWIMS and the theoretical data from X-ray and modelled structures using the Siu parameters for L1Cu complex.**

2.5 CONCLUSIONS

DTIMS and TWIMS have been used to determine the collision cross sections of ligand species (containing nitrogen and oxygen binding atoms) and their complexes with copper and zinc. TWIMS measurements were carried out in nitrogen, using TAAH and peptide calibration compounds, with reported helium-derived collision cross sections. Intra-day and inter-day reproducibility for the TWIMS collision cross sections gave % RSDs of less than 2%. TWIMS measurements gave larger collision cross sections than DTIMS in helium, by 9% using TAAH calibration and 3% using peptide calibration, indicating that peptide standards may be better for measurements of small ligands and their metal complexes. The experimental collision cross sections were compared with theoretical cross sections determined using modified MOBCAL calculations from molecular geometries derived from *in-silico* modelling and x-ray data. CCS data calculated from modelled structures showed a good correlation with experimental CCS measurements made by DTIMS in helium and TWIMS measurements made in nitrogen, when peptide calibrants were used for the TWIMS measurements.

2.7 CHAPTER TWO REFERENCES

1. Creaser, C.S., Bramwell, C.J., Noreen S., Hill, C.A., Thomas, C.L., *Analyst*, 2004, **129**, 984.
2. Giles, K., Pringle, S.D., Worthington, K.R., Little, D., Wildgoose, J.L., Bateman, R.H., *Rapid Comm. Mass. Spectrom*., 2004, **18**, 2401.
3. Scarff, C.A., Snelling, J.R., Knust, M.M., Wilkins, C.L., Scrivens, J.H., *J. Am. Chem. Soc*., 2012, **134**, 9193.
4. Cuyckens, F., Wassvik, C., Mortishire-Smith, R.J., Tresadern, G., Campuzano, I., Claereboudt, J., *Rapid Comm. Mass Spectrom*., 2011, **25**, 3497.
5. Campuzano, I., Bush, M.F., Robinson, C.V., Beumont, C., Richardson, K., Kim, H., Kim, H.I., *Anal. Chem.*, 2012, **84**, 1026.
6. Scarff, C.A., Thalassinos, K., Hilton, G.R., Scrivens, J.H., *Rapid Comm. Mass Spectrom*., 2008, **22**, 3297.
7. Thalassinos, K., Grabenaur, M., Slade, S.E., Hilton, G.R., Bowers, M.T., Scrivens, J.H., *Anal. Chem.* 2009, **81**, 248.
8. Salbo, R., Bush, M.F., Naver, H., Campuzano, I., Robinson, C.V., Pettersson, I., Jørgensen, T.J.D., Haselmann, K.F., (2012) *Rapid Comm. Mass Spectrom.*, 2012, **26**, 1181.
9. Michaelevski, I., Eisenstein, M., Sharon, M., *Anal Chem.*, 2010, **82**, 9484.
10. Atmanene, C., Petiot-Bécard, S., Zeyer, D., Dorsselaer, A.V., Hannah, V.V., Sanlier-Cianférani, S., *Anal. Chem*., 2012, **84**, 4703.
11. Knapman, T.W., Berryman, J.T., Campuzano, I., Harris, S.A., Ashcroft, A.E., *Int. J. Mass Spectrom*., 2010, **298**, 17.
12. Williams, J.P., Bugarcic, T., Habtemariam, A., Giles, K., Campuzano, I., Rodger, P.M., Sadler, P.J., *J. Am. Chem. Soc. Mass Spectrom*., 2009, **20**, 1119.

13. Williams, J.P., Lough. J.A., Campuzano, I., Richardson, K., Sadler, P.J., *Rapid Comm. Mass Spectrom.*, 2009, **23**, 3563.
14. Wyttenbach, T., Batka, J.J., Gidden, J., Bowers, M.T., *Int. J. Mass Spectrom.*, 1999, **193**, 143.
15. Wyttenbach, T., Witt, M., Bowers, M.T., *J. Am. Chem. Soc.*, 2000, **122**, 3458.
16. Clowers, B.H., Hill, Jr. H.H., *J. Mass Spectrom.*, 2006, **41**, 339.
17. Moision, R.M., Armentrout, P.B., *J. Phys. Chem. A*, 2006, **2**, 3933.
18. Taraszka, J.A., Li, J., Clemmer, D.E., *J. Phys. Chem. B*, 2000, **104**, 4545.
19. Leavell, M.D., Gaucher, S.P., Leary, J.A., Taraszka, J.A., Clemmer, D.E., *J. Am. Chem. Soc. Mass Spectrom.*, 2002, **13**, 284.
20. Baker, E.S., Manard, M.J., Gidden, J., Bowers, M.T., *J Phys Chem B*, 2005, **109**, 4808.
21. Wyttenbach, T., Liu, D.F., Bowers, M.T., *J. Am. Chem. Soc.*, 2008, **130**, 5993.
22. Berezovskaya, Y., Armstrong, C.T., Boyle, A.L., Porrini, M., Woolfson, D.N., Barran, P.E., *Chem. Commun.*, 2011, **47**, 412.
23. Chepelin, O., Ujma, J., Barran, P.E., Lusby, P.J., *Angew. Chem. Int.*, 2012, **51**, 4194.
24. Gidden, J., Bowers, M.T., Jackson, A.T., Scrivens, J.H., *J. Am. Chem. Soc.*, 2002, **13**, 499.
25. www.indiana.edu/~nano/Software/mobcal.txt.
26. Smith, D.P., Knapman, T.W., Campuzano, I., Malham, R.W., Berryman, J.T., Radford, S.E., Ashcroft, A.E., *Eur. J. Mass Spectrom.*, 2009, **15**, 113.
27. McCullough, B. J., Kalapothakis, J., Eastwood, H., Kemper, P., MacMillan, D., Taylor, K., Dorin, J., Barran, P.E., *Anal. Chem.*, 2008, **80**, 6336.

28. Von Helden, G., Hsu, M.T., Gotts, N., Bowers, M.T., *J. Phys. Chem*., 1993, **97**, 8182.
29. Shvartsburg, A.A., Jarrold, M.F., *Chem. Phys. Lett*., 1996, **261**, 86.
30. Mesleh, M.F., Hunter, J.M., Shvartsburg, A.A., Schatz, G.C., Jarrold, M.F., *J. Phys. Chem*., 1996, **100**, 16082.
31. http://cds.dl.ac.uk/cds/datasets/crys/cweb/cweb.html, Date accessed November 2009.
32. Siu, C., Guo, Y., Saminathan, I.S., Hopkinson, A.C., Siu, K.W.M., *J. Phys. Chem*., 2010, **114**, 1204.
33. Gaussian 09, Revision **A.1**, Frisch, M. J.; Trucks, G. W.; Schlegel, H. B.; Scuseria, G. E.; Robb, M. A.; Cheeseman, J. R.; Scalmani, G.; Barone, V.; Mennucci, B.; Petersson, G. A.; Nakatsuji, H.; Caricato, M.; Li, X.; Hratchian, H. P.; Izmaylov, A. F.; Bloino, J.; Zheng, G.; Sonnenberg, J. L.; Hada, M.; Ehara, M.; Toyota, K.; Fukuda, R.; Hasegawa, J.; Ishida, M.; Nakajima, T.; Honda, Y.; Kitao, O.; Nakai, H.; Vreven, T.; Montgomery, Jr., J. A.; Peralta, J. E.; Ogliaro, F.; Bearpark, M.; Heyd, J. J.; Brothers, E.; Kudin, K. N.; Staroverov, V. N.; Kobayashi, R.; Normand, J.; Raghavachari, K.; Rendell, A.; Burant, J. C.; Iyengar, S. S.; Tomasi, J.; Cossi, M.; Rega, N.; Millam, J. M.; Klene, M.; Knox, J. E.; Cross, J. B.; Bakken, V.; Adamo, C.; Jaramillo, J.; Gomperts, R.; Stratmann, R. E.; Yazyev, O.; Austin, A. J.; Cammi, R.; Pomelli, C.; Ochterski, J. W.; Martin, R. L.; Morokuma, K.; Zakrzewski, V. G.; Voth, G. A.; Salvador, P.; Dannenberg, J. J.; Dapprich, S.; Daniels, A. D.; Farkas, Ö.; Foresman, J. B.; Ortiz, J. V.; Cioslowski, J.; Fox, D. J. Gaussian, Inc., Wallingford CT, 2009.

34. Valentine, S.J., Conterman, A.E., Clemmer, D.E., *J. Am. Chem. Soc. Mass Spectrom*., 1999, **10**, 1188.

35. Jurneczko, E.J., Kalapothakis, J., Campuzano, I.D.G., Morris, M., Barran, P.E., *Anal. Chem*., 2012, **84**, 8524.

36. Morsa, D., Gabelica, V., De Pauw, E., *Anal. Chem*., 2011, **83**, 5775.

CHAPTER 3

MONITORING OF AN ENANTIOSELECTIVE ORGANOCATALYTIC DIELS-ALDER CYCLOADDITION REACTION BY ION MOBILITY-MASS SPECTROMETRY

3.1 INTRODUCTION

Organocatalysis is an area of research which has grown rapidly since the year 2000.[1] Until then little work had been published on the use of small organic molecules as catalysts. Organocatalysis is a beneficial replacement for organometallic and enzyme catalysis, due to the wide variety of compounds from biological sources which are cheap and readily available. They are also typically insensitive to air and moisture eliminating the need for specialist facilities such as gloveboxes and dried solvents. Furthermore, in medicinal chemistry and the pharmaceutical industry, removing traces of toxic metals associated with organometallic catalysts that are harmful to the human body and the environment can be expensive and difficult, however, extremely important. Using organic catalysts removes any risk of toxic metal residues and they are cheaper and easier to recover than organometallic catalysts.[1]

One of the most well studied organocatalytic reactions, developed between 1968 and 1997 is the Hajos-Parrish[2] reaction and in 2000 List *et al.*[3] used the mechanism to broaden the applications to proline catalysed reactions. In parallel with this development, was the first report of the use of an iminium catalyst for an enantioselective Diels-Alder reaction. This work demonstrated the benefits of organocatalysis as well as describing a general activation strategy that could be applied to other reaction classes.[4] This reaction occurs when an α,β-unsaturated aldehyde is reacted with a chiral Lewis acid amine catalyst in a condensation reaction, which creates a reactive iminium ion. The iminium ion reacts with a diene to undergo the Diels-Alder cycloaddition that hydrolyses to produce the enantiopure product and the chiral amine catalyst. The reaction can be performed on a bench in an aerobic atmosphere with wet solvents.

This catalyst scaffold has been further developed using imidazolidinone catalysts. Of particular note is the imidazolidinone catalytic cycle shown in **Figure 3.1**, which has been used in the acceleration of [4+2][4-6] and [3+2][7] cycloadditions, as well as the conjugate addition of pyrroles to α,β-unsaturated aldehydes[8]. Diels-Alder cycloaddition reactions using imidazolidinone salts (**1**) have been widely studied by investigating not only the reactivities[9] compared to diarylprolinol ethers, but also the solvents in which the reactions take place[10]. A variety of techniques have been used to monitor these reactions, including HPLC, NMR, X-ray and MS.[9-12] However, intermediate **2** (**Figure 3.1**) created using an imidazolidinone HCl salt has never been observed.

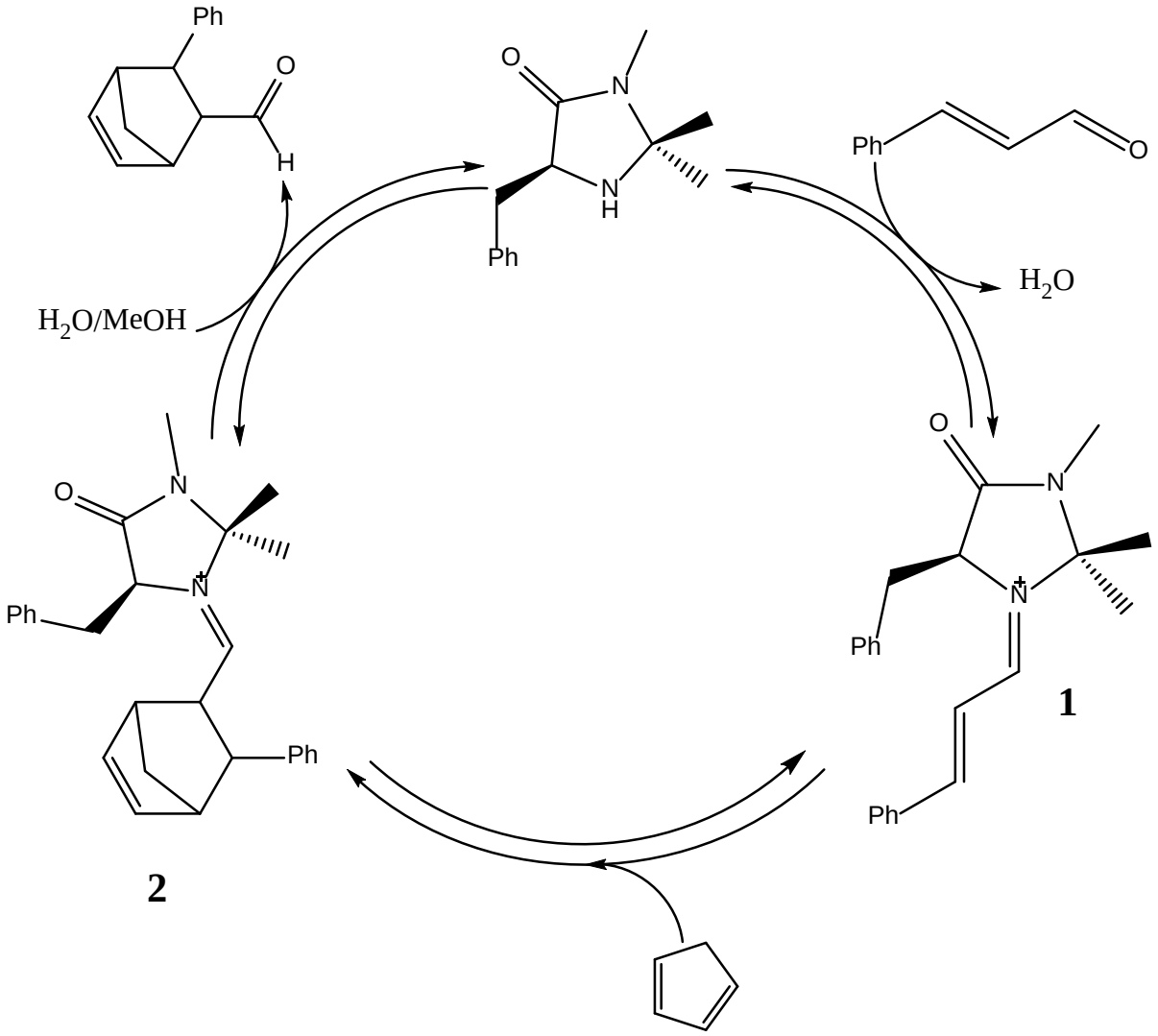

Figure 3. 1 Catalytic cycle of an imidazolidinone catalysed Diels-Alder reaction.

Ion mobility spectrometry (IMS) has the potential to yield structural information on selected ions (Chapter 1) and has been used for many monitoring applications including online monitoring of trihalomethane and haloacetic acid concentrations in drinking water,[13] ammonia in water and waste water,[14] volatile organic carbons (VOCs) in laboratory air,[14] monomer concentrations in (semi-) batch emulsion polymerisation reactors,[15] VOCs in air during yeast fermentation,[16] and nicotine in air during the manufacture of transdermal systems. Reaction monitoring by IM-MS was first reported by Harry *et al*.[16] and was shown to have potential to significantly enhance selectivity and data quality in reaction monitoring compared to MS alone. It has since been used for pharmaceutical reaction monitoring be Hill *et al*.[17]

Reaction monitoring can be carried out on-line or off-line. Off-line monitoring involves mixing the reactants in a suitable vessel and then taking samples at various time intervals. This approach works if the intermediates are sufficiently stable, but transient species may go undetected. On-line reaction monitoring can be performed using a PEEK mixing tee as a microreactor which allows two reactants to be mixed prior to infusion into the MS. To change the reaction time the capillary into the MS can be lengthened or shortened.[18-20] In both cases, a further challenge is to dilute the reaction mixture sufficiently to quench the reaction and not overload the mass spectrometer.

In this chapter we report the use of IM-MS to monitor the iminium catalysed Diels-Alder reaction (**Figure 3.1**) on-line by infusing the reactants into a t-piece mixer and off-line by quenching aliquots removed from the reaction mixture. IM-MS was used to simultaneously detect the catalyst and all intermediates within the enantioselective organocatalytic Diels-Alder cycloaddition reaction and determine their CCS.

3.2 AIMS AND OBJECTIVES

In this chapter the analysis and monitoring of an imidazolidinone catalysed Diels-Alder reaction by IM-MS is reported. The CCS were measured by TWIMS using peptide and TAAH calibrants. The reaction was also analysed using FAIMS-MS.

The aims were:-

- To analyse reaction mixtures from an imidazolidinone catalysed Diels-Alder reaction using TWIMS and FAIMS and identify the components of the catalytic cycle.
- To monitor the reaction over a period of time.
- To determine the CCS of the catalyst and intermediates.

3.3 EXPERIMENTAL

3.3.1 Materials

HPLC grade methanol, water and the peptide standards; $(Glycine)_2$, $(Alanine)_3$, $(Alanine)_5$, $(Lysine)_4$, $(Phenylalanine)_4$, $(Phenylalanine)_5$ were purchased from Fisher Scientific (Loughborough, UK). Cinnamaldehyde was purchased from Sigma-Aldrich (Gillingham, UK) The catalyst was synthesised by Nick Tomkinsons group in Strathclyde.

3.3.2 Reaction Monitoring

On-line

A solution of the imidazolidinium salt catalyst in acetonitrile (0.1 mg/mL, 0.00046 mmol) was drawn up into a syringe and the syringe attached to an arm of a t-piece mixer. Cinnamaldehyde (0.1 mg/mL, 0.00076 mmol) and cyclopentadiene (0.1 mg/mL, 0.0015 mmol) were placed in a second syringe and connected to the other arm of the t-piece. These solutions were mixed by infusion into a t-piece mixer before being diluted (x 200) by acetonitrile using a second t-piece and a Waters Acquity LC (Waters, Manchester, UK) prior to the ESI source. The sample introduction set-up is shown in **Figure 3.2**.

Off-line

The imidazolidinium salt catalyst (17 mg, 0.0625 mmol) (**Figure 3.1**) was dissolved in acetonitrile (2 mL). Cinnamaldehyde (160 μL, 1.25 mmol) and freshly distilled cyclopentadiene (300 μL, 3.75 mmol) were added to the dissolved catalyst. The reaction was stirred at 25 °C for 24 hours. An aliquot of the reaction mixture (10 μL) was removed and diluted in acetonitrile (1990 μL) before infusion into the mass

spectrometer. The mixture was further diluted (x 200) with acetonitrile using a t-piece mixer and a Waters Acquity LC (Waters, Manchester, UK) prior to the ESI source. The sample introduction set-up is shown in **Figure 3.2**.

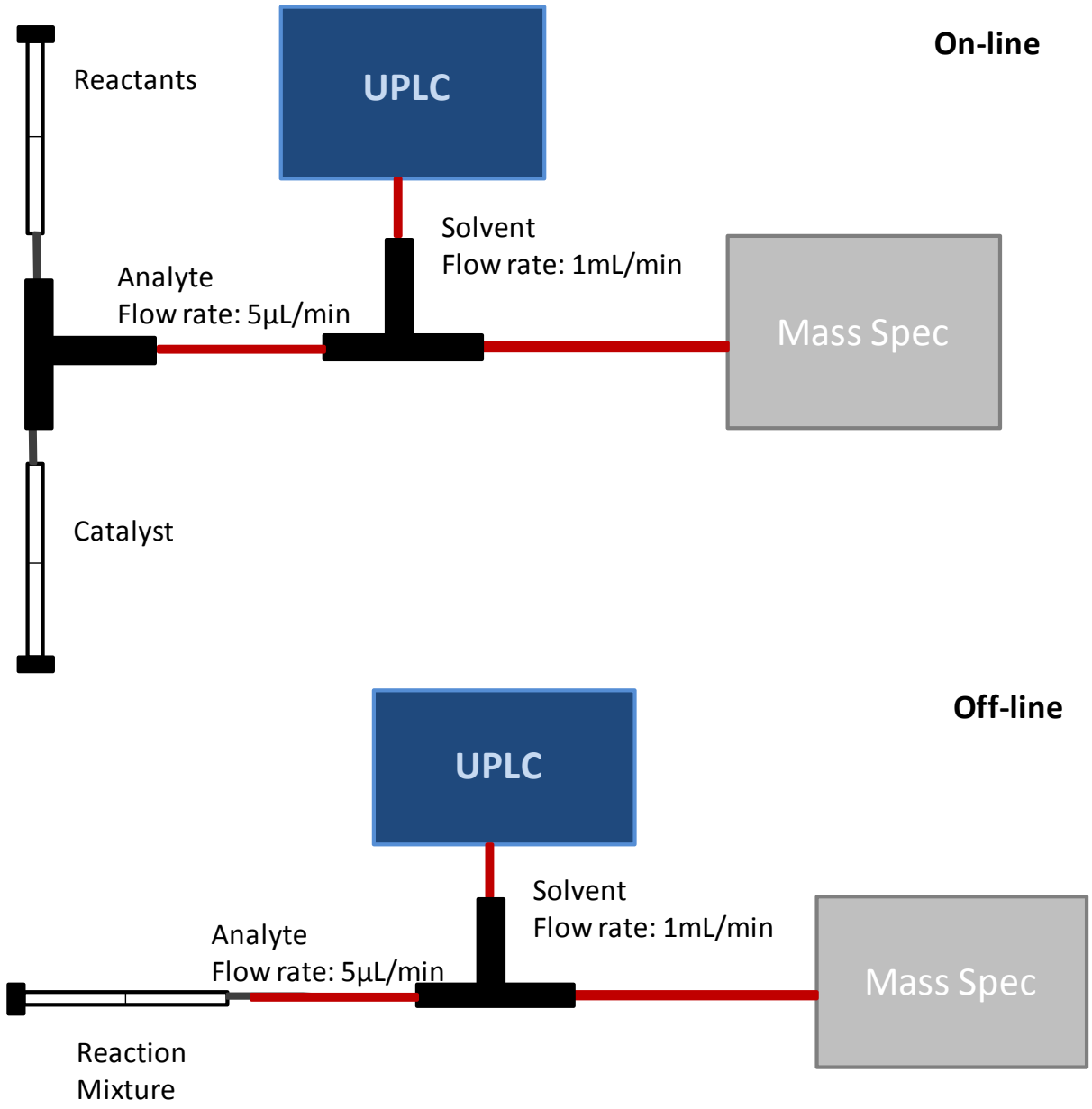

Figure 3. 2 **Schematic of the sample introduction set-up for on-line reaction monitoring (Top) and off-line reaction monitoring (Bottom).**

3.3.3 Ion mobility - Mass Spectrometry

TWIMS analyses were performed using a Waters Synapt HDMS spectrometer (Waters Corporation, Manchester, UK), with a hybrid quadrupole/ion mobility/orthogonal acceleration time-of-flight (oa-ToF) geometry controlled by Waters MassLynx operating software. Samples were introduced into the electrospray ionisation source via the sample introduction set-ups shown in **Figure 3.2**. The source and desolvation temperatures were set to 120°C and 250°C, respectively, gas flow (N_2) rates were set to 20 L/h and 600 L/h respectively. The tri-wave drift cell conditions were set at 30 mL/min drift gas (N_2) with travelling wave heights of 12 V, 8-18 V and 0-30 V and a wave velocity of 300 m/s. The ToF scan time was 45 μs/scan so each ion mobility spectrum consisted of 200 sequentially acquired time-of-flight mass spectra over the IM acquisition time of 9 ms. The acquired IM-MS data were processed using DriftScope and MassLynx 4.1 (Waters, Manchester, UK). Collision cross sections were determined using peptide standards of known CCS in helium[21]. They were analysed by IM-MS and the data used to produce a calibration curve. The CCS of the analytes were then determined from the graph using **Eqn. 2.1**.

3.3.4 High-field asymmetric waveform ion mobility-mass spectrometry

FAIMS-MS analysis were performed using a prototype miniaturised FAIMS device (Owlstone, Cambridge, UK), interfaced to an Agilent 6230 orthogonal acceleration time-of-flight mass spectrometer (Agilent Technologies, Santa Clara, CA, USA) as described in Section 1.3.3. FAIMS data were acquired with analytes transmitted through the FAIMS chip with the DF set to 200-300 Td and CF set to -4 - +6Td with 10s/scan. The FAIMS chip (NC) had a 78.1 mm trench length, 100 μm gap and 700 μm path

length. The waveform frequency was 25 MHz. ToF spectral acquisitions were performed at a rate of 10 spectra/sec, analytes were infused into the JetStream-ESI ion source at 15 µL/min and ionized using a voltage of 3.0 kV. Source conditions were: nozzle voltage 2000 V; drying gas temperature, 150 °C; sheath gas temperature, 250 °C; nebulizer gas pressure, 30 psig, drying gas flow, 7 L/min and sheath gas flow, 9 L/min. The fragmentor voltage was set to 200 V.

3.4 RESULTS AND DISCUSSION

3.4.1 Mass Spectrometry and Reaction Monitoring

TWIMS-MS has been used to analyse the imidazolidinone catalysed Diels-Alder reaction cycle shown in **Figure 3.1**. The reaction was initially carried out in a glass vial and aliquots were taken and diluted off-line in acetonitrile (x 200) prior to analysis. The mixture was diluted further during infusion as shown in **Figure 3.2**. The cinnamaldehyde reactant and catalyst ionise in the ESI source to produce $[M+H]^+$ ions at *m/z* 133 and 219, respectively, whereas, the intermediates are quaternary ammonium ions and are detected as $[M]^+$. Intermediate **2** has been postulated but not previously detected in the reaction mixture. The mass spectrum of the reaction mixture is shown in **Figure 3.3**.

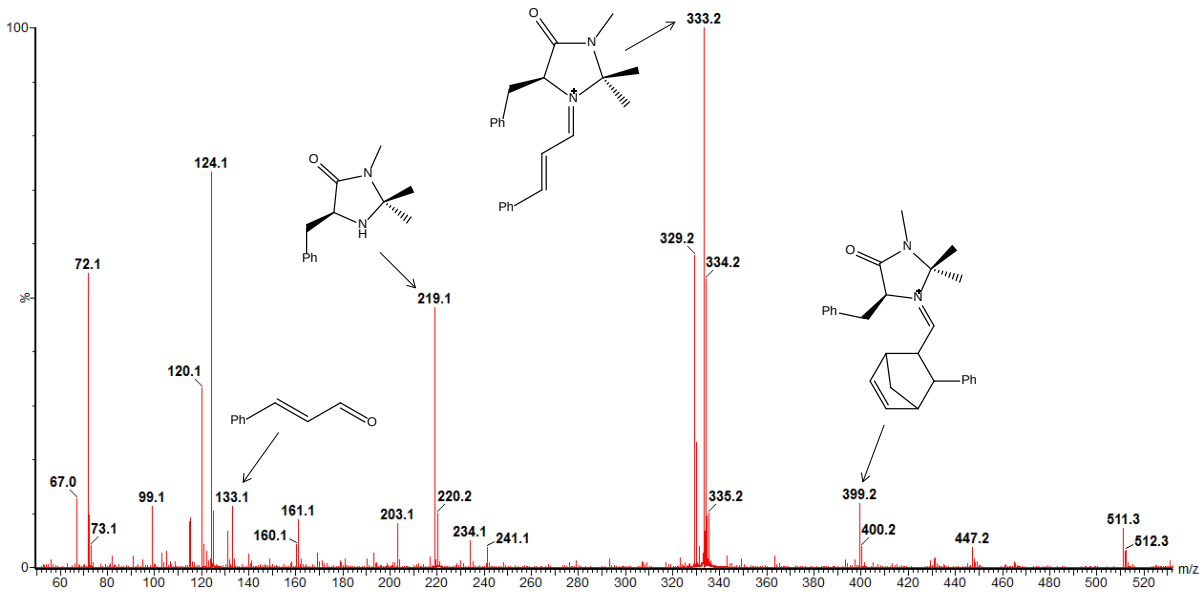

Figure 3. 3 Mass spectrum of the reactant, catalyst and intermediates 1 and 2.

All species in the catalytic cycle were observed simultaneously with the exception of cyclopentadiene which is not amenable to electrospray ionisation. The product shows a very weak response in comparison to the other compounds in the catalytic cycle because

of its low proton affinity. The reactants and products are of less concern than the intermediates as they can be characterised via other analytical techniques.

The reaction was also monitored on-line by infusing the catalyst and intermediates simultaneously via two syringes and diluting on-line using a Waters Acquity LC. The sample introduction set-up is shown in **Figure 3.2**.

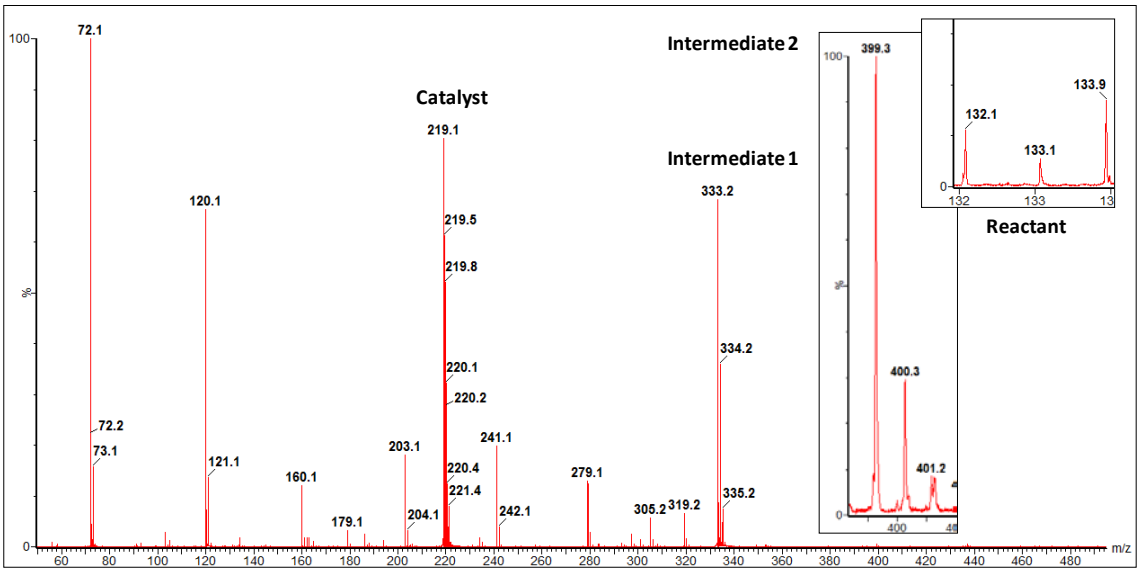

Figure 3. 4 Mass spectrum obtained from online reaction analysis.

The resulting mass spectrum (**Figure 3.4**) showed that the reactant, catalyst and intermediates **1** and **2** could be detected within the reaction mixture by on-line analysis. However, the intensities of the components vary from those observed in **Figure 3.3**. The intensity of intermediate **2** is much lower for the on-line reaction than when infusing aliquots from the off-line reaction, which is to be expected as the reactants have less time to react. The reactant ion intensity was low in comparison to the other species. The reactant, catalyst and intermediates within the reaction were observed which means the reaction can be monitored over time by the on-line and off-line methods. Continuously monitoring on-line produces large data files that are difficult to process and so for this work the off-line method was used for monitoring the course of

the reaction and for CCS measurements. Aliquots of sample were taken from the reaction vessel at timed intervals and diluted on-line using the LC. The variation in intensities of the catalyst and intermediates **1** and **2** over a period of 24 hours is shown in **Figure 3.5**.

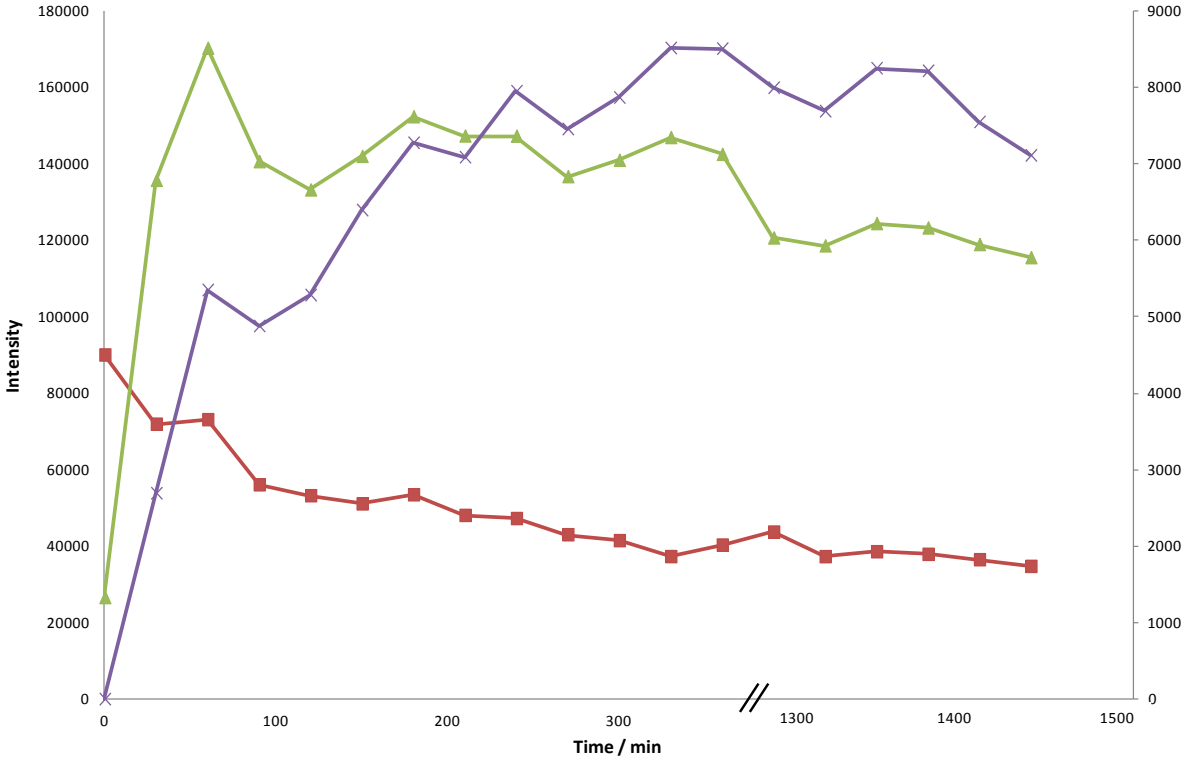

Figure 3. 5 **Variation of the intensity of the catalyst (*m/z* 219.14, squares), intermediate 1 (*m/z* 333.20, triangles) and intermediate 2 (*m/z* 399.24, crosses) over time for the iminiun catalysed Diels-Alder reaction.**

Intermediate **2** was present in the mass spectrum at a low intensity in comparison to those of the catalyst and intermediate **1** and therefore has been plotted on a secondary axis (right hand side). The intensity of the catalyst declines during the initial stages of the reaction before reaching a steady state. Intermediate **1** shows a rapid increase in intensity over the first 80 minutes, before declining gradually and intermediate **2** increases over 300 minutes and then remains at a stable intensity for the next 19 hours.

3.4.2 Ion Mobility and Determination of CCS

The mass-selected ion mobility spectra obtained from the TWIMS-MS analysis of the reaction mixture are shown in **Figure 3.6**. The beam was attenuated to limit the number of ions entering the drift cell for the most intense ions to prevent detector saturation.

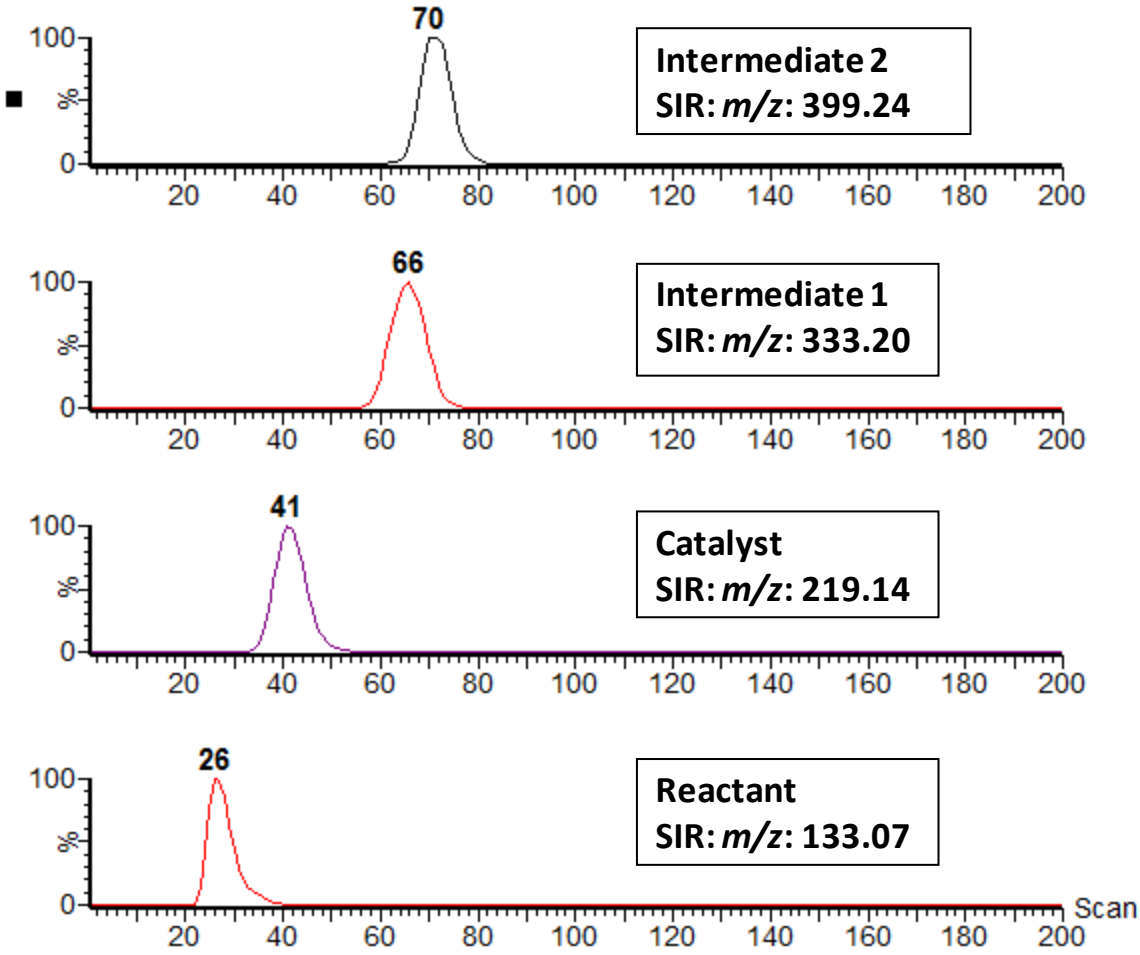

Figure 3. 6 Ion mobility spectra for the reactant, catalyst and intermediates in the imidazolidinone catalysed Diels-Alder reaction.

The results show that IM can distinguish between the reactant, catalyst and intermediates of the reaction. The components have mobilities in the expected order with the smallest ion, the cinnamaldehyde reactant having the shortest drift time (bin 26, t_d 1.17 ms), followed by the imidazolidinone catalyst (bin 41, t_d 1.85 ms). Intermediate

2 has a longer drift time (bin 70, t_d 3.15 ms) than intermediate **1** (bin 66, t_d 2.97 ms) because of the cycloaddition of cyclopentadiene.

The CCS of the catalyst and intermediates were determined by calibrating the TWIMS drift cell using peptide and TAAH standards. The calibration process has been discussed in detail in Chapter 2, however, previously the analytes had only been measured using one wave height setting, 8-18 V. In this work the catalyst and intermediates were measured using peptide standards at ramped wave heights of 8-18 V, 0-30 V and a fixed wave height of 12 V. The resulting calibration plots are shown in **Figure 3.7**.

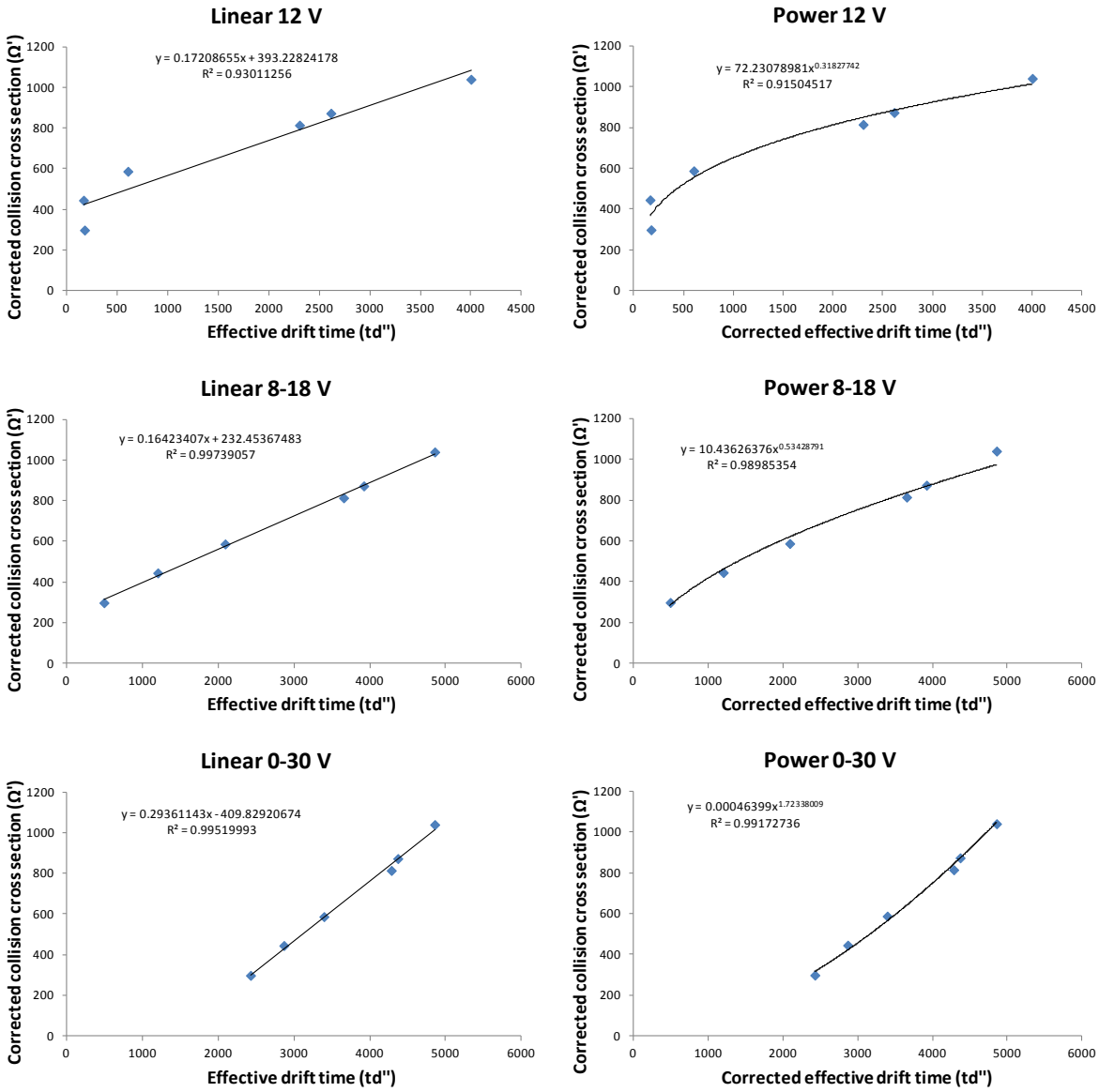

Figure 3. 7 Calibration graphs of corrected collision cross section (Ω'/Å^2) against effective drift time (td"/μs) for wave heights 12 V, 8-18 V and 0-30 V using peptides.

There is a lack of separation in the 12 V plot for the lower mass peptides which are pushed in front of the travelling wave causing them to have the same or very similar scan numbers. The 12 V and 8-18 V linear trendlines intercept the y-axis above zero whereas the 0-30 V linear trendline intercepts the y-axis below zero. The CCS data for the catalyst and intermediates derived from the power and linear fits are shown in **Table 3.1**.

Table 3. 1 **CCS data for the catalyst and Intermediates for power and linear trendlines at varying wave heights.**

Compounds	CCS/ Å^2 (Peptides)					
	12 V		8-18 V		0-30 V	
	Power	Linear	Power	Linear	Power	Linear
Catalyst	80	86	88	83	80	81
Intermediate 1	116	102	127	118	114	118
Intermediate 2	129	112	137	129	123	127

Differences were observed between the CCS calculated using the linear and power plot, using all three wave heights. The power data produces larger CCS for the 8-18 V data, however, for the 0-30 V data the power CCS values are smaller. The 12 V CCS are larger for the linear data for the catalyst but smaller for the intermediates. This may be due to the lack of separation of the first two calibration points, which are pushed in front of the travelling wave and therefore have effective drift times close to the dead time of the mobility cell (610 μs). If the bottom two points are removed from the calibration line the power data changes by an average 3% difference in CCS results. However, for the linear calibration the CCS increase by 19%. The power data does not change because the intercept is being forced through zero creating a similar trendline. The linear trendline is not forced through zero and the catalyst and intermediate **1** fall outside of the calibration range.

There is no variable to compensate for gas pressure or wave height in the calibration process and altering these parameters effects the drift time of the standards, shifting the

points left or right in the calibration graphs as demonstrated in **Figure 3.7**. The linear plots using ramped wave heights provide the most consistent results.

The CCS were also determined using TAAH standards. A comparison of CCS for TAAH and peptide standards obtained using an 8-18 V ramp are shown in **Table 3.2**.

Table 3. 2. Experimental CCS data determined using TAAH and peptide standards.

Compounds	**CCS/ Å^2 (TAAH)[a]**	**CCS/ Å^2 (Peptides)[b]**
Catalyst	86 ± 3	83 ± 3
Intermediate 1	125 ± 3	118 ± 5
Intermediate 2	134 ± 6	129 ± 4

[a] Calculated from six repeats on one day and three repeats on separate days. [b]Calculated from six repeats on separate days. Error values are ± 3*Standard deviation.

The CCS results show the catalyst to have the smallest CCS followed by intermediate **1** and then intermediate **2** for both peptide and TAAH calibrations. There is a large increase from the catalyst ion to intermediate **1**, with the addition of the aromatic ring and a small increase between intermediate **1** and intermediate **2** as a result of the incorporation of the cyclopentadiene. As observed in Chapter 2 the peptide data is systematically smaller than the TAAH data with an average 4% difference. The reason for the differences were discussed in detail in Section 2.5.2 but in brief, the difference is due to calibrating using standards with CCS determined in a helium (He) gas. The calibration process therefore provides a CCS estimation in He gas, but does not correct fully for the compound dependent interaction of the polarisable nitrogen drift gas with the calibrants and analytes.

Ion mobility is able to separate ions by *m/z* and size and shape which can enhance selectivity and data quality in reaction monitoring (**Figure 3.8**).

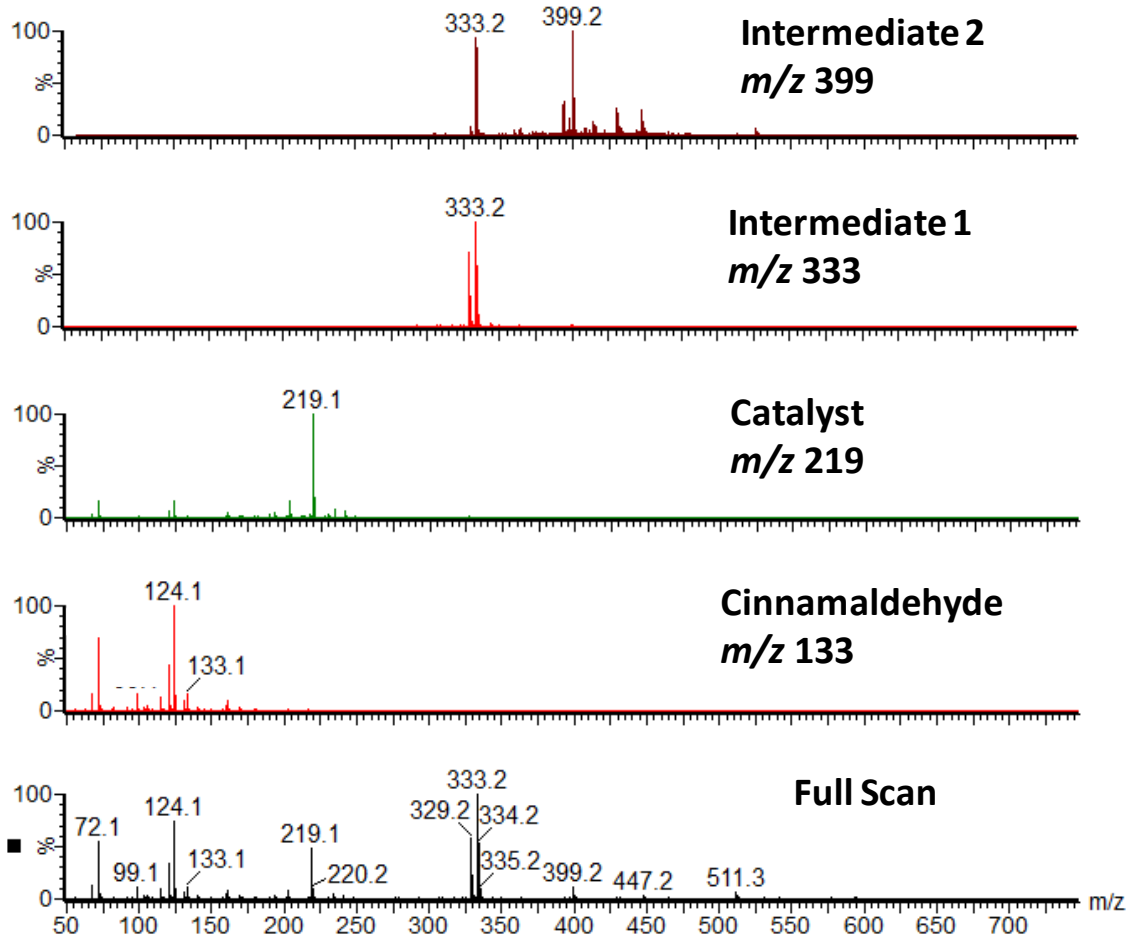

Figure 3. 8 **Mass spectrum for the reaction mixture and mass/mobility-selected spectra for cinnamaldehyde (*m/z* 133, bins 22-36), the catalyst (*m/z* 219, bins 34-48) Intermediate 1 (*m/z* 333, 58-74) and Intermediate 2 (*m/z* 399, bins 70-78).**

The mass spectrum obtained by averaging the 200 scans (bins) acquired during the IM-MS analysis (i.e. removing the mobility separation) shows a complex spectrum (**Figure 3.8 bottom**), but selecting the scans at the drift time of the reactant, intermediates and the catalyst results in enhanced spectral quality (**Figure 3.8**).

3.4.3 FAIMS-MS

The imidazolidinone-catalysed Diels-Alder reaction mixture was analysed using field asymmetric ion mobility-mass spectrometry. This technique is based on the same fundamental principles as DTIMS and TWIMS, however, FAIMS separates ions based on the difference in an ions behaviour in high and low electric fields, termed differential mobility.

The imidazolidinone catalysed Diels-Alder reaction was reacted in a vial and then aliquots were taken and diluted in acetonitrile (1:2000). A mass spectrum of the reaction mixture is shown in **Figure 3.9**.

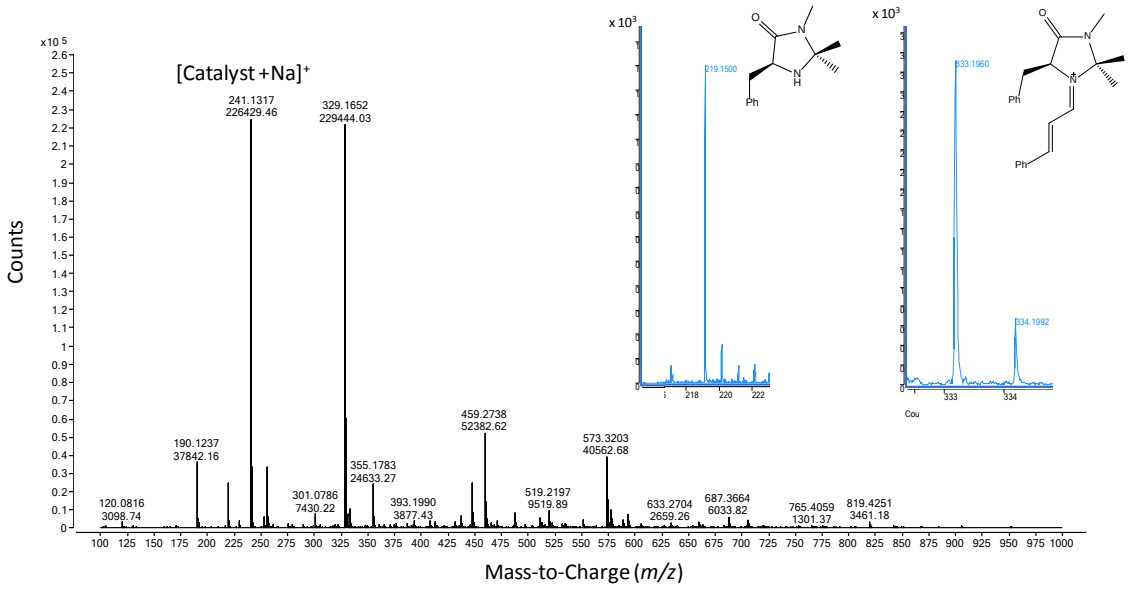

Figure 3. 9 **A mass spectrum of the Diels-Alder reaction mixture showing the [catalyst+Na]$^+$, the [catalyst+H]$^+$ (insert, left) and Intermediate 1 (insert, right).**

All the intermediates are observed in the mass spectrum with catalyst and protonated intermediate **1** shown in inserts (**Figure 3.9**). Intermediate **2** is shown in **Figure 3.10** for clarity. The [catalyst+Na]$^+$ (*m/z* 241) is at a much higher intensity than the protonated catalyst ion. Intermediates **1** and **2** have a less intense signal compared to other components in the cycle. High mass accuracy was obtained for the catalyst (3.65 ppm), intermediates **1** (0.30 ppm) and Intermediate **2** (0.75 ppm). **Figure 3.10** demonstrates the ability of FAIMS to enhance the selectivity of particular species within a mixture allowing it to be distinguished from other reaction components.

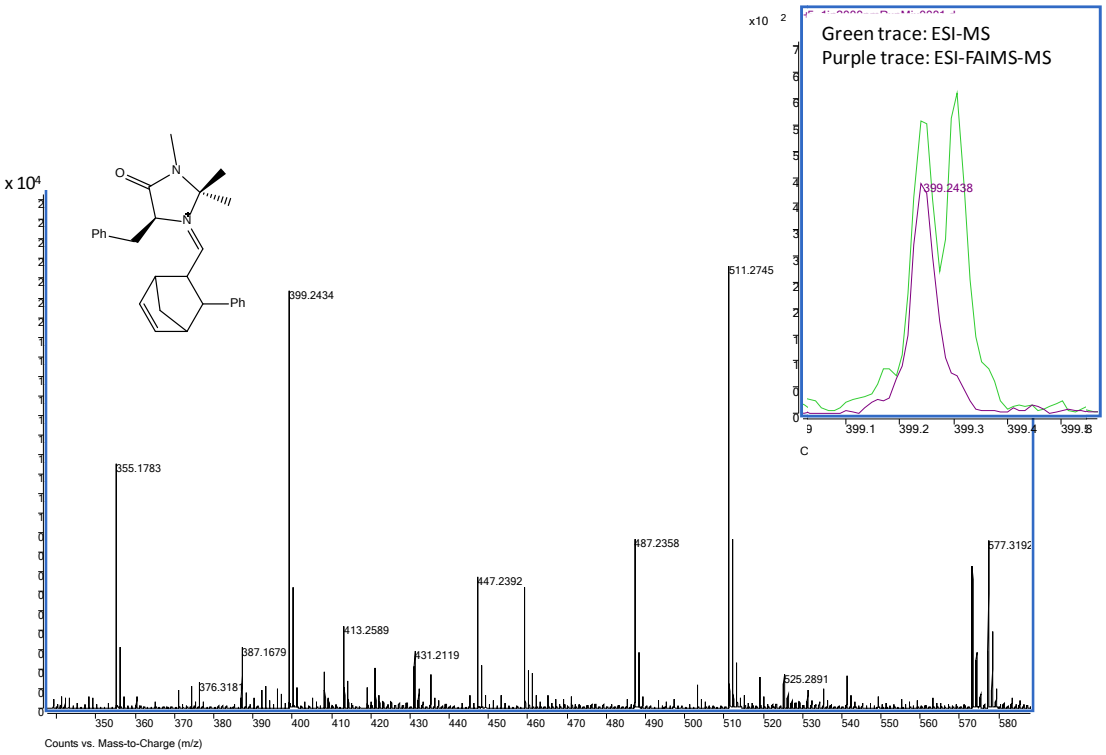

Figure 3. 10 Mass spectra of intermediate 2 with FAIMS (purple trace) and without FAIMS (green trace) (Insert).

The FAIMS-MS data for the catalyst and intermediates **1** and **2** are shown in **Figure 3.11**. The FAIMS-MS data shows that the catalyst (*m/z* 219) and intermediate **1** (*m/z* 333) require different compensation fields for maximum transition through the FAIMS device, but there is no separation between the intermediates **1** and **2** (*m/z* 399).

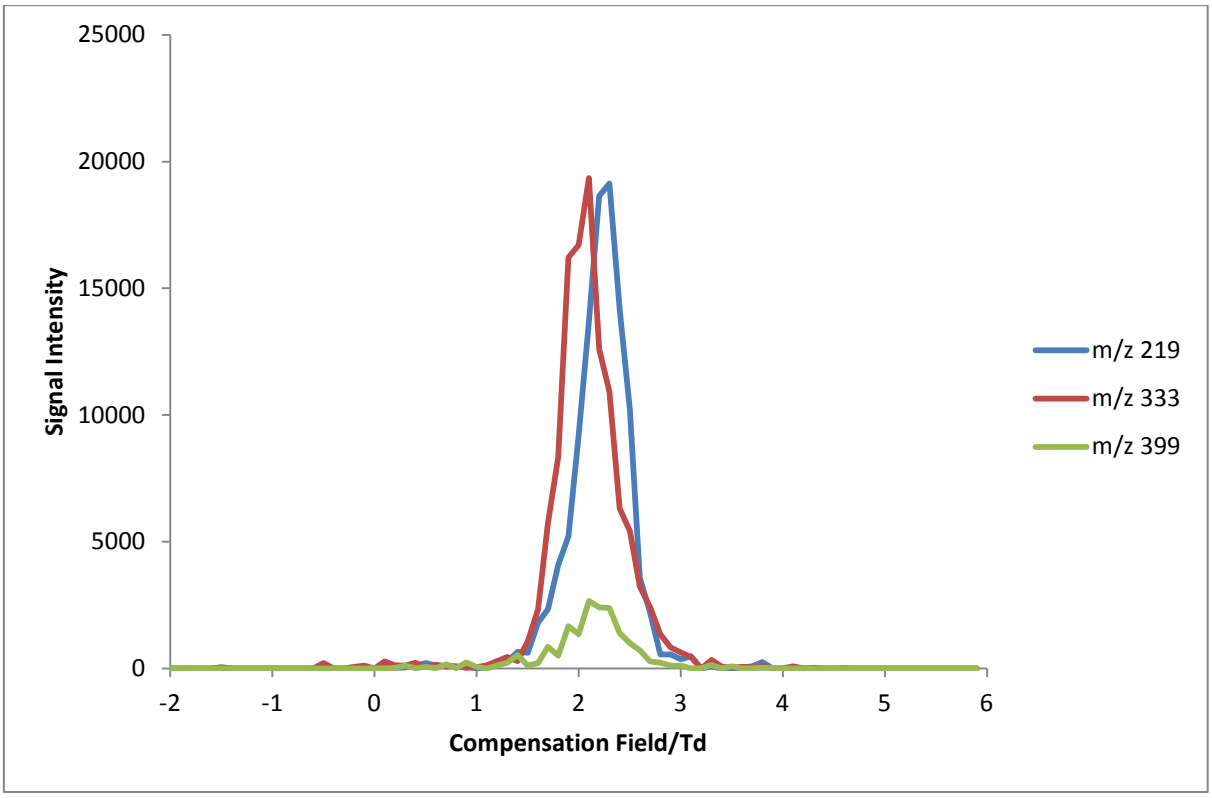

Figure 3. 11 Compensation field scan for the FAIMS-MS analysis of the catalyst (blue), intermediate 1 (red) and intermediate 2 (green).

The differential mobility of an ion is dependent on the mass, charge, functionality and conformation of the ion and does not have as much emphasis on size and shape like DTIMS and TWIMS. The intermediates have identical functional groups meaning their differential mobility are very similar making them indistinguishable.

3.5 CONCLUSIONS

The reactant, catalyst and reaction intermediates of an imidazolidinone catalysed Diels-Alder cycloaddition reaction have been analysed by IM-MS by on-line direct infusion and off-line by dilution of aliquots removed from the reaction mixture. The results show IM separation of the catalyst and intermediates, which were monitored over a 24 hour period by removing aliquots from the reaction mixture at specific time intervals. The CCS of the reactive species were determined by T-wave IM using peptide and TAAH standards and varying wave heights. The CCS determined from the linear trendlines using the ramped wave heights produced the most consistent results. The TAAH standards gave significantly larger (4%) CCS values than the peptide standards. The reaction was also monitored using FAIMS which showed separation between the catalyst and intermediates but not between intermediate **1** and intermediate **2** due to their similarity in functional groups. The data reported in this chapter demonstrates that IM-MS may be used for reaction monitoring and to identify trace intermediates, including a previously undetected intermediate, during the course of an organocatalytic reaction. Structural information based on *m/z* and CCS measurements may be acquired simultaneously for all components of the reaction mixture.

3.6 CHAPTER THREE REFERENCES

1. MacMillan, D.W.C., *Nature*, 2008, **455**, 304.
2. Hajos, Z. G. & Parrish, D. R. German patent DE 2102623 (1971).
3. List, B., Lerner, R.A., Barbas III, C.F., *J. Am. Chem. Soc*., 2000, **122**, 2395.
4. Adhrendt, K.A., Borths, C.J., MacMillan, D.W.C., *J. Am. Chem. Soc*., 2000, **122**, 4243.
5. Northrup, A.B., MacMillan, D.W.C., *J. Am. Chem. Soc*., 2002, **124**, 11, 2458.
6. Wilson, R.M., Jen, W.S., MacMillan, D.W.C., *J. Am. Chem. Soc*., 2005, **127**, 11616.
7. Jen, W.S., Wiener, J.J.M., MacMillan, D.W.C., *J. Am. Chem. Soc*., 2000, **122**, 9874.
8. Paras, N.A., MacMillan, D.W.C., *J. Am. Chem. Soc*., 2001, **123**, 4370.
9. Brazier, J.B., Hopkins, G.P., Jirari, M., Mutter, S., Pommereuil, R., Samulis, L., Platts, J.A., Tomkinson, N.C.O., *Tetrahedron Letters*, 2011, **52**, 2783.
10. Brazier, J.B., Jones, K.M., Platts, J.A., Tomkinson, N.C.O., *Angew. Chem. Int. Ed*., 2011, **50**, 1613.
11. Samulis, L., Tomkinson, N.C.O., *Tetrahedron*, 2011, **67**, 4263.
12. Brazier, J.B., Evans, G., Gibbs, T.J.K., Coles, S.J., Hursthouse, M.B., Platts, J.A., Tomkinson, N.C.O., *Org. Lett*., 2009, **11**, 133.
13. Meyer, S., Koch, R., and Metzger, J.O., *Angew. Chem. Int. ed.*, 2003, **42**, 4700.
14. Meyer, S., Metzger, J.O., *Anal. Bioanal. Chem.*, 2003, **377**, 1108.
15. Wilson, D.J., and Konermann, L., *Anal. Chem.*, 2003, **75**, 6408.
16. Harry, E.L., Bristow, A.W.T., Wilson, I.D., Creaser, C.S., *Analyst*, 2011, **136**, 1728.

17. Roscioli, K. M., Zhang, X., Li, S. X., Goetz, G. H., Cheng, G., Zhang, Z., Siems, W. F., Hill, H. H. Jr., *Int. J. Mass Spectrom*., 2013, **336** 27.
18. Emmert, G.L., Geme, G., Brown, M.A., Simone, P.S., *Anal. Chim. Acta*, 2009, **656**, 1.
19. Eiceman, G.A., *Trends Anal. Chem.*, 2002, **21**, 259.
20. Vautz, W., Mauntz, W., Engell, S., Baumbach, J.I., *Macromol. React. Eng.*, 2009, **3**, 85.
21. Valentine, S.J., Conterman, A.E., Clemmer, D.E., *J. Am. Chem. Soc. Mass Spectrom.*, 1999, **10**, 1188.

CHAPTER 4

STRUCTURAL STUDIES OF METAL CATALYSED REACTION INTERMEDIATES BY ION MOBILITY-MASS SPECTROMETRY

4.1 INTRODUCTION

Mass spectrometry (MS) has always been an important tool when analysing organometallics as exemplified by a paper on metal chelates dating back to 1975 using a Hitachi RMU-7 mass spectrometer.[1] MS investigations into organometallic compounds have been carried out on copper (Cu) complexes[2,3] , palladium (Pd) complexes[4], tin (Sn) compounds[5] and cobalt (Co) complexes[3,6]. A variety of ionisation sources have been used in conjunction with this technique. Cold-spray ionisation (CSI),[7] matrix-assisted laser desorption ionisation (MALDI),[8,9] direct analysis in real time (DART)[10] and flowing afterglow (FA)[11] are some of the ionisation techniques used for MS in the analysis of organometallics.

The most common ionisation source used, however, is electrospray ionisation (ESI) due to the wide range of analytes which can be ionised using this technique. ESI sources have also been modified to enhance the technique for specific purposes using methods such as photolysis[12,13]. In this method the sample passes through a quartz cell and is photoirradiated by a xenon (Xe) lamp[12] or by a mercury (Hg) lamp[13]. An electrochemical cell (EC) has been developed to analyse electrochemical reactions, using a radial-flow cell[14] and for the analysis of photochemical reactions, nanospray photochemical apparatus was used to irradiate samples in a transparent nanospray tip of the ESI source.[15] The use of ESI-MS for the study of organometallics has been extensively reviewed elsewhere.[16-18] However, an area more challenging is the detection of trace organometallic catalytic intermediates in real time as they are formed in reaction mixtures.

Electrospray ionisation mass spectrometry (ESI-MS) has been used widely in reaction monitoring, due to its ability to detect a wide range of ionised and neutral species in

solution, and to provide information on reaction kinetics.[19-22] Emphasis has been placed on the detection and identification of low level and transient intermediates, and the monitoring of the levels of these intermediates along with the reactants and products over the course of a reaction.

A wide range of work has been carried out on reaction monitoring by MS including work on catalytic cycles. Examples are the Suzuki,[23] Suzuki-Miyaura[24,25] and Stille[26] reactions. Mechanistic studies of catalytic intermediates are important in reaction understanding, design and process control.[27] A variety of analytical methods have been used to monitor reactions including infrared spectroscopy (IR),[28] near infrared spectroscopy (NIR),[29] nuclear magnetic resonance (NMR),[30] and liquid chromatography (LC).[31] However, all these methods have limitations for the simultaneous monitoring of trace levels of catalytic intermediates in complex reaction mixtures. It has recently been shown that the combination of ion mobility spectrometry with mass spectrometry (IM-MS) has the potential to significantly enhance selectivity and data quality in reaction monitoring.[32]

This chapter describes the incorporation of IM analysis into mass spectrometric reaction monitoring studies of reactants, products and low level reaction intermediates of an organometallic catalytic cycle using a palladium catalyst.

The palladium catalysed Stille reaction for the conversion of 3,4-dichloroiodobenzene to its styrene analogue, which is well known and characterized both experimentally and theoretically, and has been previously studied using ESI-MS,[26,33,34] was selected to demonstrate proof of principle of the IM-MS approach.

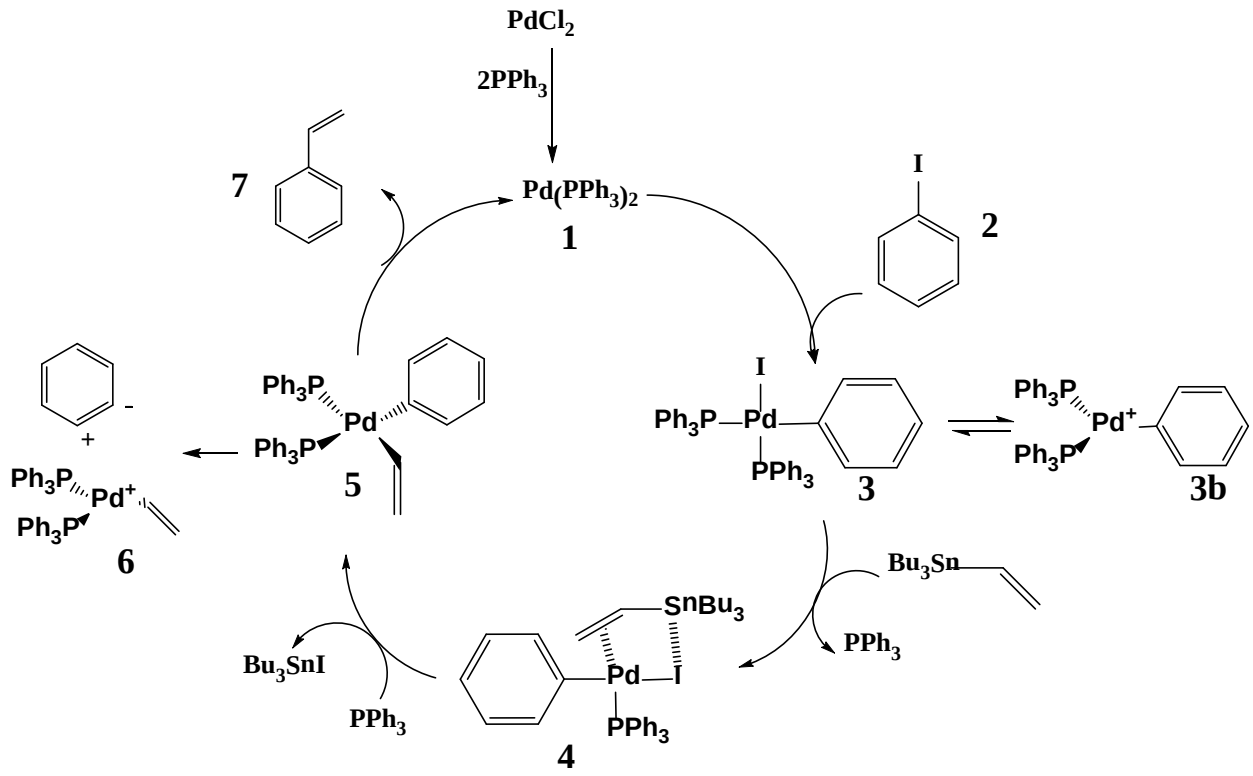

Scheme 4. 1 A schematic of the Stille reaction.

Several trace palladium-containing species have been reported for the reaction, but these were all by-products of the reaction. The product is not ionisable by ESI and was only detected via gas chromatography-mass spectrometry (GC-MS). This chapter describes the study of the reaction using IM-MS using free and tagged iodobenzene as the reactant. The catalytic cycle is shown in **Scheme 4.1**.

4.2 AIMS AND OBJECTIVES

This chapter reports the analysis and monitoring of an organometallic catalysed reaction. The CCS were measured by TWIMS using TAAH and peptide standards.

The aims were:-

- To analyse the Stille reaction mixture using TWIMS and identify the components within the reaction.
- To monitor the Stille reaction over a period of time to observe changes of reactant, product and intermediates.
- To determine the CCS of selected intermediates.
- To react the Stille reactant with an ESI active tag.
- To compare model structures to experimental data to investigate the structure/conformation of selected intermediates.

4.3 EXPERIMENTAL

4.3.1 Chemicals

Acetonitrile (HPLC gradient grade) was purchased from Thermo Fisher Scientific (Loughborough, UK). Lutidine and tetraalkyl ammonium halides (TAAHs): tetraethylammonium bromide, tetrapropylammonium iodide, tetrabutylammonium iodide, tetrahexylammonium iodide, tetraoctylammonium bromide, tetradodecylammonium bromide, Palladium(II)chloride, triphenylphosphine, tributyl(vinyl)tin, and 1-methylimidazole were purchased from sigma-aldrich (Gillingham, UK) and tetrapentylammonium bromide, tetraheptylammonium bromide were obtained from Thermo Fisher Scientific (Loughborough, UK). Benzene boronic acid and iodbenzene are from Lancaster Synthesis. 4-iodobenzyl bromide was bought from Acros Organics (Geel, Belgium).

4.3.2 Sample preparation

Stille reaction (Non-Tagged)

Triphenylphosphine (31.47 mg) was added to palladium(II)chloride (10.64 mg) in acetonitrile (1 mL). Iodobenzene (6.7 μL) and tributyl(vinyl)tin (17.6 μL) were then added. This was left to stir at room temperature for approximately 4 hrs.

Stille reaction (Tagged)

The tag was synthesised by the addition of 1-methylimidazole (4.8 μL) to 4-iodobenzyl bromide (17.77 mg) in acetonitrile (1 mL) and the mixture was left to stir for 2 hrs. Triphenylphosphine (31.47 mg) was added to palladium(II)chloride (10.64 mg) in acetonitrile (1 mL) and the tagged iodobenzene and tributyl(vinyl)tin (17.6 μL) were then added. The reaction is left to stir on a hotplate at 50°C for 24 hrs.

4.3.3 Ion Mobility-Mass Spectrometry

The Stille reaction was investigated off-line by removing aliquots of the reaction mixture at periodic intervals, diluted in acetonitrile (x 200) and infused into the ESI source of a Waters Synapt HDMS spectrometer (Waters Corporation, Manchester, UK) at 5 μL/min, using a syringe pump. The reaction mixture was further diluted on-line with acetonitrile delivered *via* a t-piece mixer at 1 mL/min using a Waters Acquity UPLC pump (**Figure 3.2**). Accurate mass data was obtained for the tagged intermediate by lockmassing to the C13 isotope of the tagged reactant ion (m/z 300.0075). This was carried out by James Reynolds (Loughborough University).

IM-MS data were acquired using a T-wave drift tube pulse height of 8-18 V and a wave velocity of 300 m/s, with nitrogen buffer gas. Each ion mobility spectrum consisted of 200 sequentially acquired time-of-flight mass spectra over the IM acquisition time of 9 ms. CCS were measured using the procedure described in section 2.3.5 with peptide calibrants.

4.3.4 Theoretical determination of CCS

Molecular structures were optimized using a Density Functional Theory (DFT) based method. DFT optimisation was carried out by Carles Bo and Fernando Castro-Gómez from the Institute of Chemical Research of Catalonia (ICIQ). The 6-311G(d,p) triple-zeta basis set were used for H, C, N and P atoms, whereas the relativistic effective core pseudo potential LANL2DZ together with its associated basis set was used for Pd and I atoms. Geometry optimizations were performed without constraints and the nature of the stationary points were characterized as minima by means of harmonic vibrational frequencies analysis. All calculations were carried out using the Gaussian09 package.[35]

Calculation of the theoretical CCS from the DFT optimized structures were carried out using methods implemented in MOBCAL[36]: projection approximation (PA),[37] exact hard sphere scattering (EHSS)[38] and trajectory method (TM). [39,40] This has been discussed in Section 1.4.2. For H, C, and N atoms, the 12-6 default parameters in MOBCAL as well as recently developed parameter sets by Siu et al.[41] and by Campuzano et al.[42] were considered. For Pd, P and I atoms, the 12-6 parameters for silicon were used. For all the atoms, charge-induced dipole interaction was included from Mulliken atomic charges computed at the DFT level. Helium parameters were assumed when carrying out MOBCAL calculations.

4.4 RESULTS AND DISCUSSION

4.4.1 Stille reaction

The Stille reaction was monitored by removal of aliquots from the reaction mixture at periodic intervals and infusion into the ESI source after dilution. Reactants, intermediates and products were detected directly by ESI-IM-MS and a typical mass spectrum obtained from the reaction mixture of the Pd-catalysed conversion of iodobenzene to styrene is shown in **Figure 4.1a**. A complex mass spectrum is observed consisting of ions associated with the catalytic cycle and side reactions, as well as palladium clusters and complexes with other ligands present in solution or formed as artefacts of the ESI process. However, Stille reaction species can still be observed, such as intermediates **1** (*m/z* 630), **3b** (*m/z* 707) and **6** (*m/*z 657); (**Scheme 4.1**).

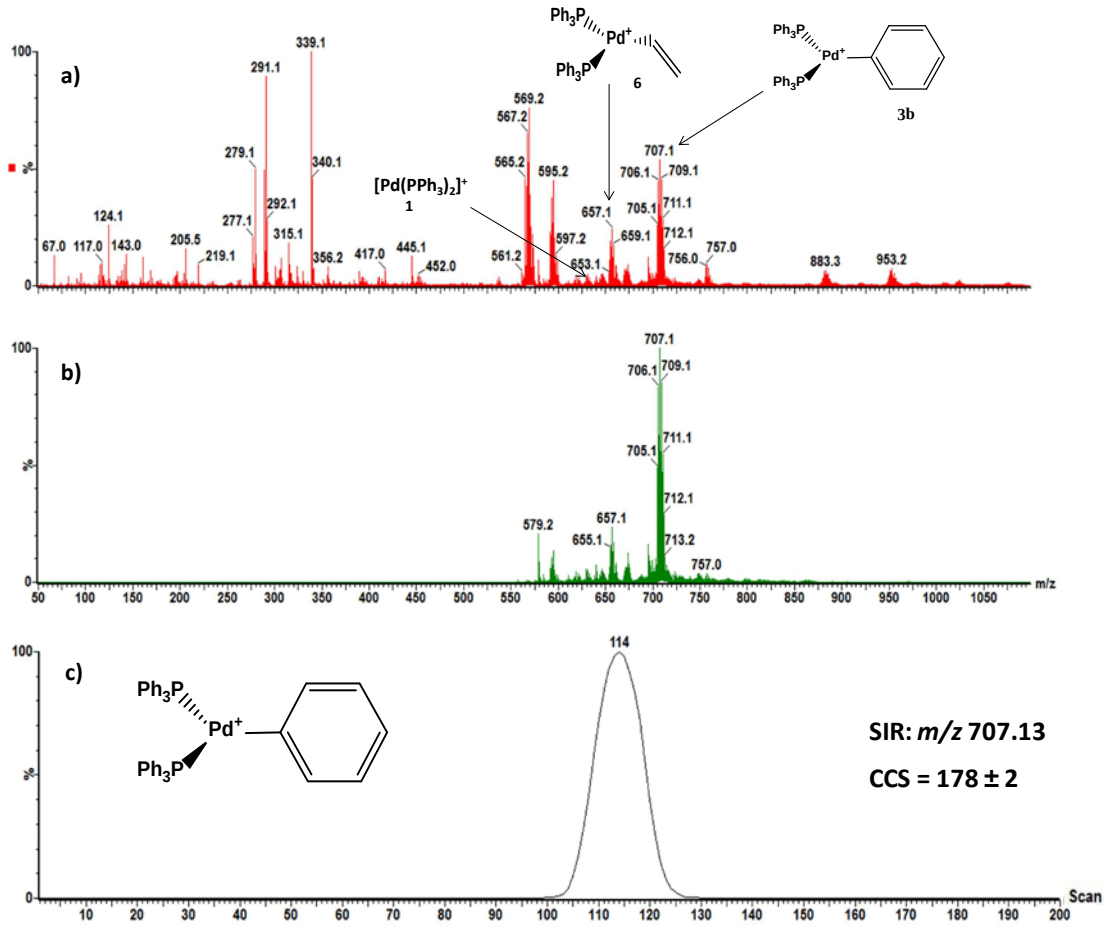

Figure 4. 1 **ESI mass spectrum of Stille reaction mixture showing the complexity of the spectrum and identified intermediates 1, 3b and 6 (a), ESI-IM-MS of intermediate 3b combining mass spectra in the drift time range 4.68 -5.85 ms (b) and (c) the selected ion mobility spectra of intermediate 3b (*m/z* 707.13).**

Figure 4.1 demonstrates the complexity of the spectra obtained using this technique, but also shows that low level Pd-containing catalytic intermediates can be identified in the mixture and selected for IM measurement. Summing the mass spectra obtained between td 4.68 ms and 5.85 ms, gives a simplified mass spectrum with *m/z* 707 as the base peak as a result of IM separation of **3b** from other components of the reaction mixture (**Figure 4.1b**). The selected ion mobility spectrum from the *m/z* 707 ion of **3b** (**Figure 4.1c**), shows a sharp symmetric peak centred at a t_d of 5.13 ms, indicating the presence of a single species.

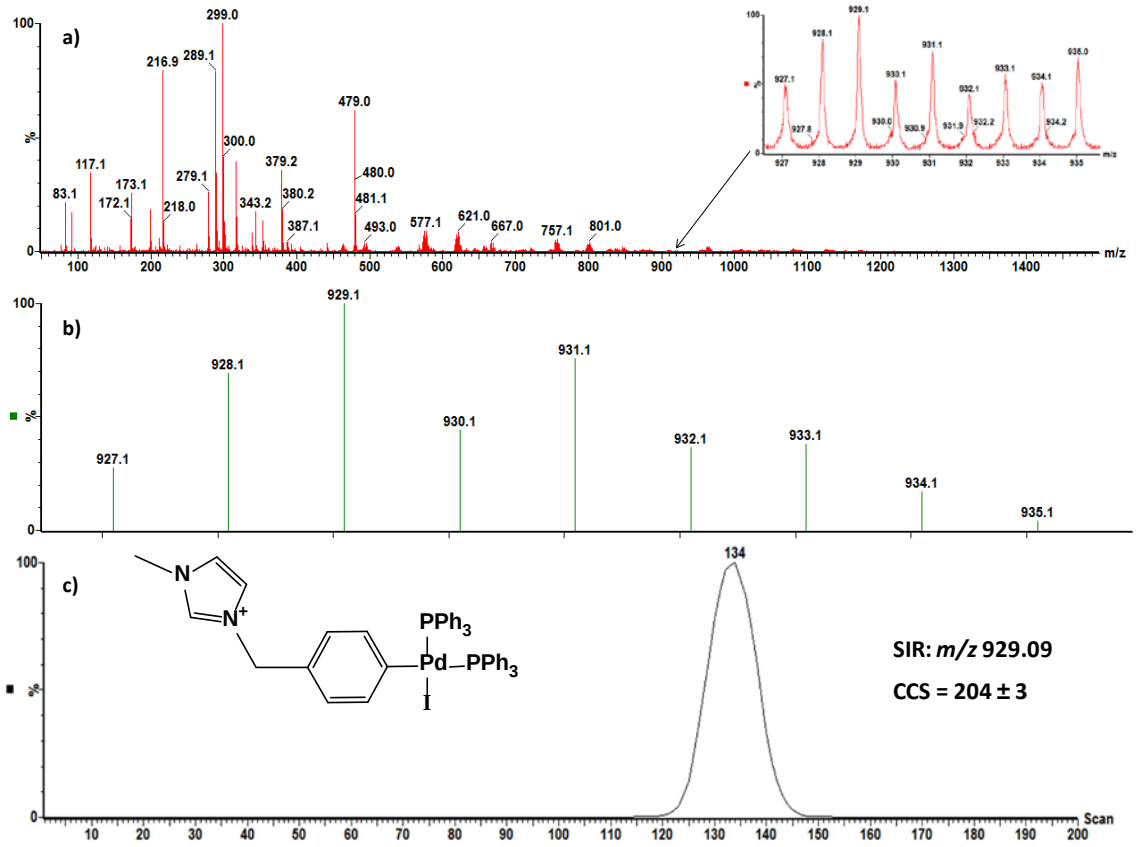

Figure 4. 2 **ESI mass spectrum of Stille reaction mixture showing the isotope pattern of the intermediate (insert) (a), the theoretical isotope pattern (b) and (c) the selected ion mobility spectra of the methyl imidazole tagged intermediate 3 (*m/z* 926.09).**

Several key intermediates in the Stille reaction are neutral species with low proton affinities and, therefore, were not detected by ESI. A method of ionising components whilst limiting changes to the reaction is by the addition of a charge bearing group to the reactant. This carries a permanent charge but does not take part in the reaction.[20,21] In this study, iodobenzene was tagged with 1-methylimidazole by reaction with 1,4-iodobenzylbromide to give $\mathbf{2}_{\mathbf{tag}}$. This adds a quaternary ammonium ion to the reactant, giving it a permanent charge which is incorporated into subsequent intermediates and products.

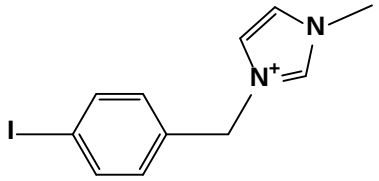

2_{tag}

The mass spectrum for the reaction using the tagged reactant (**2_{tag}**) is shown in **Figure 4.2a**. The mass spectrum is complex and the tagged intermediate is at trace levels. Accurate mass data was obtained for the tagged intermediate by lockmassing to the C13 isotope of the tagged reactant ion (m/z 300.0075) which produced an average error of 4.7 ppm for the isotope peaks. An expansion of the isotope pattern of tagged intermediate **3** (**3_{tag}**) is displayed in an insert. The isotope pattern matches the theoretical isotope pattern shown in **Figure 4.2b** with the exception of the final two isotope peaks. This is due to an overlapping Pd complex adjacent to the intermediate.

Figure 4.3 shows the progress of the reaction for the tagged reactant, product, and the intermediate **3** ions over a period of 6 hours**.** The intensity of the tagged reactant gradually decreases with time, whilst the intensities of tagged intermediate **3** (**3_{tag}**) and the product **7** increase over the first 200 minutes, before reaching a steady state and then declining. The IM spectrum of the tagged intermediate **3_{tag}** is shown in **Figure 4.2c**.

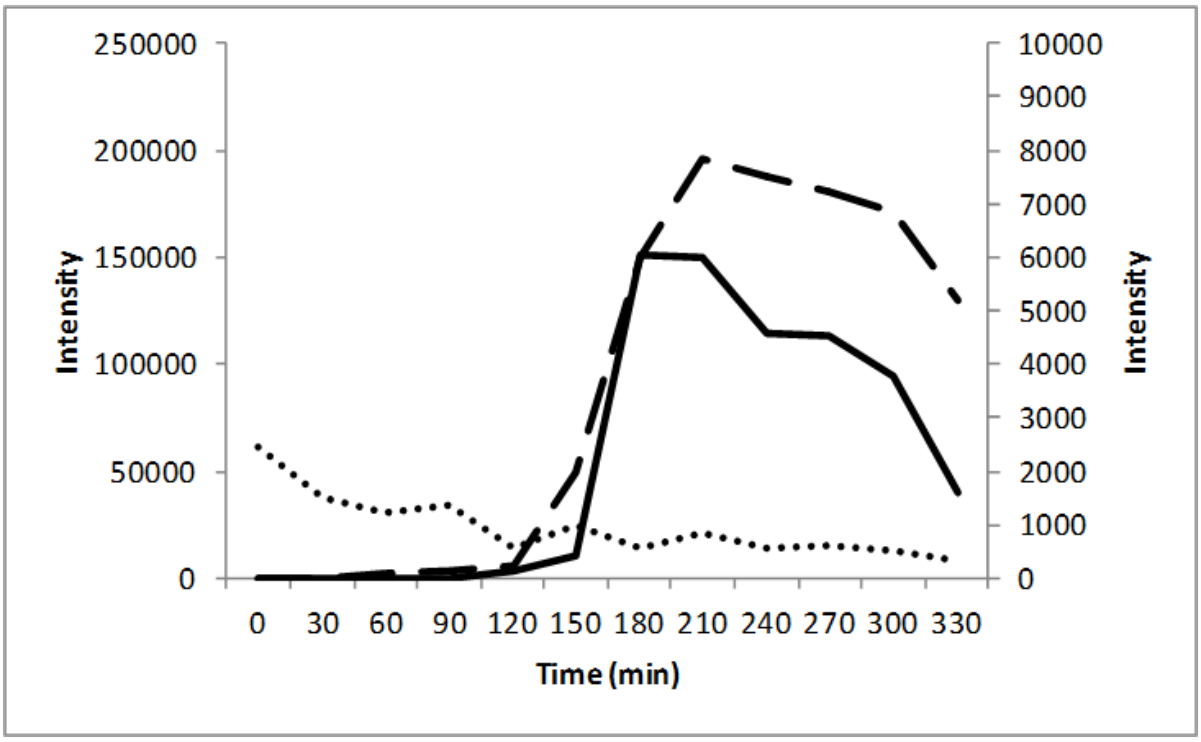

Figure 4. 3 **Variation of ion intensity for the methyl imidazole tagged reactant (*m/z* 299.00, dotted line), intermediate 3 (*m/z* 929.09, solid line, secondary axis) and the product ion of the Pd-catalysed Stille reaction of iodobenzene to styrene (*m/z* 199.12, dashed line).**

Reaction monitoring provides important information about the progress of the reaction and some structural information may be deduced from the *m/z* values of fragment ions obtained by collision-induced dissociation of the intact ions by using MS/MS. However, the three dimensional structures of low level intermediates remain unknown. Combining IM with mass analysis has the potential to provide structural identification of the intermediates by comparing the experimental CCS with data derived from modelled structures. In order to demonstrate this novel approach to structural studies of trace intermediates, we selected the ion mobility spectra for the tagged Pd-containing intermediate $\mathbf{3}_{\mathbf{tag}}$ (**Figure 4.1c**) and the untagged intermediate **3b** (**Figure 4.2c**) were selected for further study. It should, however, be noted that IM-MS data of all ions in the ESI spectrum of the reaction mixture were acquired simultaneously at all points in

the monitoring process and therefore structural information may be extracted for any detected species.

The CCS of **3b** and $\mathbf{3_{tag}}$ were measured by calibrating the effective drift time in the T-wave drift cell of the IM-MS spectrometer used in this study using standards of known CCS and using the resulting calibration graph to determine the CCS of the selected intermediate, as described in Chapter 2.[43-46] It was shown in Chapter 2 that peptides provide good CCS measurements for small organometallic complexes so they were used to measure CCS of **3b** and $\mathbf{3_{tag}}$. The experimentally determined CCS for **3** and **3b**, measured in nitrogen, using peptide calibration standards with CCS_{He} determined using a linear drift tube[47] are given in **Tables 4.1 and 4.2**. The measured CCS for $\mathbf{3_{tag}}$ (204 $Å^2$) is significantly larger than **3b** (178 $Å^2$), as expected from the presence of the iodine and the tagging group.

The experimental data were compared to modelled data (**Tables 4.1 and 4.2**). Molecular structures of species $\mathbf{3_{tag}}$ and **3b** were fully optimized using two density functional theory (DFT) GGA based methods; the hybrid B3LYP[48] (**Appendix 3**) and the non-hybrid B97D[49] which include empirical dispersion corrections. Calculation of the theoretical CCS from the DFT optimized structures were carried out using methods implemented in MOBCAL[36]: projection approximation (PA),[37] exact hard sphere scattering (EHSS)[38] and trajectory method (TM).[39,40]

The relative position of the phosphine groups with respect to the metal center defines isomers *cis* and *trans* for species **3b** (**Figure 4.4**). The optimized structures of both isomers present a T-shape conformation. According to the relative energies obtained through the DFT studies, the *trans* isomer is slightly more stable than the *cis* isomer. At the B97D level, the *trans* is favoured by only 1.0 $kcal.mol^{-1}$, whereas the energy difference increases to 6.0 $kcal.mol^{-1}$ at the B3LYP level. (**Appendices 4 and 5**).

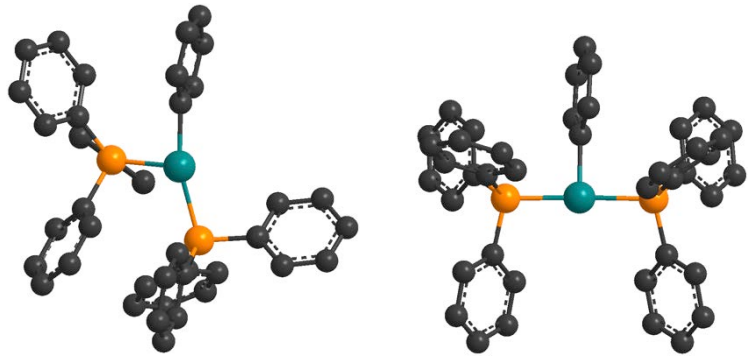

cis *trans*

Figure 4. 4 **Optimized structures of intermediate 3b isomers at B97D/6-311G(d,p) level. Hydrogen atoms omitted for clarity.**

Table 4.1 shows the comparison between the experimental CCS value and the theoretical values calculated for the *cis* and *trans* isomers of species **3b**. The TM correlates well with experimental measurements, followed closely by EHSS whereas, the PA consistently underestimates the CCS values. B97D values are systematically lower than those obtained with B3LYP because all metal-ligand bond lengths are slightly shorter. It is worth noting that small changes in the geometry of the metal complex may significantly affect the calculated CCS by as much as 4 $Å^2$, which is close to the uncertainty of the experimental measurement.

Table 4. 1 **Comparison of experimental and theoretical CCS calculated by the three methods used by MOBCAL for 3b species.**

Experimental $\Omega/Å^2$	Intermediate	Computed $\Omega/Å^2$					
		B3LYP			B97D		
		PA	EHSS	TM	PA	EHSS	TM
178 ± 2	*trans*	169	185	183	167	183	182
	cis	166	181	180	161	174	174

Although the *trans* isomer is the most energetically stable structure, comparison of the theoretical CCS values for *cis* and *trans* isomers indicate that it is not possible to distinguish between the two configurations based on CCS. The variation in the experimental measurements falls in the same order of magnitude as the uncertainty associated with the computed values. Nonetheless, the difference in computed CCS values between the two isomers provides a larger value for the *trans* isomer than for the *cis* isomer.

Species **3** also presents *cis* and *trans* configurations, but taking into account the relative orientation of the 1-methylimidazole moiety, four structures as is depicted in **Figure 4.5** were considered. DFT optimized geometries correspond to square-planar complexes for all the isomers, with intermediate *cis-1* being the most stable structure according to their relative energies. (**Appendices 4 and 5**).

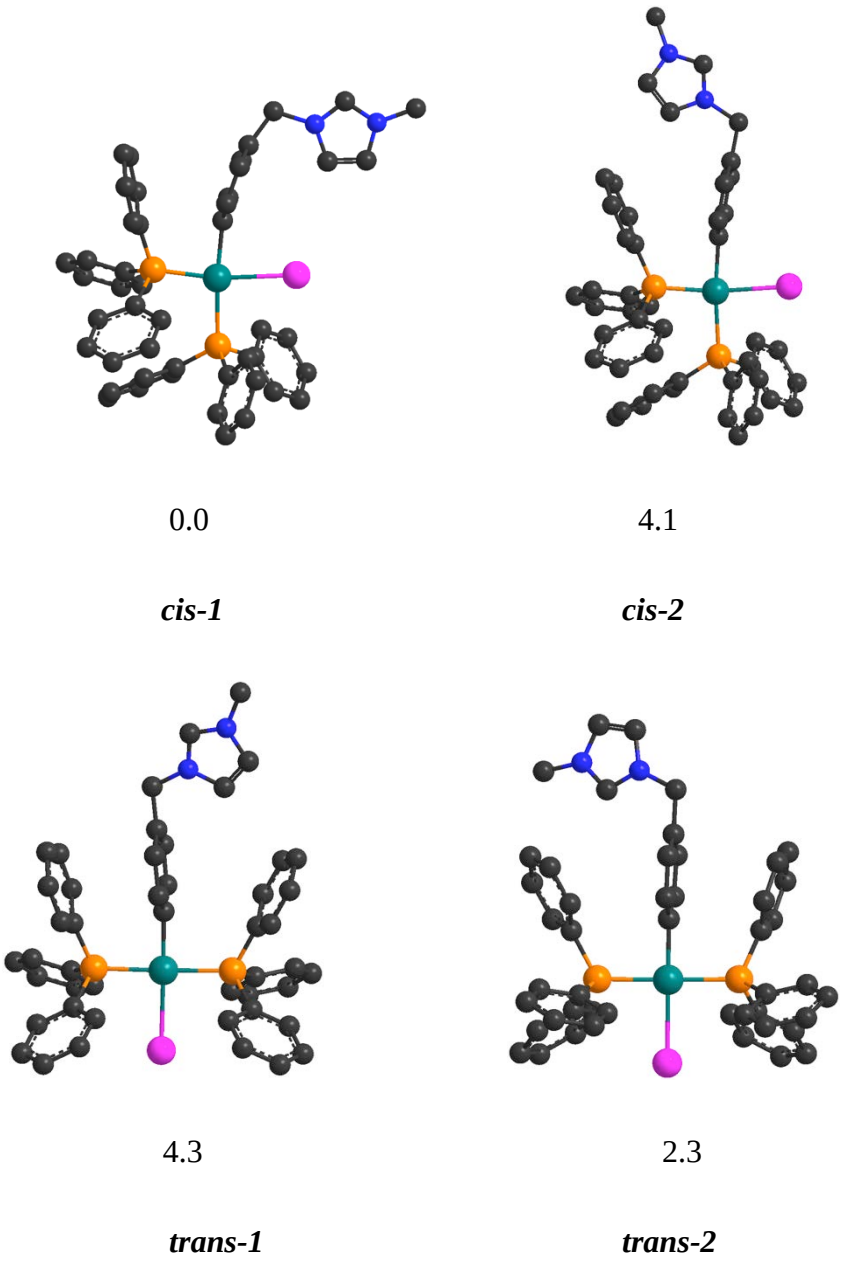

Figure 4. 5 **Optimized structures and relative energies (kcal mol^{-1}) of the different isomers of intermediate 3 at B97D/6-311G(d,p) level. Hydrogen atoms have been omitted for clarity.**

The modelled and experimental results for species $\mathbf{3}_{\mathbf{tag}}$ are shown in **Table 4.2**. Both DFT methods show the PA to give systematically lower values than the EHSS and TM. The B3LYP method results in systematically larger CCS values than the B97D method. The computed CCS values for the four isomers fall in a very narrow range, 4 Å^2 on

average. The DFT method used has a more pronounced effect on CCS than the integration method EHSS or TM. This is because, in these particular systems, B97D reproduces the **π**-stacking interactions between the phenyl rings in the structures better than B3LYP, thus small differences in the geometries are obtained. In any case, uncertainty regarding the method used is also approximately 4 $Å^2$.

Table 4. 2 Experimental and theoretical CCS values for species 3_{tag}.

Experimental Ω/$Å^2$	Intermediate	Modelled Ω/$Å^2$					
		B3LYP			B97D		
		PA	EHSS	TM	PA	EHSS	TM
204 ± 3	*trans*-1	194	212	210	191	209	207
	trans-2	194	212	211	189	206	205
	cis-1	193	210	208	188	204	203
	cis-2	192	209	207	188	203	202

In conclusion the accuracy of both the experimental setup and the computational methodology reached the same level and the agreement between the measured and computed values are excellent. Due to the similarity of the size and shape of the different isomers, isomeric resolution could not be achieved, however, where more bulky and sophisticated phosphine and phosphite ligands are commonly used, we envision new opportunities to improve the selectivity of this technique.

ESI is a soft ionisation technique which provides information on the composition of reaction solutions in which solution phase structure is conserved in the gas phase.[50] This is supported by many experiments showing that the gross reactivity of reactions in the gas-phase resembles that of solution-phase.[51] The time between ionisation and detection of an analyte during MS analysis means that little structural change can occur. In this

work, analysis is undertaken using IM-MS in which multiple collisions occur with an inert gas in the drift cell before the ions enter the vacuum of the mass analyser. Energy is lost upon collision and any reactions or changes in structure are unlikely once the ions enter the drift cell. The similarity observed between the theoretical and experimental measurements demonstrates that molecular structure is conserved during the ionization and IM-MS analysis for small molecules, which has been shown for the limited number of small molecule studies reported to date.[42]

4.5 CONCLUSIONS

We have demonstrated proof of principle that ion mobility measurements of collision cross section, combined with mass spectrometry, can provide simultaneous structural information on reactants, intermediates and products present in a reaction mixture, including low level catalytic species that cannot be studied by other techniques. This novel approach to reaction understanding has the potential to provide new insights into the nature of catalytic and other reactions, the study of transient species and transition states.

4.6 CHAPTER FOUR REFERENCES

1. Naga, S., Kidani, Y., Koike, H., *Bulletin of the Chemical Society of Japan*, 1975, **48**, 863.
2. Gianelli, L., Amendola, V., Fabbrizzi, L., Pallavicini, P., Mellerio, G.G., *Rapid Commun, Mass Spectrom.*, 2001, **15**, 2347.
3. Pakarinen J.M.H., Vainiotalo, P., *Rapid Commun. Mass Spectrom.*, 2009, **23**, 1767.
4. Agrawal, D., Schröder, D., Sale, D.A., Lloyd-Jones, G.C., *Organometallics*, 2010, **29**, 3979.
5. Jirásko, R., Holčapek, M., Kolářová, L., Basu Baul, T.S., *J. Mass Spectrom.*, 2007, **42**, 918-928.
6. Gimbert, Y., Lesage, D., Milet, A., Fournier, F., Greene, A.E., Tabet, J.C., *Org. Lett*, 2003, **5**, 4073.
7. He, J., Abliz, Z., Zhang, R., Liang, Y., Ding, K., *Anal. Chem.*, 2006, **78**, 4737.
8. Hughes, L., Wyatt, M.F., Stein, B.K., Brenton, A.G., *Anal. Chem.*, 2009, **81**, 543.
9. Vitalini, D., Spina, E., Rapisardi, R., Scamporrino, E., Mineo, P., *Rapid Commun. Mass Spectrom.*, 2006, **20**, 2961.
10. Borges, D.L.G., Sturgeon, R.E., Welz, B., Curtius, A.J., Mester, Z., *Anal. Chem.*, 2009, **81**, 9834.
11. Damrauer, R., *Organometallics*, 2004, **23**, 1462.
12. Arakawa, R., Mimura, Si., Matsubayashi, Ge, and Matsuo, T., *Inorg. Chem.*, 1996, **35**, 5725.
13. Brum J., Dell'Orco, P., *Rapid Commun. Mass Spectrom.*, 1998, **12**, 741.

14. Modestov, A.D., Gun, J., Savotine, I., Lev, O., *J. Electroanal. Chem.*, 2004, **565**, 7-19.
15. Ding, W., Johnson, K.A., Amster, I.J., Kutal, C., *Inorg. Chem.*, 2001, **40**, 6865.
16. Weston, D.J., Bateman, R., Wilson, I.D., Wood, T.R., Creaser, C.S., *Anal. Chem.*, 2005, **77**, 7572.
17. Colton, R., D'Agostino, A., Traeger, J.C., *Mass Spectrom. Rev.*, 1995, **14**, 79.
18. Henderson, W., Nickleson, B.K., McCaffrey, L.J., *Polyhedron*, 1998, **17**, 4291.
19. Aliprantis, A.O., Canary, J.W., *J. Am. Chem. Soc.*, 1994, **116**, 6985.
20. Adlhart, C., Chen, P., *Helv. Chim. Acta.*, 2000, **83**, 2192.
21. Vikse, K.L., Ahmadi, Z., Manning, C.C., Harrington, D.A., Mcindoe, J.S., *Angew. Chem. Int. Ed.*, 2011, **50**, 8304.
22. Hinderling, C., Adlhart, C., Chen, P., *Angew. Chem. Int. Ed.*, 1998, **37**, 2658.
23. Aliprantis A.O., and Canary, J.W., *J. Am. Chem. Soc.*, 1994, **116**, 6985.
24. Zawartka, Gniewek, W.A., Trzeciak, A.M., Ziółkowski, J.J., Pernak, J., *Journal Mol. Catal. A: Chem.*, 2009, **304**, 8.
25. Cella, R., Cunha, R.L.O.R., Reis, A.E.S., Pimenta, D.C., Klitzke, C.F., Stefani, H.A., *J. Org. Chem.*, 2006, **71**, 244.
26. Santos, L.S., Rosso, G.B., Pilli, R.A., Eberlin, M.N., *J. Org. Chem.*, 2007, **72**, 5809.
27. *Reactive Intermediates: MS Investigations in* Solution (Ed.: L. S. Santos), Whiley, Weinham, 2010, 63.
28. Tewari, J., Dixit, V., Malik, K., *Sensors and Actuators B: Chemical*, 2010, **144**, 104.
29. Hammond, J., Moffat, C.A., Jee, R.D., Kellam, B., *Anal. Comm.*, 1999, **36**, 127.
30. Gibson, S.E., Hardick, D.J., Haycock, P.R., Kaufmann, K.A.C., Miyazaki, A., Tozer, M.J., White, A.J.P., *Chem. Eur. J.*, 2007, **13**, 7099.
31. Radhakrishna, T., Screenivas Rao, D., Om Reddy, G., *J. Pharm. Biomed. Anal.*, 2001, **26**, 617.

32. Harry, E.L., Bristow, A.W.T., Wilson, I.D., Creaser, C.S., *Analyst*, 2011, **136**, 1728.

33. Espinet, P., Echavarren, A.M., *Angew. Chem. Int. Ed*., 2004, **43**, 4704.

34. Nova, A., Ujaque, G., Maseras, F., Lledos, A., Espinet, P., *J. Am. Chem. Soc*., 2006, **128**, 14571.

35. www.indiana.edu/~nano/Software/mobcal.txt

36. Gaussian 09, Revision **A.1**, M. J. Frisch, G. W. Trucks, H. B. Schlegel, G. E. Scuseria, M. A. Robb, J. R. Cheeseman, G. Scalmani, V. Barone, B. Mennucci, G. A. Petersson, H. Nakatsuji, M. Caricato, X. Li, H. P. Hratchian, A. F. Izmaylov, J. Bloino, G. Zheng, J. L. Sonnenberg, M. Hada, M. Ehara, K. Toyota, R. Fukuda, J. Hasegawa, M. Ishida, T. Nakajima, Y. Honda, O. Kitao, H. Nakai, T. Vreven, J. A. Montgomery, Jr., J. E. Peralta, F. Ogliaro, M. Bearpark, J. J. Heyd, E. Brothers, K. N. Kudin, V. N. Staroverov, R. Kobayashi, J. Normand, K. Raghavachari, A. Rendell, J. C. Burant, S. S. Iyengar, J. Tomasi, M. Cossi, N. Rega, J. M. Millam, M. Klene, J. E. Knox, J. B. Cross, V. Bakken, C. Adamo, J. Jaramillo, R. Gomperts, R. E. Stratmann, O. Yazyev, A. J. Austin, R. Cammi, C. Pomelli, J. W. Ochterski, R. L. Martin, K. Morokuma, V. G. Zakrzewski, G. A. Voth, P. Salvador, J. J. Dannenberg, S. Dapprich, A. D. Daniels, Ö. Farkas, J. B. Foresman, J. V. Ortiz, J. Cioslowski, and D. J. Fox, Gaussian, Inc., Wallingford CT, 2009.

37. Von Heldon, G., Hsu, M.T., Gotts, N., Bowers, M.T., *J. Phys. Chem.*, 1993, **97**, 8182.

38. Shvartsburg, A.A., Jarrold, M.F., *Chem. Phys. Lett.*, 1996, **261**, 86.

39. Mesleh, M.F., Hunter, J.M., Shvartsburg, A.A., Schatz, G.C., Jarrold, M.F., *J. Phys. Chem.*, 1996, **100**, 16082.

40. Wyttenbach, T., Bushnell, J.E., Bowers, M.T., *J. Am. Chem. Soc.*, 1998, **120**, 5098.

41. Siu, C., Guo, Y., Saminathan, I.S., Hopkinson, A.C., Siu, K.W.M., *J. Phys. Chem.*, 2010, **114**, 1204.

42. Campuzano, I., Bush, M.F., Robinson, C.V., Beaumont, C., Richardson, K., Kim, H., Kim, H.I., *Anal. Chem.*, 2012, **84**, 1026.

43. Ruotolo, B., Benesch, J.L.P., Sanderock, A.M., Hyung, S.J., Robinson, C.V., *Nature Protocols*, 2008, **3**, 1139.

44. Smith, D.P., Knapman, T.W., Campuzano, I., Malham, R.W., Berryman, J.T., Radford, S.E., Ashcroft, A.E., *Euro J. Mass Spectrom.*, 2009, **15**, 113.

45. Scarff, C.A., Thalassinos, K., Hilton, G.R., Scrivens, J.H., *Rapid commun. Mass Spectrom.*, 2008, **22**, 3297.

46. Thalassinos, K., Grabenauer, M., Slade, S.E., Hilton, G.R., Bowers, M.T., Scrivens, J.H., *Anal. Chem.*, 2009, **81**, 248.

47. Kaur-Atwal, G., O'Connor, G., Aksenov, A.A., Bocos-Bintintan, V., Thomas, C.L., Creaser, C.S., *Int. J. Mobil. Spec.*, 2009, **12**, 1.

48. a).Becke, A.D., *J. Chem. Phys.*, 1993, **98**, 5648; b) Lee, C., Yang, W., Parr, R.G., *Phys. Rev. B*, 1988, **37**, 785.

49. Grimme, S., *J. Comp. Chem.*, 2006, **27**, 1787.

50. a) *Reactive Intermediates: MS Investigations in* Solution (Ed.: L. S. Santos), Whiley, Weinham, 2010; b) Santos, L.S., Pavam, C.H., Almeida, W.P., Coelho, F., Eberlin, M.A., *Angew. Chem.. Int. Ed.*, 2004, **43**, 4330.

51. Chen, P., *Angew. Chem. Int. Ed.*, 2003, **42**, 2832.

CHAPTER 5

CONCLUSIONS AND FURTHER WORK

5.1 THESIS OVERVIEW

The work presented in this thesis describes the use of ion mobility-mass spectrometry (IM-MS) to derive structural information for organic and organometallic complexes by the measurement of collision cross sections (CCS). CCS have been compared with theoretical modelled and x-ray structures. This approach has been applied to reaction monitoring of organic and organometallic catalytic cycles to aid the identification of components within reaction mixtures including low level intermediates.

5.1.1 IM-MS analysis of salen ligands and complexes

Chapter 2 describes the use of DTIMS and TWIMS to determine the CCS of three salen ligand species (containing nitrogen and oxygen binding atoms) and their complexes with copper and zinc. TWIMS measurements were carried out in nitrogen, using TAAH and peptide calibration compounds, with reported helium-derived CCS, to calibrate the TWIMS drift cell. TWIMS measurements gave larger CCS than DTIMS in helium, by 9% using TAAH calibration and 3% using peptide calibration, indicating that the choice of calibration standards influences the CCS obtained. Peptide standards may be better for measurements of small ligands and their metal complexes. The experimental CCS were compared with theoretical cross sections determined using modified MOBCAL calculations from molecular geometries derived from *in-silico* modelling (modelled at ICIQ, Tarragona) and x-ray data. CCS data calculated from modelled structures showed good correlation with experimental CCS measurements made by DTIMS in helium and TWIMS measurements made in nitrogen, when peptide calibrants were used for the TWIMS measurements.

Further work in this area could focus on trying other calibration sets to explore the effect of calibrant structure on TWIMS CCS measurements. It would also be interesting

to analyse these ligands using other TWIMS wave heights and drift gases to observe how the CCS change with differing IMS parameters.

5.1.2 IM-MS monitoring of an organocatalytic reaction

Chapter 3 describes the monitoring of enantioselective imidazolidinone catalysed Diels-Alder cycloaddition reaction by IM-MS using on-line direct infusion and by off-line and on-line dilution of aliquots removed from a reaction mixture. The reactant, product, catalyst and intermediates were detected, including an intermediate not previously observed in the reaction mixture. IM-MS was used to monitor the catalyst and intermediates over a 24 hour period by removing aliquots from the reaction mixture at specific time intervals. The CCS of the reactive species were determined via TWIMS using peptide standards, varying wave heights and power and linear calibration plots. The CCS determined from the linear trendlines using the ramped wave heights produced the most consistent results. TAAH standards were used to determine CCS which were compared to those obtained using peptide standards. The TAAH standards gave significantly larger (4%) results than the peptide standards. The reaction was also monitored using FAIMS-MS which showed separation between the catalyst and intermediates but not between intermediate 1 and intermediate 2 due to their similarity in functional groups.

To develop this work further modelled data could be obtained for the reactant, catalyst, intermediates and product, the CCS calculated and then compared to experimental data. This work could also be extended to monitoring of other organocatalytic reactions. Reaction monitoring using FAIMS-MS could be attempted using other reactions which

have intermediates containing different functional groups which will therefore be separated using FAIMS-MS.

5.1.3 IM-MS reaction monitoring of an organometallic catalysed reaction

Chapter 4 extends the proof of principle demonstrated for an organocatalytic cycle in Chapter 3, that ion mobility measurements of CCS combined with mass spectrometry, can provide simultaneous structural information on reactants, intermediates and products present in a reaction mixture, including low level catalytic species that cannot be studied by other techniques. A reaction mixture for an organometallic catalysed reaction of palladium was studied by IM-MS. In cases where components are not amenable to ionisation in the ESI source an ionisable tag was added which has enabled the detection of these species. The CCS of intermediates have been determined for a palladium catalysed Stille reaction and compared to CCS calculated using MOBCAL from coordinates obtained from modelled structures. Good agreement was obtained between modelled and calculated CCS.

In this work an ionisable tag was used to aid detection which changed the structure of the component of interest. This can be undesirable in industrial applications and therefore further work could be carried out to investigate alternative tags which could be incorporated into the catalyst, such as the PPh_3 ligand rather than the reactant. It would also be of interest to study other organometallic catalytic cycles with isomeric species and explore the potential of ion mobility to distinguish between the isomers.

APPENDICES

Appendix 1 – Presentations and Publications

Publications

Structural Studies of Metal Ligand Complexes by IM-MS, V. E. Wright, F. Castro-Gomez, E. Jurneczko, J. C. Reynolds, A. Poulton, S. D. R. Christie, P. Barran, C. Bo, C. S. Creaser, *Int. J. Mobil. Spec.,* **2013,** 16, 61-67.

Presentations

- Ion Mobility-Mass Spectrometry Studies of Metal-Ligand Complexes. Presented at Structure 2010, Hinckley, 2010. (poster)

- Studies of Metal-Ligand complexes using Ion Mobility-Mass Spectrometry. Presented at Royal Society of Chemistry Analytical Research Forum, Loughborough, 2010. (poster)

- Determination of Collision Cross Sections for Metal-Ligand Complexes using Ion Mobility-Mass Spectrometry. Presented at the 31st 3 day meeting of the British Mass Spectrometry Society, Cardiff, 2010. (poster)

- A New Approach for Structural Analysis of Metal-Ligand Complexes using Ion Mobility-Mass Spectrometry. Presented at AstraZeneca annual PhD meeting, Macclesfield, 2010. (poster)

- The Application of Ion Mobility-Mass Spectrometry to Reaction Monitoring. Presented at the 32nd 3 day meeting of the British Mass Spectrometry Society, Cardiff, 2011. (oral)

- Reaction Monitoring using Ion Mobility-Mass Spectrometry. Presented at AstraZeneca annual PhD meeting, Macclesfield, 2011. (oral and poster)

- Monitoring of an Imidazolidinone-Catalysed Reaction using Ion Mobility-Mass Spectrometry. Presented at the 33rd 2 day meeting of the British Mass Spectrometry Society, Aderley Park, 2012 and 60th conference for the American Society for Mass Spectrometry, May 2012. (posters)

Appendix 2 - Cartesian coordinates and energies of all optimized species for ligands and metal complexes.

L1

Cartesian Coordinates				Mulliken Atomic Charges	
N	-1.324375	0.872207	-0.484535	N	-0.481562
N	1.245808	0.793964	0.398471	N	-0.583113
C	-2.598020	0.650455	-0.334390	C	0.186008
H	-3.249049	1.519317	-0.282340	H	0.171194
C	2.502469	0.707620	0.112034	C	0.180384
H	3.117589	1.596802	-0.060042	H	0.117697
C	-3.210030	-0.641745	-0.201675	C	0.060564
C	-4.485991	-3.087665	0.264715	C	-0.069567
C	-2.465850	-1.855802	-0.180296	C	0.341658
C	-4.610642	-0.701148	-0.005099	C	-0.117534
C	-5.245527	-1.908957	0.222111	C	-0.085712
C	-3.107068	-3.068307	0.064923	C	-0.103939
H	-5.183427	0.221587	-0.025054	H	0.127579
H	-6.318259	-1.944955	0.372451	H	0.136749
H	-2.530527	-3.987911	0.082720	H	0.131914
H	-4.977994	-4.037533	0.448552	H	0.144255
C	3.199017	-0.563110	0.006765	C	0.058380
C	4.602036	-2.977397	-0.215036	C	-0.079369
C	4.550180	-0.579592	-0.395894	C	-0.132803
C	2.564642	-1.797111	0.310220	C	0.302049
C	3.273663	-2.995398	0.197797	C	-0.098173
C	5.249651	-1.770239	-0.513273	C	-0.090568
H	5.039568	0.364762	-0.619907	H	0.106296
H	2.771595	-3.925037	0.443375	H	0.107958
H	6.287061	-1.768572	-0.828444	H	0.114858
H	5.143373	-3.914578	-0.299982	H	0.119826
O	1.272503	-1.835061	0.724795	O	-0.609277
C	-0.592649	2.150360	-0.521443	C	0.062042
C	-0.625048	4.662536	-0.382165	C	-0.196678
C	1.403153	3.364512	0.426524	C	-0.210074
C	0.531659	4.615650	0.624221	C	-0.198883
C	0.560889	2.083032	0.527968	C	0.084819
C	-1.475943	3.382389	-0.326367	C	-0.213555
H	-0.226522	4.787080	-1.397263	H	0.117519
H	1.891068	3.413856	-0.556165	H	0.113138
H	0.131839	4.623780	1.646749	H	0.114157
H	0.079996	2.067139	1.517454	H	0.123590
H	-1.980251	3.320465	0.647699	H	0.117638
H	-0.124973	2.188786	-1.515095	H	0.146534
H	-1.265025	5.528927	-0.190897	H	0.129069
H	2.198032	3.335919	1.179383	H	0.130081
H	1.150136	5.512998	0.526560	H	0.128402
H	-2.252800	3.418899	-1.099137	H	0.123409
H	0.972003	-0.887897	0.786228	H	0.350570
O	-1.140972	-1.752363	-0.433124	O	-0.582108
H	-0.577082	-2.464052	-0.081514	H	0.357337
H	-0.722183	0.045934	-0.516097	H	0.347242

Energy = -649960.05 kcal mol^{-1}

L2

Cartesian Coordinates				Mulliken Atomic Charges	
H	2.465640	3.426819	0.407224	H	0.125143
C	1.392836	3.455059	0.250286	C	-0.100467

C	-1.392923	3.546679	-0.030696	C	-0.089360
C	0.682754	2.248866	0.147946	C	0.284930
C	0.730009	4.676938	0.194318	C	-0.078666
C	-0.661354	4.725358	0.049021	C	-0.094888
C	-0.728488	2.317530	0.021110	C	0.276372
H	1.296961	5.598003	0.279879	H	0.133046
H	-1.174565	5.679860	0.013919	H	0.131354
H	-2.472543	3.593321	-0.124667	H	0.117375
N	1.272547	0.977410	0.215421	N	-0.657073
N	-1.390692	1.072870	-0.044805	N	-0.584067
C	2.454191	0.773623	-0.291151	C	0.170630
H	2.967650	1.575370	-0.833927	H	0.124556
C	-2.662589	0.796847	-0.201545	C	0.180226
H	-3.336937	1.635794	-0.347087	H	0.169400
C	3.158303	-0.481076	-0.208665	C	0.055475
C	4.589472	-2.888011	-0.120439	C	-0.076330
C	4.418731	-0.600122	-0.839012	C	-0.128524
C	2.631372	-1.610663	0.477334	C	0.302216
C	3.355122	-2.805490	0.514079	C	-0.098004
C	5.130514	-1.785586	-0.800739	C	-0.090803
H	4.823180	0.263186	-1.360631	H	0.112039
H	2.938201	-3.650474	1.051150	H	0.114792
H	6.095731	-1.862986	-1.288238	H	0.119358
H	5.143222	-3.820978	-0.082073	H	0.124642
C	-3.236930	-0.513343	-0.185264	C	0.057223
C	-4.494749	-3.016727	-0.105531	C	-0.069559
C	-2.485192	-1.700159	0.054750	C	0.346752
C	-4.634524	-0.632505	-0.387984	C	-0.117626
C	-5.258412	-1.865893	-0.351919	C	-0.086408
C	-3.118346	-2.939862	0.097586	C	-0.107378
H	-5.214650	0.267102	-0.571412	H	0.128098
H	-6.327939	-1.943806	-0.508843	H	0.137203
H	-2.535410	-3.836722	0.284720	H	0.128106
H	-4.978848	-3.987518	-0.072570	H	0.144297
O	1.432939	-1.562927	1.104501	O	-0.589476
O	-1.154124	-1.537508	0.228758	O	-0.580262
H	-0.758890	0.273843	0.063456	H	0.356111
H	1.109658	-0.632615	1.048209	H	0.353668
H	-0.662745	-2.335471	0.479597	H	0.355877

Energy = -647683.25 kcal mol^{-1}

L3

Cartesian Coordinates				Mulliken Atomic Charges	
N	-1.320180	1.705753	-0.408189	N	-0.444434
N	1.258301	1.571739	0.470247	N	-0.544364
C	-2.604220	1.537045	-0.271852	C	0.183688
H	-3.210923	2.439321	-0.208323	H	0.174894
C	2.525225	1.530006	0.218616	C	0.176341
H	3.105746	2.456051	0.106983	H	0.115316
C	-3.274226	0.274203	-0.177178	C	0.057378
C	-4.674501	-2.124856	0.157786	C	-0.067921
C	-2.584739	-0.973572	-0.163934	C	0.345918
C	-4.683074	0.272247	-0.029518	C	-0.115083
C	-5.378902	-0.911452	0.132368	C	-0.085490
C	-3.289303	-2.162448	0.011903	C	-0.104541
H	-5.212851	1.220377	-0.039895	H	0.131843
H	-6.456847	-0.903471	0.243944	H	0.140385
H	-2.756340	-3.108297	0.024472	H	0.133231
H	-5.214747	-3.056973	0.289508	H	0.147848
C	3.259064	0.289260	0.073593	C	0.053671
C	4.725505	-2.074609	-0.236566	C	-0.078180
C	4.630025	0.328177	-0.256962	C	-0.130530

C	2.634758	-0.975179	0.257281	C	0.304306
C	3.377873	-2.148199	0.099190	C	-0.097206
C	5.361572	-0.837214	-0.415111	C	-0.091433
H	5.107560	1.295429	-0.389999	H	0.108941
H	2.885038	-3.102527	0.249980	H	0.108212
H	6.414088	-0.794541	-0.671662	H	0.116149
H	5.292296	-2.992852	-0.355788	H	0.120771
O	1.325605	-1.069683	0.594422	O	-0.605015
C	-0.564677	2.959057	-0.409204	C	-0.082925
C	0.588999	2.853237	0.613159	C	-0.057549
H	0.172418	2.921244	1.625423	H	0.147937
H	-0.158854	3.101654	-1.416545	H	0.171103
H	0.999795	-0.140566	0.722073	H	0.350481
O	-1.245116	-0.920965	-0.339169	O	-0.577144
H	-0.757399	-1.730492	-0.115383	H	0.360018
H	-0.744423	0.861769	-0.450667	H	0.352685
H	-1.232919	3.792028	-0.178280	H	0.152285
H	1.261337	3.710358	0.466301	H	0.128413

Energy = -552027.22 kcal mol^{-1}

L1Zn

Cartesian Coordinates				Mulliken Atomic Charges	
N	1.312829	0.835768	0.317055	N	-0.569536
N	-1.332743	0.894852	-0.312251	N	-0.622300
C	2.591780	0.741281	0.204425	C	0.145771
H	3.202687	1.645283	0.246079	H	0.139626
C	-2.625196	0.746121	-0.374428	C	0.142536
H	-3.249297	1.615833	-0.598123	H	0.122786
C	3.370112	-0.481800	0.025579	C	0.093342
C	5.091101	-2.693876	-0.305619	C	-0.071075
C	2.861435	-1.787728	-0.158405	C	0.322470
C	4.774368	-0.335459	0.027826	C	-0.132290
C	5.629531	-1.417629	-0.130619	C	-0.078650
C	3.708226	-2.877590	-0.321980	C	-0.125733
H	5.187871	0.659867	0.162342	H	0.126944
H	6.703657	-1.270707	-0.120340	H	0.136691
H	3.290313	-3.871219	-0.463737	H	0.126321
H	5.742557	-3.552230	-0.432762	H	0.142816
C	-3.348861	-0.479430	-0.167968	C	0.040519
C	-5.015757	-2.712391	0.214450	C	-0.067959
C	-4.762360	-0.386617	-0.306497	C	-0.122519
C	-2.766692	-1.755402	0.177128	C	0.374935
C	-3.647290	-2.847339	0.362247	C	-0.124820
C	-5.590414	-1.472080	-0.124538	C	-0.101204
H	-5.189285	0.579540	-0.564868	H	0.100225
H	-3.203003	-3.801258	0.626439	H	0.108966
H	-6.664356	-1.373933	-0.237405	H	0.110795
H	-5.654796	-3.577968	0.364541	H	0.116147
O	1.487625	-1.986214	-0.187927	O	-0.624348
O	-1.472381	-1.983152	0.333726	O	-0.744496
C	0.616406	2.141006	0.472571	C	0.058609
C	0.635545	4.668833	0.505269	C	-0.193405
C	-1.437387	3.442724	-0.291476	C	-0.202377
C	-0.566464	4.699058	-0.444542	C	-0.192304
C	-0.614441	2.162845	-0.493805	C	0.091749
C	1.478807	3.396949	0.309906	C	-0.207156
H	0.285892	4.715625	1.544979	H	0.112464
H	-1.894722	3.421330	0.707109	H	0.115842
H	-0.213807	4.774899	-1.481726	H	0.109630
H	-0.210516	2.165136	-1.518623	H	0.127671
H	1.930858	3.405388	-0.691696	H	0.113276
H	0.206169	2.124969	1.493842	H	0.141110

H	1.267752	5.548638	0.350531	H	0.124433
H	-2.255799	3.476208	-1.018179	H	0.123280
H	-1.174096	5.589971	-0.258032	H	0.125624
H	2.298818	3.391162	1.037158	H	0.118789
Zn	-0.131707	-0.653681	0.162414	Zn	1.087167
H	1.267086	-2.924391	-0.297097	H	0.379634

Energy = -690391.31 kcal mol^{-1}

L2Zn

Cartesian Coordinates				Mulliken Atomic Charges	
H	2.479732	3.594970	0.042965	H	0.119078
C	1.396615	3.556351	0.017550	C	-0.101911
C	-1.392978	3.508783	-0.119914	C	-0.101447
C	0.737074	2.317688	0.009168	C	0.292959
C	0.678016	4.744770	-0.026392	C	-0.083899
C	-0.719139	4.723115	-0.101805	C	-0.091005
C	-0.688785	2.297034	-0.046284	C	0.251724
H	1.207700	5.691824	-0.021736	H	0.129464
H	-1.278243	5.650544	-0.163764	H	0.126856
H	-2.472704	3.512398	-0.220292	H	0.112939
N	1.380269	1.068902	0.020143	N	-0.699146
N	-1.317978	1.020319	-0.061009	N	-0.637062
C	2.669858	0.872336	0.178143	C	0.125772
H	3.315424	1.735088	0.359468	H	0.128737
C	-2.589861	0.865037	0.149667	C	0.127512
H	-3.198348	1.741805	0.378284	H	0.139486
C	3.342097	-0.386101	0.142084	C	0.040068
C	4.922880	-2.714359	0.092173	C	-0.065413
C	4.756791	-0.333591	0.326443	C	-0.118227
C	2.716884	-1.676003	-0.067099	C	0.380647
C	3.556482	-2.815490	-0.087357	C	-0.123227
C	5.539894	-1.463147	0.303669	C	-0.100988
H	5.216056	0.638880	0.485596	H	0.104903
H	3.081028	-3.777214	-0.248330	H	0.109831
H	6.612821	-1.395698	0.444434	H	0.115538
H	5.530102	-3.614813	0.070297	H	0.120770
C	-3.348744	-0.373446	0.127892	C	0.094990
C	-5.050451	-2.629811	0.137806	C	-0.071538
C	-2.845026	-1.680557	-0.070897	C	0.321617
C	-4.742922	-0.254251	0.337030	C	-0.132258
C	-5.586093	-1.355804	0.341058	C	-0.078228
C	-3.679767	-2.790710	-0.067137	C	-0.123359
H	-5.156139	0.737434	0.496084	H	0.128107
H	-6.650454	-1.226770	0.502113	H	0.137778
H	-3.262045	-3.782065	-0.224028	H	0.127024
H	-5.694186	-3.503196	0.138516	H	0.143684
O	1.423097	-1.865955	-0.234045	O	-0.742985
O	-1.482985	-1.854611	-0.267410	O	-0.627968
Zn	0.117195	-0.484721	-0.229308	Zn	1.138644
H	-1.240458	-2.792638	-0.317451	H	0.380531

Energy = -688113.83 kcal mol^{-1}

L3Zn

Cartesian Coordinates				Mulliken Atomic Charges	
N	-1.307510	1.542043	-0.316042	N	-0.532957
N	1.336479	1.605864	0.289766	N	-0.593341
C	-2.589941	1.481705	-0.222012	C	0.144801

H	-3.168432	2.411109	-0.269283	H	0.141854
C	2.633269	1.485005	0.323995	C	0.140833
H	3.236952	2.385145	0.490076	H	0.126021
C	-3.394429	0.277724	-0.057967	C	0.088077
C	-5.151744	-1.906747	0.242845	C	-0.069929
C	-2.905815	-1.037148	0.123301	C	0.324155
C	-4.795971	0.448292	-0.073258	C	-0.128973
C	-5.669045	-0.621292	0.070336	C	-0.078526
C	-3.771989	-2.113457	0.271932	C	-0.125266
H	-5.191390	1.451122	-0.206109	H	0.130462
H	-6.740628	-0.458005	0.050404	H	0.139472
H	-3.372945	-3.115110	0.411683	H	0.128161
H	-5.817873	-2.755441	0.358294	H	0.145188
C	3.367463	0.263965	0.155698	C	0.038889
C	5.041958	-1.971591	-0.158978	C	-0.067122
C	4.782907	0.374007	0.262197	C	-0.119300
C	2.786815	-1.030039	-0.124100	C	0.376105
C	3.672272	-2.122950	-0.276170	C	-0.123370
C	5.614289	-0.713307	0.113219	C	-0.101097
H	5.206470	1.353640	0.469971	H	0.103665
H	3.231264	-3.090815	-0.490084	H	0.110427
H	6.689434	-0.604039	0.201276	H	0.113314
H	5.684732	-2.838673	-0.281730	H	0.118252
O	-1.534532	-1.260664	0.165827	O	-0.624753
O	1.492182	-1.273016	-0.252972	O	-0.743863
C	-0.622614	2.838340	-0.464083	C	-0.077537
C	0.635839	2.874942	0.435782	C	-0.048279
H	0.327170	3.003822	1.481639	H	0.148675
H	-0.312871	2.928241	-1.512620	H	0.163948
Zn	0.131211	0.039750	-0.125788	Zn	1.094518
H	1.258445	3.735115	0.160707	H	0.139446
H	-1.291332	3.674172	-0.230001	H	0.138193
H	-1.338883	-2.203395	0.284070	H	0.379855

Energy = -592460.69 kcal mol^{-1}

L1Cu

Cartesian Coordinates				Mulliken Atomic Charges	
N	1.293928	0.876183	0.258676	N	-0.498228
N	-1.336714	0.915185	-0.208187	N	-0.534121
C	2.569589	0.737201	0.154153	C	0.147506
H	3.203789	1.625834	0.175217	H	0.143651
C	-2.621207	0.730905	-0.288783	C	0.152630
H	-3.256119	1.597799	-0.486439	H	0.136332
C	3.304732	-0.513170	0.003349	C	0.083578
C	4.912344	-2.804993	-0.315052	C	-0.072364
C	2.749198	-1.811678	0.059561	C	0.336997
C	4.696537	-0.413256	-0.208143	C	-0.131966
C	5.495620	-1.536784	-0.370233	C	-0.079767
C	3.541257	-2.943391	-0.097256	C	-0.122186
H	5.143701	0.575905	-0.247700	H	0.125061
H	6.561700	-1.429368	-0.535655	H	0.134772
H	3.089949	-3.930821	-0.046119	H	0.127041
H	5.522359	-3.694035	-0.437401	H	0.141007
C	-3.310553	-0.515011	-0.144924	C	0.033933
C	-4.828363	-2.860093	0.092881	C	-0.068209
C	-4.729431	-0.484815	-0.230577	C	-0.120547
C	-2.646898	-1.773109	0.064006	C	0.408078
C	-3.449593	-2.932648	0.178523	C	-0.126700
C	-5.485045	-1.630320	-0.113381	C	-0.099978
H	-5.216928	0.473348	-0.392161	H	0.105035
H	-2.945545	-3.880035	0.336639	H	0.111331
H	-6.566405	-1.588942	-0.179675	H	0.114552

H	-5.412838	-3.770948	0.186078	H	0.120018
O	1.395296	-1.942914	0.293606	O	-0.578030
O	-1.339652	-1.911489	0.150697	O	-0.663710
C	0.630055	2.188398	0.450776	C	0.072664
C	0.648679	4.708841	0.457186	C	-0.194060
C	-1.472613	3.464029	-0.188151	C	-0.205194
C	-0.617234	4.723728	-0.406750	C	-0.193760
C	-0.643215	2.195916	-0.435404	C	0.089098
C	1.485114	3.438407	0.220548	C	-0.209418
H	0.371939	4.766658	1.518030	H	0.114426
H	-1.864086	3.444314	0.837741	H	0.120962
H	-0.338802	4.794096	-1.466564	H	0.112398
H	-0.307208	2.194619	-1.483920	H	0.138279
H	1.874392	3.434104	-0.806898	H	0.116502
H	0.286427	2.183090	1.496266	H	0.148757
H	1.262497	5.590371	0.248160	H	0.126336
H	-2.334149	3.489098	-0.863225	H	0.124049
H	-1.216579	5.612055	-0.184491	H	0.127664
H	2.347457	3.441189	0.896559	H	0.121538
Cu	-0.096929	-0.537227	0.136884	Cu	0.687299
H	1.085913	-2.862037	0.264083	H	0.376744

Energy = -772309.05 kcal mol^{-1}

L2Cu

Cartesian Coordinates				Mulliken Atomic Charges	
H	-2.513353	3.572780	0.027389	H	0.120703
C	-1.429996	3.547450	0.011715	C	-0.098911
C	1.366988	3.541181	-0.058020	C	-0.096814
C	-0.745636	2.323187	0.003074	C	0.310141
C	-0.725873	4.745518	-0.009509	C	-0.084279
C	0.673073	4.744500	-0.047500	C	-0.090146
C	0.673650	2.322561	-0.024021	C	0.257017
H	-1.268964	5.684849	-0.005338	H	0.131154
H	1.219470	5.681050	-0.076079	H	0.128972
H	2.449827	3.563232	-0.105234	H	0.116515
N	-1.367835	1.057714	0.008921	N	-0.621628
N	1.292480	1.042928	-0.027490	N	-0.568210
C	-2.660033	0.841935	0.071624	C	0.133082
H	-3.323677	1.705608	0.137923	H	0.140523
C	2.576195	0.866931	0.056551	C	0.134333
H	3.220243	1.742262	0.150725	H	0.142635
C	-3.307634	-0.423417	0.061709	C	0.036919
C	-4.763948	-2.821689	0.036496	C	-0.065966
C	-4.731745	-0.423602	0.132621	C	-0.117280
C	-2.611018	-1.682628	-0.021030	C	0.410420
C	-3.384247	-2.867947	-0.033782	C	-0.125005
C	-5.454269	-1.593175	0.121242	C	-0.099566
H	-5.244967	0.532401	0.195837	H	0.109338
H	-2.855688	-3.812811	-0.098394	H	0.113020
H	-6.536884	-1.575266	0.175359	H	0.118922
H	-5.325668	-3.751316	0.026087	H	0.124364
C	3.302958	-0.387811	0.048340	C	0.086930
C	4.921689	-2.698827	0.063073	C	-0.072135
C	2.742417	-1.681883	-0.062626	C	0.341015
C	4.710277	-0.305945	0.165491	C	-0.133063
C	5.512773	-1.437040	0.173835	C	-0.078970
C	3.537045	-2.821470	-0.056011	C	-0.121067
H	5.164936	0.676640	0.251835	H	0.127083
H	6.588810	-1.341522	0.265599	H	0.136651
H	3.077291	-3.802188	-0.145110	H	0.128126
H	5.535408	-3.593640	0.067795	H	0.142706
O	-1.303560	-1.792754	-0.083685	O	-0.658038

O	1.373885	-1.794776	-0.184150	O	-0.581353
Cu	-0.085809	-0.389778	-0.075960	Cu	0.744545
H	1.050557	-2.709754	-0.192506	H	0.377317

Energy = -770031.41 kcal mol^{-1}

L3Cu

Cartesian Coordinates				Mulliken Atomic Charges	
N	-1.345292	1.641633	-0.171502	N	-0.507709
N	1.289266	1.597785	0.236935	N	-0.466459
C	-2.634379	1.479009	-0.229667	C	0.149613
H	-3.254133	2.369296	-0.380595	H	0.141578
C	2.569166	1.481822	0.154933	C	0.147087
H	3.179622	2.390799	0.184077	H	0.146926
C	-3.329251	0.236055	-0.119007	C	0.034100
C	-4.847967	-2.112736	0.051230	C	-0.067367
C	-2.664176	-1.031104	0.033788	C	0.407744
C	-4.749613	0.273392	-0.181627	C	-0.117430
C	-5.505161	-0.874483	-0.097663	C	-0.099728
C	-3.468393	-2.192172	0.114709	C	-0.125154
H	-5.236341	1.238096	-0.300041	H	0.108672
H	-6.587240	-0.829312	-0.146835	H	0.117326
H	-2.965228	-3.146158	0.229398	H	0.113033
H	-5.433430	-3.025297	0.117217	H	0.122421
C	3.324060	0.244731	0.025371	C	0.080628
C	4.965781	-2.027815	-0.236811	C	-0.071145
C	4.722964	0.360731	-0.125214	C	-0.129261
C	2.777075	-1.059729	0.045770	C	0.339479
C	3.587437	-2.181627	-0.083414	C	-0.121655
C	5.539150	-0.753882	-0.257821	C	-0.079584
H	5.160847	1.354661	-0.138188	H	0.128580
H	3.145324	-3.174303	-0.062553	H	0.128532
H	6.610471	-0.635665	-0.374540	H	0.137577
H	5.589351	-2.910156	-0.337441	H	0.143424
O	-1.356143	-1.177778	0.100192	O	-0.660898
O	1.413810	-1.209420	0.209034	O	-0.579917
C	-0.673390	2.925668	-0.374291	C	-0.054436
C	0.644690	2.908525	0.417551	C	-0.069950
H	0.427748	3.024215	1.486447	H	0.170633
H	-0.458445	3.051565	-1.443107	H	0.159824
Cu	-0.100833	0.182630	0.109346	Cu	0.704042
H	1.302029	3.728690	0.108030	H	0.143781
H	-1.299120	3.765992	-0.051722	H	0.148631
H	1.125593	-2.135342	0.179979	H	0.377061

Energy = -674377.97 kcal mol^{-1}

Appendix 3 – Cartesian Coordinates for Stille Intermediates

Ph-Pd-(PPh_3)$_2$ *cis* B3LYP

	Cartesian Coordinates			Mulliken Atomic Charges
C	2.255305	-1.666494	-5.072261	-0.093635
C	2.231283	-2.712674	-5.992115	-0.080262
C	3.464413	-1.058021	-4.738439	-0.075128
C	3.416292	-3.155094	-6.587300	-0.047436
H	1.293290	-3.193546	-6.246741	0.111744
C	4.655347	-1.494891	-5.321433	-0.046731
H	3.487367	-0.249431	-4.016403	0.112556
C	4.616655	-2.521515	-6.267078	-0.265743
H	3.389273	-3.982968	-7.286530	0.116853
H	5.593881	-1.034564	-5.032210	0.110430
Pd	6.202847	-2.660449	-7.480329	-0.173886
C	8.512612	-4.996128	-6.677216	-0.362751
C	8.853205	-6.326603	-6.951770	-0.037428
C	9.511429	-4.012955	-6.691722	-0.070315
C	10.175938	-6.663445	-7.233463	-0.087039
H	8.095383	-7.099276	-6.947386	0.130025
C	10.831128	-4.356765	-6.968072	-0.071961
H	9.262044	-2.977642	-6.493411	0.136265
C	11.165008	-5.682666	-7.241085	-0.076307
H	10.431020	-7.695557	-7.443671	0.119543
H	11.594081	-3.587676	-6.977474	0.119199
H	12.192143	-5.949433	-7.460603	0.121918
C	5.752020	-5.957745	-6.725464	-0.380089
C	5.311438	-6.056124	-8.052528	-0.054081
C	5.443934	-6.980922	-5.820271	-0.044483
C	4.573745	-7.160773	-8.466338	-0.087963
H	5.548739	-5.270703	-8.761728	0.153451
C	4.700642	-8.082226	-6.240214	-0.079260
H	5.778658	-6.922990	-4.792465	0.130794
C	4.264805	-8.173896	-7.559671	-0.071449
H	4.237596	-7.228446	-9.494311	0.116071
H	4.463386	-8.867983	-5.532730	0.121009
H	3.684623	-9.030881	-7.881068	0.122654
H	1.334823	-1.332037	-4.608229	0.117321
P	6.789546	-4.526392	-6.245616	0.946398
C	6.764045	-4.442896	-4.409502	-0.344665
C	7.954847	-4.472150	-3.671700	-0.047742
C	5.539354	-4.359387	-3.728363	-0.052626
C	7.919730	-4.414124	-2.279667	-0.085753
H	8.911229	-4.550501	-4.170517	0.127555
C	5.513142	-4.314192	-2.339278	-0.084995
H	4.606747	-4.331286	-4.275967	0.144253
C	6.702343	-4.336144	-1.611204	-0.074246
H	8.848387	-4.437757	-1.721797	0.116114
H	4.560712	-4.255741	-1.825891	0.115991
H	6.677494	-4.294722	-0.528596	0.120491
P	7.646470	-2.042002	-9.418653	0.811822
C	6.523233	-0.747517	-10.098534	-0.374335
C	7.960290	-3.193735	-10.814715	-0.379583
C	9.237410	-1.178531	-9.108435	-0.363970
C	5.173794	-1.091755	-10.285769	-0.040515
C	6.937184	0.560192	-10.377588	-0.046628
C	8.491821	-4.459777	-10.531956	-0.047342
C	7.691785	-2.843588	-12.143727	-0.037444
C	10.311484	-1.235746	-10.002963	-0.039806
C	9.366239	-0.430919	-7.929308	-0.066834
C	4.262263	-0.149214	-10.752400	-0.074447
H	4.835131	-2.104520	-10.088075	0.123200
C	6.019484	1.500673	-10.841229	-0.077393

H	7.972017	0.846220	-10.236767	0.125150
C	8.758101	-5.354907	-11.564132	-0.099781
H	8.704851	-4.745155	-9.508624	0.155163
C	7.954307	-3.746680	-13.171875	-0.088382
H	7.275855	-1.871648	-12.378966	0.123947
C	11.493075	-0.551408	-9.721687	-0.086133
H	10.230521	-1.813326	-10.915552	0.124661
C	10.544097	0.257822	-7.656164	-0.081409
H	8.540890	-0.381657	-7.225802	0.123327
C	4.684216	1.149854	-11.028978	-0.081456
H	3.225322	-0.428614	-10.897032	0.114580
H	6.351132	2.509347	-11.058546	0.117477
C	8.487659	-5.001025	-12.884919	-0.075892
H	9.172159	-6.330095	-11.335708	0.106364
H	7.742262	-3.467224	-14.197336	0.116432
C	11.611032	0.196128	-8.552431	-0.083179
H	12.320073	-0.601347	-10.420427	0.117114
H	10.630675	0.839359	-6.745654	0.113844
H	3.974990	1.885701	-11.389151	0.119684
H	8.690437	-5.700902	-13.687174	0.117654
H	12.530179	0.729134	-8.338925	0.119449

Energy = -1525648.92 kcal mol^{-1}

Ph-Pd-$(PPh_3)_2$ *cis* B97D

Cartesian Coordinates				Mulliken Atomic Charges
C	2.243077	-2.161266	-4.624271	-0.089640
C	2.276311	-2.988997	-5.754712	-0.077734
C	3.401042	-1.487424	-4.209347	-0.061075
C	3.471116	-3.147287	-6.475951	-0.032337
H	1.380778	-3.522429	-6.071309	0.104172
C	4.600982	-1.644831	-4.918219	-0.054974
H	3.377342	-0.850386	-3.326120	0.105594
C	4.616507	-2.446907	-6.068952	-0.266863
H	3.508373	-3.819412	-7.332556	0.119445
H	5.508406	-1.153412	-4.569516	0.109224
Pd	6.200697	-2.334413	-7.331667	-0.260474
C	8.562669	-4.557214	-6.720189	-0.329773
C	9.023914	-5.836166	-7.076049	-0.019434
C	9.456346	-3.475033	-6.656702	-0.080760
C	10.379671	-6.020870	-7.371921	-0.087810
H	8.330035	-6.671304	-7.139360	0.119807
C	10.807397	-3.662992	-6.962746	-0.061419
H	9.087618	-2.485873	-6.397025	0.136067
C	11.268631	-4.937247	-7.323332	-0.084150
H	10.739205	-7.009777	-7.650867	0.112287
H	11.487300	-2.814005	-6.938820	0.117291
H	12.318539	-5.085160	-7.569924	0.113532
C	5.870673	-5.639522	-7.082185	-0.349003
C	5.557689	-5.550158	-8.451991	-0.034329
C	5.543232	-6.798564	-6.356402	-0.049775
C	4.916995	-6.615798	-9.089703	-0.086220
H	5.824725	-4.658498	-9.015682	0.185207
C	4.894475	-7.858600	-7.002316	-0.074224
H	5.790729	-6.870597	-5.299974	0.123974
C	4.581118	-7.768723	-8.365079	-0.065091
H	4.683440	-6.543511	-10.150081	0.103743
H	4.636326	-8.753987	-6.439786	0.113720
H	4.076078	-8.595614	-8.861318	0.113846
H	1.319146	-2.050690	-4.059083	0.111497
P	6.799430	-4.265904	-6.324472	0.905955
C	6.669400	-4.435978	-4.508838	-0.312806
C	7.826515	-4.402658	-3.707588	-0.048643
C	5.405185	-4.600514	-3.906648	-0.057560

C	7.716518	-4.529377	-2.317052	-0.079573
H	8.808305	-4.290578	-4.160895	0.120627
C	5.307999	-4.739630	-2.520555	-0.076975
H	4.505417	-4.614573	-4.514938	0.142202
C	6.460942	-4.698742	-1.722406	-0.068404
H	8.614972	-4.502349	-1.703337	0.109631
H	4.329080	-4.871110	-2.063535	0.107761
H	6.378901	-4.799672	-0.641645	0.113459
P	7.603461	-1.921152	-9.247812	0.836058
C	6.627467	-0.656637	-10.158175	-0.336721
C	7.731514	-3.368415	-10.366301	-0.333134
C	9.284677	-1.221682	-9.082600	-0.356140
C	5.220528	-0.724270	-10.077532	-0.065276
C	7.233251	0.381707	-10.887204	-0.038421
C	8.678532	-4.372131	-10.085228	-0.049125
C	6.798488	-3.562330	-11.401321	-0.078473
C	10.319085	-1.509439	-9.988733	-0.054127
C	9.525806	-0.356543	-7.998906	-0.064753
C	4.430415	0.231698	-10.726088	-0.073872
H	4.737386	-1.531171	-9.521271	0.137870
C	6.437887	1.336131	-11.532192	-0.073943
H	8.318239	0.445438	-10.942016	0.114878
C	8.684890	-5.555737	-10.829437	-0.075682
H	9.408165	-4.231630	-9.293448	0.145175
C	6.808824	-4.753045	-12.139097	-0.074406
H	6.072667	-2.785990	-11.634538	0.122090
C	11.588372	-0.947591	-9.800306	-0.078563
H	10.137304	-2.175404	-10.829326	0.119243
C	10.791814	0.209113	-7.819037	-0.087937
H	8.722985	-0.132183	-7.295528	0.123995
C	5.039866	1.262915	-11.453251	-0.070525
H	3.345545	0.173308	-10.659604	0.108824
H	6.910033	2.138643	-12.096228	0.111411
C	7.747123	-5.752951	-11.852366	-0.074617
H	9.422898	-6.324086	-10.605770	0.097349
H	6.089410	-4.892545	-12.944436	0.107954
C	11.827117	-0.091660	-8.716957	-0.076655
H	12.388293	-1.175751	-10.502654	0.111743
H	10.972221	0.879548	-6.980509	0.109234
H	4.427109	2.010133	-11.954245	0.113722
H	7.753171	-6.676890	-12.427943	0.108700
H	12.814580	0.343676	-8.573909	0.114130

Energy = -1525037.06 kcal mol^{-1}

Ph-Pd-$(PPh_3)_2$ *trans* B3LYP

Cartesian Coordinates				Mulliken Atomic Charges
C	1.700528	-2.686131	-4.153723	-0.096804
C	1.758548	-3.062496	-5.493560	-0.087459
C	2.801403	-2.072895	-3.560029	-0.081566
C	2.914440	-2.831021	-6.246001	-0.043077
H	0.907468	-3.541830	-5.964400	0.111896
C	3.962924	-1.832281	-4.299384	-0.062063
H	2.765200	-1.772958	-2.518615	0.111608
C	4.003804	-2.217109	-5.636455	-0.204126
H	2.944822	-3.132715	-7.285030	0.107366
H	4.809826	-1.351280	-3.825919	0.117090
Pd	5.667069	-1.843491	-6.685662	-0.183600
P	4.984024	0.376555	-7.341536	0.887425
C	6.584101	1.245252	-7.604160	-0.364769
C	7.533547	1.211530	-6.570006	-0.066111
C	6.891579	1.914219	-8.794400	-0.037546
C	8.759291	1.853222	-6.719314	-0.078930
H	7.306719	0.699631	-5.640198	0.126964

C	8.124528	2.546974	-8.941681	-0.078989
H	6.172891	1.944921	-9.603750	0.127523
C	9.056946	2.520361	-7.907330	-0.081392
H	9.479746	1.834343	-5.909748	0.115355
H	8.352850	3.065305	-9.865601	0.119000
H	10.012123	3.018617	-8.024887	0.120766
C	3.994550	1.455212	-6.237201	-0.369712
C	2.720014	1.024242	-5.840494	-0.036464
C	4.467786	2.697532	-5.798275	-0.046258
C	1.932818	1.830861	-5.025592	-0.085951
H	2.338309	0.064842	-6.167366	0.135437
C	3.675663	3.496388	-4.975626	-0.087387
H	5.446777	3.048927	-6.098040	0.124361
C	2.409298	3.066418	-4.589442	-0.078059
H	0.948175	1.490334	-4.727765	0.112048
H	4.049913	4.457534	-4.643079	0.115045
H	1.794544	3.691151	-3.952021	0.117859
C	4.122442	0.407131	-8.960236	-0.375786
C	3.248512	1.442874	-9.312728	-0.033827
C	4.375302	-0.620605	-9.878495	-0.046019
C	2.643290	1.448505	-10.567482	-0.082763
H	3.034259	2.238853	-8.610327	0.128678
C	3.773908	-0.606943	-11.133359	-0.086781
H	5.044683	-1.432196	-9.611781	0.123776
C	2.905620	0.427633	-11.478313	-0.075643
H	1.965800	2.251942	-10.831800	0.118747
H	3.977988	-1.404152	-11.838588	0.111141
H	2.431966	0.435455	-12.452986	0.120162
C	8.175542	-3.866349	-7.261848	-0.366316
C	8.597156	-4.872927	-8.138917	-0.039821
C	8.928423	-2.685021	-7.159907	-0.058268
C	9.756654	-4.701488	-8.891423	-0.078716
H	8.024541	-5.786805	-8.235685	0.127909
C	10.086198	-2.519672	-7.914860	-0.075613
H	8.623002	-1.897562	-6.477152	0.124664
C	10.500906	-3.528294	-8.782334	-0.079711
H	10.079098	-5.487874	-9.563807	0.119606
H	10.659890	-1.604776	-7.826582	0.114110
H	11.400806	-3.400230	-9.372268	0.121007
C	5.731941	-5.444828	-6.937098	-0.369792
C	4.963241	-5.285546	-8.097763	-0.050732
C	5.825526	-6.708177	-6.341896	-0.038430
C	4.307178	-6.375493	-8.660474	-0.083249
H	4.881347	-4.308607	-8.562079	0.118032
C	5.159534	-7.794990	-6.904747	-0.081999
H	6.412020	-6.845725	-5.442036	0.128048
C	4.402795	-7.631438	-8.062349	-0.076731
H	3.716671	-6.244941	-9.559785	0.111704
H	5.234566	-8.769702	-6.437189	0.118531
H	3.886019	-8.479189	-8.496692	0.120240
H	0.802543	-2.870051	-3.575808	0.115601
P	6.631067	-3.994541	-6.275304	0.899881
C	7.132213	-4.434434	-4.568684	-0.369680
C	8.470296	-4.666764	-4.228736	-0.043835
C	6.140426	-4.539910	-3.581691	-0.049197
C	8.809715	-5.000704	-2.918947	-0.086097
H	9.247241	-4.594241	-4.979279	0.124380
C	6.487501	-4.880181	-2.278319	-0.086404
H	5.100648	-4.362716	-3.827949	0.137538
C	7.821909	-5.108271	-1.943877	-0.076545
H	9.847636	-5.181335	-2.664890	0.115979
H	5.714837	-4.965205	-1.523174	0.113700
H	8.089257	-5.370453	-0.926912	0.119038

Energy = -1525654.99 kcal mol^{-1}

Ph-Pd-(PPh_3)$_2$ *trans* B97D

Cartesian Coordinates				Mulliken Atomic Charges
C	1.930957	-2.882515	-4.291771	-0.095402
C	2.120163	-3.348743	-5.599631	-0.086190
C	2.890727	-2.050291	-3.701658	-0.072846
C	3.271681	-2.992658	-6.322424	-0.029640
H	1.378725	-3.995803	-6.066510	0.104808
C	4.044523	-1.681184	-4.411682	-0.044170
H	2.751651	-1.680943	-2.686539	0.105214
C	4.216508	-2.163351	-5.712606	-0.244060
H	3.425848	-3.374403	-7.328276	0.117191
H	4.784564	-1.030512	-3.953082	0.119252
Pd	5.916823	-1.688877	-6.674938	-0.207046
P	5.035287	0.364015	-7.393339	0.846427
C	6.465649	1.188389	-8.185309	-0.324181
C	7.710785	1.099530	-7.529163	-0.062230
C	6.369924	1.850116	-9.421922	-0.040936
C	8.846945	1.684332	-8.098708	-0.068061
H	7.783680	0.580542	-6.571868	0.119627
C	7.511399	2.431305	-9.986844	-0.071163
H	5.412839	1.903684	-9.937011	0.117177
C	8.746560	2.350635	-9.327879	-0.072133
H	9.806196	1.617650	-7.588402	0.104003
H	7.437026	2.946571	-10.942815	0.112761
H	9.630379	2.802863	-9.774168	0.113850
C	4.355690	1.515716	-6.152692	-0.317285
C	3.118523	1.199335	-5.556038	-0.052868
C	5.058606	2.665345	-5.750510	-0.053268
C	2.590511	2.036920	-4.569157	-0.079275
H	2.573915	0.309070	-5.861859	0.133392
C	4.522858	3.495513	-4.757754	-0.079162
H	6.009020	2.916421	-6.217204	0.115751
C	3.291796	3.182987	-4.166941	-0.072055
H	1.632350	1.793080	-4.113623	0.105526
H	5.064690	4.389023	-4.452761	0.108324
H	2.877246	3.832260	-3.397758	0.110775
C	3.745517	0.164253	-8.665853	-0.341919
C	2.853776	1.206642	-8.977971	-0.043699
C	3.672624	-1.056123	-9.360660	-0.041552
C	1.901697	1.025902	-9.988039	-0.075622
H	2.898369	2.143914	-8.426450	0.120867
C	2.720619	-1.230322	-10.370485	-0.090091
H	4.352579	-1.864815	-9.094160	0.127263
C	1.836041	-0.189233	-10.684543	-0.065998
H	1.209958	1.831093	-10.228958	0.112616
H	2.661621	-2.177375	-10.904369	0.099628
H	1.091067	-0.326642	-11.466310	0.112906
C	8.544971	-3.687790	-6.722233	-0.340993
C	9.166995	-4.651606	-7.535138	-0.037213
C	9.263764	-2.549439	-6.303053	-0.059881
C	10.502696	-4.477573	-7.917081	-0.072062
H	8.609378	-5.525483	-7.866128	0.118971
C	10.599551	-2.385350	-6.683783	-0.069566
H	8.778353	-1.804888	-5.670521	0.118036
C	11.218238	-3.348856	-7.492999	-0.072108
H	10.985802	-5.224723	-8.544205	0.113523
H	11.155183	-1.509603	-6.352913	0.105157
H	12.256347	-3.219854	-7.793859	0.114142
C	6.011864	-5.059190	-7.289881	-0.342147
C	5.694713	-4.671510	-8.606507	-0.057589
C	5.718438	-6.361665	-6.853971	-0.041911
C	5.096626	-5.582944	-9.481207	-0.081231
H	5.921895	-3.658721	-8.941495	0.126852
C	5.110020	-7.268392	-7.732423	-0.076666
H	5.956874	-6.661412	-5.835669	0.121628

C	4.800086	-6.882536	-9.042705	-0.069047
H	4.859637	-5.281960	-10.500425	0.105587
H	4.881173	-8.276617	-7.391801	0.112830
H	4.328143	-7.590784	-9.721340	0.113284
H	1.038516	-3.165692	-3.736586	0.109752
P	6.794612	-3.814065	-6.208365	0.863587
C	6.759951	-4.475980	-4.509850	-0.338340
C	7.949014	-4.752870	-3.811079	-0.043900
C	5.510792	-4.691545	-3.892171	-0.039226
C	7.886951	-5.243380	-2.500869	-0.082369
H	8.913888	-4.591868	-4.287412	0.117103
C	5.461181	-5.187749	-2.586172	-0.090395
H	4.588202	-4.478153	-4.425641	0.142767
C	6.646461	-5.461164	-1.888110	-0.067415
H	8.808378	-5.459387	-1.963040	0.108669
H	4.495166	-5.356274	-2.113562	0.102863
H	6.602570	-5.844073	-0.870009	0.110803

Energy = -1525038.08 kcal mol^{-1}

Py-Ph-I-Pd-$(PPh_3)_2$ *cis1* B3LYP

Cartesian Coordinates				Mulliken Atomic Charges
C	2.519563	-2.429503	-4.413642	-0.057410
C	4.342374	-1.827765	-2.956985	-0.056824
C	3.423398	-2.641730	-5.450730	-0.019681
H	1.456920	-2.574101	-4.589004	0.084685
C	5.241513	-2.043179	-3.995109	0.007344
H	4.709446	-1.502824	-1.987318	0.083638
C	4.789289	-2.392868	-5.272235	-0.240532
H	3.045019	-2.944758	-6.420366	0.110185
H	6.297557	-1.883750	-3.813012	0.107401
Pd	5.992803	-2.305620	-6.913070	-0.494649
C	8.539936	-4.663855	-6.507120	-0.388987
C	9.198437	-5.856189	-6.828395	-0.023284
C	9.298719	-3.529598	-6.192442	-0.065039
C	10.590013	-5.909860	-6.831035	-0.090124
H	8.633915	-6.740283	-7.093898	0.112991
C	10.690893	-3.587443	-6.190892	-0.076175
H	8.800223	-2.594469	-5.963893	0.147552
C	11.338801	-4.778408	-6.510528	-0.082544
H	11.089441	-6.837592	-7.086087	0.110152
H	11.264463	-2.699307	-5.953220	0.111030
H	12.421715	-4.823937	-6.516024	0.113385
C	5.988996	-5.846636	-7.475172	-0.377121
C	5.345404	-5.492603	-8.664908	-0.035362
C	6.060116	-7.202406	-7.118109	-0.057909
C	4.800174	-6.470666	-9.493714	-0.091750
H	5.269462	-4.449004	-8.941241	0.147498
C	5.517210	-8.177180	-7.949266	-0.089847
H	6.520227	-7.498127	-6.183190	0.127469
C	4.888438	-7.813515	-9.139546	-0.075850
H	4.307322	-6.180085	-10.413916	0.102254
H	5.579360	-9.220954	-7.663522	0.110499
H	4.463275	-8.575136	-9.783011	0.111983
P	6.702899	-4.525958	-6.409781	0.986483
C	6.354799	-5.155624	-4.705576	-0.352383
C	7.331077	-5.131855	-3.704126	-0.050028
C	5.072171	-5.625310	-4.390249	-0.037617
C	7.032386	-5.574273	-2.415903	-0.089207
H	8.331648	-4.782191	-3.923318	0.119399
C	4.779961	-6.071516	-3.106261	-0.078725
H	4.300389	-5.652130	-5.149318	0.114106
C	5.759128	-6.046341	-2.113757	-0.088286
H	7.803087	-5.558061	-1.653689	0.105454

H	3.786427	-6.442832	-2.882043	0.100322
H	5.531635	-6.399423	-1.114393	0.105317
P	7.209676	-1.865204	-9.117327	0.900366
C	6.124854	-0.878065	-10.241290	-0.351918
C	7.727936	-3.261956	-10.228776	-0.369950
C	8.767244	-0.885057	-8.947220	-0.380673
C	4.758294	-1.179961	-10.280076	-0.031455
C	6.621708	0.124437	-11.078624	-0.031822
C	8.837123	-4.048980	-9.888334	-0.051916
C	7.017130	-3.574322	-11.394421	-0.056177
C	9.758088	-0.892299	-9.939784	-0.058826
C	8.958678	-0.097030	-7.805658	-0.038883
C	3.910155	-0.511844	-11.157452	-0.083116
H	4.349874	-1.924726	-9.606511	0.123534
C	5.767819	0.803777	-11.945681	-0.086266
H	7.670600	0.390544	-11.051002	0.113870
C	9.222087	-5.117365	-10.692824	-0.086609
H	9.417064	-3.819970	-9.004158	0.141211
C	7.402684	-4.648513	-12.194824	-0.087760
H	6.169747	-2.971569	-11.693333	0.121637
C	10.912343	-0.127623	-9.790769	-0.086998
H	9.635993	-1.500611	-10.827297	0.125714
C	10.114065	0.668096	-7.661408	-0.101242
H	8.194047	-0.064211	-7.039818	0.137546
C	4.413799	0.483741	-11.992441	-0.081840
H	2.854135	-0.756236	-11.176289	0.096850
H	6.164553	1.585858	-12.582913	0.104286
C	8.504532	-5.423907	-11.847295	-0.082036
H	10.088422	-5.707480	-10.416783	0.099860
H	6.844436	-4.868383	-13.097873	0.103227
C	11.093686	0.653475	-8.651192	-0.080616
H	11.669082	-0.142999	-10.566875	0.107466
H	10.243895	1.279000	-6.775225	0.102699
H	3.752332	1.013066	-12.668697	0.104934
H	8.807755	-6.254735	-12.473962	0.105750
H	11.992564	1.248784	-8.537560	0.108049
I	5.174349	0.331263	-6.861582	-0.250870
C	2.967421	-1.975610	-3.169378	-0.212409
C	1.991291	-1.485648	-2.148287	-0.004693
H	2.378267	-1.578319	-1.132280	0.164299
H	1.032557	-2.002295	-2.215204	0.163888
N	1.697094	-0.014394	-2.357711	-0.341583
C	2.219103	0.794532	-3.348725	0.063656
C	0.874697	0.717710	-1.601525	0.291244
C	1.688264	2.035859	-3.169284	0.021373
H	2.914028	0.430431	-4.089203	0.214841
N	0.849878	1.969939	-2.072958	-0.319812
H	0.320165	0.361001	-0.749852	0.167608
H	1.837610	2.945770	-3.724617	0.165844
C	0.069962	3.083215	-1.520564	-0.157601
H	0.743504	3.877678	-1.200031	0.170673
H	-0.614330	3.461186	-2.279726	0.170307
H	-0.501095	2.727278	-0.665422	0.144525

Energy = -1723783.94 kcal mol^{-1}

Py-Ph-I-Pd-(PPh_3)$_2$ *cis1* B97D

Cartesian Coordinates			Mulliken Atomic Charges
C	2.466812	-2.635661	-4.373651	-0.066963
C	4.307543	-2.085379	-2.890142	-0.063882
C	3.371290	-2.807115	-5.426020	-0.013446
H	1.395952	-2.754187	-4.548388	0.079545
C	5.206906	-2.262800	-3.942661	0.019550
H	4.669529	-1.779167	-1.907258	0.077254

C	4.739790	-2.548324	-5.236709	-0.233644
H	2.998307	-3.070227	-6.414469	0.109497
H	6.270819	-2.121720	-3.765678	0.107372
Pd	5.937312	-2.334555	-6.890388	-0.584411
C	8.536914	-4.499072	-6.609384	-0.369697
C	9.251910	-5.647218	-6.988113	-0.019512
C	9.226352	-3.306496	-6.331645	-0.062260
C	10.644673	-5.590101	-7.108191	-0.085942
H	8.725273	-6.567785	-7.225916	0.102466
C	10.618308	-3.249816	-6.460488	-0.064293
H	8.668666	-2.415290	-6.051689	0.153355
C	11.328236	-4.391745	-6.854125	-0.081458
H	11.195714	-6.477765	-7.414951	0.103106
H	11.136578	-2.310510	-6.277950	0.107055
H	12.410132	-4.348257	-6.968385	0.105482
C	6.011348	-5.742932	-7.571407	-0.344821
C	5.280453	-5.338490	-8.699206	-0.031102
C	6.176293	-7.115914	-7.300403	-0.057258
C	4.743283	-6.294346	-9.568504	-0.081460
H	5.138873	-4.276901	-8.886584	0.151157
C	5.639492	-8.067825	-8.172746	-0.084189
H	6.702107	-7.434091	-6.402244	0.117195
C	4.927009	-7.657725	-9.309637	-0.069252
H	4.185426	-5.972625	-10.445847	0.092098
H	5.769588	-9.128169	-7.962454	0.104488
H	4.508718	-8.401993	-9.985401	0.104648
P	6.707568	-4.463463	-6.467857	0.972504
C	6.396703	-5.118177	-4.779886	-0.333247
C	7.363756	-4.993577	-3.769004	-0.056589
C	5.126385	-5.638017	-4.468374	-0.031147
C	7.060938	-5.383434	-2.457701	-0.082146
H	8.350123	-4.598743	-4.003475	0.113756
C	4.830286	-6.026422	-3.159942	-0.067315
H	4.371481	-5.730539	-5.245816	0.112521
C	5.795237	-5.896310	-2.150332	-0.080445
H	7.818047	-5.291495	-1.680409	0.099140
H	3.845677	-6.429075	-2.927478	0.093774
H	5.562841	-6.200700	-1.130935	0.098524
P	7.131955	-1.887301	-8.964073	0.896356
C	6.092144	-0.872289	-10.088625	-0.323233
C	7.606111	-3.305772	-10.051836	-0.336860
C	8.701919	-0.961045	-8.728209	-0.346887
C	4.703255	-1.086309	-10.075627	-0.035471
C	6.648687	0.044110	-10.994114	-0.031712
C	8.758834	-4.060732	-9.768464	-0.059080
C	6.781524	-3.692936	-11.124889	-0.065669
C	9.740405	-1.004737	-9.677010	-0.067309
C	8.860274	-0.191413	-7.561978	-0.040628
C	3.878901	-0.403486	-10.975556	-0.080847
H	4.271714	-1.765011	-9.341493	0.137148
C	5.818428	0.739413	-11.882113	-0.083694
H	7.721628	0.225031	-10.997828	0.104178
C	9.066347	-5.193146	-10.529576	-0.080197
H	9.427005	-3.757006	-8.969493	0.148833
C	7.093855	-4.826401	-11.883509	-0.077033
H	5.899677	-3.106696	-11.373456	0.113771
C	10.926742	-0.295773	-9.453658	-0.080617
H	9.628026	-1.603744	-10.577975	0.119975
C	10.046433	0.518223	-7.344397	-0.101538
H	8.051687	-0.145958	-6.835398	0.144191
C	4.435932	0.512119	-11.878831	-0.073133
H	2.802955	-0.570459	-10.958483	0.091080
H	6.252317	1.458993	-12.574679	0.098411
C	8.232213	-5.584788	-11.584107	-0.071403
H	9.963462	-5.764515	-10.297110	0.090885
H	6.448738	-5.112043	-12.713055	0.094276
C	11.083008	0.463968	-8.286398	-0.074200

H	11.726756	-0.336728	-10.191291	0.102256
H	10.159173	1.114575	-6.440101	0.097866
H	3.793507	1.053544	-12.571626	0.099001
H	8.473226	-6.467198	-12.174682	0.098155
H	12.007060	1.014001	-8.114181	0.102615
I	5.040277	0.310478	-6.722043	-0.282946
C	2.926038	-2.223540	-3.111651	-0.174400
C	1.962621	-1.627432	-2.136988	-0.020987
H	2.325150	-1.669397	-1.102851	0.161879
H	0.962833	-2.073514	-2.200854	0.161654
N	1.787578	-0.147691	-2.464213	-0.327724
C	2.409292	0.541190	-3.495367	0.075575
C	0.996135	0.702552	-1.792436	0.278422
C	1.969765	1.836285	-3.427948	0.015675
H	3.102982	0.074108	-4.185926	0.209604
N	1.089489	1.918190	-2.360994	-0.305580
H	0.382976	0.457018	-0.937036	0.160202
H	2.208628	2.691334	-4.044286	0.156444
C	0.383409	3.132659	-1.921583	-0.161998
H	1.116661	3.887080	-1.616156	0.170670
H	-0.225608	3.514512	-2.748042	0.169654
H	-0.261579	2.880296	-1.075018	0.144361

Energy = -1723062.88 kcal mol^{-1}

Py-Ph-I-Pd-(PPh_3)$_2$ *cis2* B3LYP

Cartesian Coordinates				Mulliken Atomic Charges
C	2.843018	-2.082541	-4.343903	-0.051436
C	4.778310	-1.616485	-2.989423	-0.066685
C	3.668332	-2.290810	-5.443858	-0.026723
H	1.765314	-2.158077	-4.463351	0.076877
C	5.599948	-1.826804	-4.093381	-0.006466
H	5.221819	-1.324782	-2.041108	0.082707
C	5.058790	-2.138487	-5.344717	-0.222424
H	3.212733	-2.514939	-6.401565	0.107223
H	6.668959	-1.693159	-3.978345	0.104060
Pd	6.194827	-2.195566	-7.042810	-0.518947
C	8.623951	-4.662224	-6.585153	-0.398002
C	9.253835	-5.885295	-6.844224	-0.022356
C	9.410884	-3.538333	-6.304165	-0.063137
C	10.642887	-5.978717	-6.817871	-0.090111
H	8.670895	-6.763750	-7.086605	0.109627
C	10.800750	-3.635599	-6.273136	-0.076058
H	8.935023	-2.580252	-6.128740	0.153629
C	11.418956	-4.856724	-6.529708	-0.081691
H	11.119585	-6.929688	-7.026763	0.109426
H	11.395408	-2.754319	-6.063619	0.112385
H	12.500017	-4.933279	-6.513738	0.113780
C	6.042291	-5.752932	-7.604897	-0.378384
C	5.365794	-5.367589	-8.765927	-0.035951
C	6.102793	-7.117018	-7.277040	-0.057160
C	4.780053	-6.321178	-9.596152	-0.088458
H	5.296121	-4.317811	-9.018780	0.150564
C	5.521194	-8.067547	-8.109597	-0.092418
H	6.583692	-7.439622	-6.361715	0.122162
C	4.860716	-7.671737	-9.272398	-0.077262
H	4.263383	-6.004756	-10.494417	0.103169
H	5.578396	-9.117793	-7.847140	0.108275
H	4.406191	-8.414537	-9.917801	0.111524
P	6.789690	-4.452156	-6.534267	0.982330
C	6.384125	-5.091786	-4.841288	-0.341338
C	7.336718	-5.110101	-3.816713	-0.044796
C	5.091641	-5.559217	-4.569730	-0.024417
C	7.011645	-5.604250	-2.554439	-0.082963

H	8.343503	-4.758139	-4.002199	0.123193
C	4.773813	-6.068369	-3.314223	-0.115954
H	4.336672	-5.551719	-5.346118	0.117110
C	5.733740	-6.095142	-2.301768	-0.113109
H	7.767160	-5.624349	-1.777344	0.108237
H	3.779526	-6.465045	-3.137644	0.094778
H	5.496435	-6.515154	-1.330065	0.098547
P	7.369263	-1.890557	-9.298808	0.883262
C	6.292164	-0.911023	-10.435869	-0.353049
C	7.803033	-3.352324	-10.363291	-0.373661
C	8.976411	-0.978492	-9.220124	-0.374749
C	4.912491	-1.147699	-10.411750	-0.029010
C	6.804884	0.018725	-11.344630	-0.031342
C	8.876388	-4.177781	-10.000107	-0.048539
C	7.070981	-3.672606	-11.513163	-0.054000
C	9.922641	-1.065140	-10.251857	-0.059185
C	9.254808	-0.165554	-8.114586	-0.037403
C	4.065074	-0.486563	-11.295023	-0.081425
H	4.494390	-1.831854	-9.682105	0.123226
C	5.952628	0.691449	-12.218371	-0.084851
H	7.865355	0.234793	-11.367242	0.114032
C	9.205815	-5.292144	-10.765674	-0.086695
H	9.473915	-3.940264	-9.129870	0.139922
C	7.400934	-4.792371	-12.275487	-0.087335
H	6.250935	-3.041453	-11.829559	0.122382
C	11.116356	-0.352133	-10.177588	-0.087671
H	9.734670	-1.694821	-11.112384	0.125355
C	10.449547	0.547955	-8.045114	-0.100315
H	8.526337	-0.069283	-7.319694	0.131324
C	4.584146	0.436655	-12.200658	-0.081684
H	2.998385	-0.676932	-11.262177	0.097001
H	6.361795	1.418866	-12.910130	0.104444
C	8.467009	-5.606095	-11.904869	-0.082668
H	10.045961	-5.911516	-10.473037	0.098754
H	6.827815	-5.018068	-13.167783	0.102531
C	11.383124	0.455864	-9.074236	-0.080941
H	11.836734	-0.428320	-10.984161	0.106408
H	10.644688	1.180779	-7.186749	0.104209
H	3.923663	0.962569	-12.880464	0.105501
H	8.726899	-6.472314	-12.502480	0.104556
H	12.312084	1.012047	-9.019431	0.107652
I	5.574738	0.457769	-7.072610	-0.166200
C	3.389078	-1.726291	-3.105487	-0.182650
C	2.506423	-1.407189	-1.936932	-0.021964
H	1.614600	-0.856703	-2.241081	0.158312
H	3.041147	-0.815655	-1.191899	0.176753
N	1.999822	-2.634200	-1.224082	-0.327642
C	2.666154	-3.834421	-1.101272	0.056692
C	0.849121	-2.716234	-0.554169	0.293297
C	1.886598	-4.647886	-0.335402	0.015324
H	3.614057	-4.008683	-1.582996	0.203883
N	0.752556	-3.931805	-0.001720	-0.320685
H	0.115514	-1.931983	-0.470503	0.174155
H	2.037011	-5.662215	-0.008289	0.159609
C	-0.371822	-4.426216	0.801946	-0.157901
H	-0.839555	-5.271918	0.298248	0.171035
H	-0.010923	-4.731195	1.783771	0.170329
H	-1.101633	-3.627773	0.919584	0.148261

Energy = -1723780.07 kcal mol^{-1}

Py-Ph-I-Pd-(PPh_3)$_2$ *cis2* B97D

	Cartesian Coordinates			Mulliken Atomic Charges
C	2.760625	-1.966009	-4.381149	-0.051295
C	4.753394	-1.603647	-3.045692	-0.079302
C	3.558335	-2.151063	-5.514067	-0.028292
H	1.673317	-2.013048	-4.466742	0.070898
C	5.546060	-1.803589	-4.179527	-0.002522
H	5.220850	-1.368070	-2.087542	0.073339
C	4.959790	-2.046860	-5.433886	-0.192669
H	3.083182	-2.324739	-6.478037	0.105942
H	6.628427	-1.729384	-4.091668	0.098731
Pd	6.104483	-2.106839	-7.145787	-0.606786
C	8.476707	-4.491741	-6.683360	-0.372264
C	9.117142	-5.708673	-6.968524	-0.013594
C	9.246721	-3.348238	-6.407491	-0.058641
C	10.514395	-5.772892	-6.989786	-0.084363
H	8.534946	-6.592395	-7.213843	0.097911
C	10.644280	-3.413288	-6.436169	-0.072304
H	8.751110	-2.399722	-6.211126	0.152994
C	11.279677	-4.626741	-6.729823	-0.079999
H	11.006318	-6.715040	-7.226507	0.101941
H	11.227343	-2.512421	-6.255222	0.106724
H	12.366676	-4.678638	-6.765138	0.106292
C	5.879940	-5.512445	-7.774855	-0.337612
C	5.125150	-5.036381	-8.858142	-0.041999
C	5.968638	-6.900311	-7.546093	-0.052932
C	4.485317	-5.933913	-9.720795	-0.082540
H	5.041738	-3.962719	-9.013215	0.153600
C	5.338099	-7.794731	-8.416187	-0.086233
H	6.505874	-7.277121	-6.678105	0.110186
C	4.597847	-7.311998	-9.506017	-0.068227
H	3.905248	-5.555082	-10.560485	0.095075
H	5.415505	-8.866416	-8.239841	0.102216
H	4.104037	-8.011021	-10.179161	0.104603
P	6.650405	-4.288027	-6.650126	0.953948
C	6.199133	-4.946597	-4.986345	-0.320545
C	7.122520	-4.940572	-3.927309	-0.042553
C	4.898795	-5.437044	-4.767744	-0.007749
C	6.757509	-5.438345	-2.669912	-0.073318
H	8.131875	-4.567613	-4.088897	0.116827
C	4.542874	-5.950670	-3.517146	-0.122596
H	4.176023	-5.440163	-5.580552	0.115803
C	5.472268	-5.955665	-2.465255	-0.126745
H	7.485600	-5.443282	-1.860243	0.101471
H	3.543281	-6.359078	-3.370719	0.090410
H	5.205531	-6.378122	-1.496384	0.091705
P	7.372421	-1.937041	-9.223617	0.880239
C	6.394622	-1.036082	-10.493958	-0.321938
C	7.867290	-3.461938	-10.149157	-0.330191
C	8.962926	-1.040469	-9.008107	-0.335559
C	4.996577	-1.176319	-10.466408	-0.034658
C	7.000814	-0.295532	-11.520283	-0.029467
C	9.034088	-4.166010	-9.798139	-0.066574
C	7.046657	-3.969085	-11.173932	-0.064465
C	9.990318	-1.120738	-9.967866	-0.072046
C	9.159523	-0.270198	-7.848596	-0.040457
C	4.211960	-0.598965	-11.470003	-0.080935
H	4.526617	-1.704312	-9.638020	0.139081
C	6.211289	0.296529	-12.513665	-0.082567
H	8.080826	-0.167053	-11.536983	0.101589
C	9.363076	-5.358565	-10.451250	-0.080505
H	9.694627	-3.779128	-9.028146	0.146675
C	7.376830	-5.164548	-11.820546	-0.069380
H	6.155066	-3.424086	-11.475623	0.112776
C	11.194785	-0.436269	-9.768812	-0.083022

H	9.855754	-1.732075	-10.857464	0.120857
C	10.365241	0.413014	-7.653158	-0.098593
H	8.362492	-0.198539	-7.111999	0.142211
C	4.819121	0.139284	-12.494808	-0.072672
H	3.128667	-0.704978	-11.439025	0.092000
H	6.683956	0.882981	-13.300026	0.098040
C	8.533446	-5.866076	-11.458933	-0.076944
H	10.272379	-5.887016	-10.169715	0.089712
H	6.732064	-5.543058	-12.612214	0.091444
C	11.384525	0.330942	-8.611133	-0.072337
H	11.983240	-0.502562	-10.516976	0.101099
H	10.503970	1.013648	-6.755383	0.098769
H	4.208475	0.601462	-13.268899	0.099559
H	8.791938	-6.794500	-11.965908	0.096268
H	12.322004	0.863848	-8.458695	0.101799
I	5.448517	0.554422	-7.279291	-0.177874
C	3.352398	-1.667213	-3.141618	-0.166580
C	2.505372	-1.426206	-1.929822	-0.019742
H	1.540552	-0.972711	-2.185291	0.157523
H	3.021185	-0.793125	-1.197589	0.176603
N	2.170735	-2.717610	-1.206754	-0.319358
C	2.902792	-3.886561	-1.274200	0.058630
C	1.143488	-2.896873	-0.364791	0.281446
C	2.290680	-4.790113	-0.445363	0.010873
H	3.769327	-3.973832	-1.916184	0.216750
N	1.193803	-4.153596	0.113775	-0.306149
H	0.396196	-2.158397	-0.111008	0.166703
H	2.531808	-5.817264	-0.211751	0.147957
C	0.232037	-4.757995	1.051210	-0.162088
H	-0.285080	-5.587947	0.557267	0.171346
H	0.769343	-5.120476	1.934041	0.169933
H	-0.493979	-3.996693	1.350216	0.148680

Energy = -1723058.81 kcal mol^{-1}

Py-Ph-I-Pd-(PPh_3)$_2$ *trans1* B3LYP

Cartesian Coordinates				Mulliken Atomic Charges
C	3.404588	-1.096924	-3.100414	-0.205215
C	2.745911	-1.655186	-4.197881	-0.047771
C	4.736094	-0.691583	-3.248097	-0.038811
C	3.409705	-1.816280	-5.414157	-0.091329
H	1.714585	-1.983748	-4.101211	0.084523
C	5.385130	-0.840124	-4.467675	-0.030270
H	5.274729	-0.270273	-2.403367	0.076324
C	4.742537	-1.416369	-5.575279	-0.222934
H	2.874927	-2.273200	-6.240134	0.114845
H	6.421197	-0.528902	-4.542009	0.100127
Pd	5.734729	-1.712986	-7.334918	-0.407218
I	7.062063	-2.124123	-9.735998	-0.208610
P	4.926474	0.381737	-8.219952	0.883322
C	6.355585	1.411514	-8.757485	-0.320975
C	7.444987	1.518730	-7.882423	-0.051469
C	6.406561	2.066428	-9.990239	-0.034728
C	8.550537	2.291277	-8.221920	-0.083224
H	7.436483	0.980596	-6.940774	0.110171
C	7.521315	2.830037	-10.332216	-0.082600
H	5.594333	1.966658	-10.697790	0.119202
C	8.590395	2.950380	-9.449593	-0.078874
H	9.387657	2.364775	-7.537029	0.099345
H	7.554812	3.322516	-11.297133	0.108231
H	9.456991	3.541714	-9.721639	0.108586
C	3.971866	1.533327	-7.110411	-0.331269
C	2.631261	1.235765	-6.825964	-0.015734
C	4.521924	2.708852	-6.589307	-0.051887

C	1.853106	2.108892	-6.072201	-0.127950
H	2.178734	0.337575	-7.227509	0.115688
C	3.744893	3.579633	-5.824590	-0.084943
H	5.549650	2.970102	-6.804634	0.124004
C	2.406724	3.289892	-5.573872	-0.124721
H	0.806201	1.881142	-5.901772	0.103222
H	4.183657	4.499687	-5.454715	0.103489
H	1.789261	3.992521	-5.023732	0.098623
C	3.754328	0.265934	-9.638722	-0.382087
C	3.092164	1.409580	-10.112892	-0.051449
C	3.489219	-0.969477	-10.236325	-0.024662
C	2.199147	1.315550	-11.175162	-0.087062
H	3.265872	2.373674	-9.649978	0.120003
C	2.586895	-1.060569	-11.294800	-0.095610
H	4.005484	-1.853833	-9.888905	0.138884
C	1.944922	0.079368	-11.768519	-0.077602
H	1.700422	2.207045	-11.537883	0.106878
H	2.394723	-2.024171	-11.752093	0.105704
H	1.247987	0.007716	-12.595682	0.110825
C	8.472267	-3.928037	-6.761171	-0.339357
C	9.092788	-5.164652	-6.960587	-0.033636
C	9.254413	-2.767408	-6.736752	-0.032072
C	10.474827	-5.237555	-7.121247	-0.085351
H	8.505348	-6.072128	-7.010682	0.113628
C	10.635889	-2.845208	-6.882937	-0.077592
H	8.779346	-1.799209	-6.632622	0.125163
C	11.249018	-4.081382	-7.076050	-0.080590
H	10.943591	-6.200405	-7.288777	0.105605
H	11.229801	-1.938636	-6.869981	0.100067
H	12.323569	-4.141180	-7.205063	0.107699
C	5.875730	-5.299556	-7.144906	-0.375006
C	5.194053	-5.244647	-8.365775	-0.021938
C	5.965051	-6.527305	-6.470550	-0.064726
C	4.617285	-6.393381	-8.903272	-0.097707
H	5.139780	-4.309920	-8.908051	0.131906
C	5.388176	-7.672255	-7.012487	-0.088030
H	6.476419	-6.592558	-5.518290	0.125365
C	4.712505	-7.607808	-8.229740	-0.077084
H	4.098330	-6.336171	-9.853134	0.104800
H	5.467729	-8.614565	-6.482503	0.106958
H	4.264182	-8.500777	-8.650112	0.109763
P	6.660162	-3.774300	-6.464926	0.921255
C	6.530892	-4.038348	-4.633961	-0.344971
C	7.624917	-3.830631	-3.786590	-0.049572
C	5.306217	-4.422979	-4.070497	-0.036919
C	7.499361	-4.010612	-2.409330	-0.091795
H	8.585378	-3.547191	-4.197442	0.123332
C	5.186049	-4.610567	-2.697636	-0.086359
H	4.447035	-4.596358	-4.706030	0.113515
C	6.282795	-4.404818	-1.860982	-0.097436
H	8.362233	-3.859298	-1.770534	0.103782
H	4.237008	-4.932882	-2.283290	0.093839
H	6.193101	-4.566605	-0.792452	0.099298
C	2.703732	-0.961558	-1.780566	-0.000701
H	3.297154	-1.370713	-0.960183	0.158195
N	2.437719	0.471207	-1.411837	-0.333507
C	2.263467	1.519737	-2.290703	0.057134
C	2.291168	0.930737	-0.166890	0.293915
C	2.005680	2.628259	-1.542603	0.016935
H	2.359722	1.396346	-3.356702	0.216612
N	2.026629	2.241544	-0.215982	-0.320992
H	2.373516	0.343660	0.732386	0.172761
H	1.822051	3.646609	-1.838118	0.159513
C	1.815159	3.121805	0.939683	-0.157962
H	2.581210	3.896701	0.954323	0.171861
H	0.827126	3.576680	0.875168	0.171377
H	1.881142	2.532037	1.851687	0.147637

H	1.738324	-1.470097	-1.796611	0.168395

Energy = -1723783.22 kcal mol^{-1}

Py-Ph-I-Pd-(PPh_3)$_2$ *trans1* B97D

	Cartesian Coordinates			Mulliken Atomic Charges
C	3.435051	-1.220926	-3.211431	-0.202286
C	2.775249	-1.698012	-4.353252	-0.048174
C	4.772247	-0.798568	-3.312763	-0.045357
C	3.457605	-1.790423	-5.572995	-0.072703
H	1.736229	-2.024748	-4.281389	0.075983
C	5.438261	-0.869862	-4.535209	-0.005650
H	5.296720	-0.436925	-2.427016	0.069089
C	4.802713	-1.392733	-5.679671	-0.230727
H	2.942457	-2.196758	-6.442619	0.116998
H	6.480476	-0.560898	-4.589654	0.103704
Pd	5.847729	-1.689966	-7.406244	-0.522901
I	7.218608	-2.184136	-9.782556	-0.213983
P	5.039158	0.349551	-8.244750	0.884912
C	6.393226	1.381342	-8.926285	-0.319392
C	7.676524	1.218179	-8.376762	-0.027925
C	6.174924	2.350029	-9.918459	-0.028708
C	8.730353	2.032433	-8.803274	-0.078949
H	7.847729	0.430152	-7.645551	0.143251
C	7.236759	3.151960	-10.354498	-0.081741
H	5.190489	2.464859	-10.365578	0.102550
C	8.511663	2.999486	-9.793846	-0.071791
H	9.725121	1.894953	-8.382530	0.092436
H	7.068624	3.890054	-11.137089	0.099461
H	9.335703	3.622064	-10.138682	0.102226
C	4.236368	1.491884	-7.028502	-0.306638
C	2.886108	1.303177	-6.678518	-0.018226
C	4.957023	2.543965	-6.437247	-0.037012
C	2.256513	2.180617	-5.789723	-0.134240
H	2.318548	0.493675	-7.130379	0.114286
C	4.330491	3.411688	-5.532668	-0.080796
H	5.998984	2.705319	-6.706218	0.120478
C	2.975950	3.242307	-5.219272	-0.120995
H	1.199356	2.047226	-5.560932	0.094120
H	4.895047	4.236782	-5.100658	0.097447
H	2.475907	3.949298	-4.556897	0.089942
C	3.741484	0.168196	-9.530157	-0.351764
C	2.919818	1.252725	-9.898355	-0.061637
C	3.564275	-1.079713	-10.151114	-0.013936
C	1.946515	1.090142	-10.889708	-0.088308
H	3.031411	2.214545	-9.402118	0.115825
C	2.586660	-1.237228	-11.141188	-0.094691
H	4.207816	-1.910227	-9.872295	0.138284
C	1.780245	-0.154716	-11.513671	-0.067449
H	1.318954	1.933302	-11.174401	0.100531
H	2.460725	-2.205224	-11.623374	0.098631
H	1.022631	-0.278741	-12.285929	0.104090
C	8.492251	-3.867823	-6.723109	-0.308142
C	9.111820	-5.115634	-6.887625	-0.031391
C	9.268966	-2.696042	-6.700857	-0.028173
C	10.504089	-5.188323	-7.022527	-0.082142
H	8.513002	-6.022277	-6.933615	0.105969
C	10.659711	-2.774879	-6.817866	-0.079475
H	8.775983	-1.728001	-6.622666	0.129025
C	11.278612	-4.022178	-6.980824	-0.070121
H	10.981407	-6.156159	-7.167108	0.099876
H	11.257199	-1.864645	-6.807885	0.091377
H	12.360233	-4.083107	-7.089870	0.101507
C	5.865339	-5.195261	-7.128222	-0.352704

C	5.144555	-5.116557	-8.332014	-0.016312
C	5.948745	-6.423371	-6.442482	-0.062934
C	4.524971	-6.259100	-8.852475	-0.093947
H	5.093937	-4.168625	-8.862233	0.136215
C	5.328983	-7.561999	-6.968699	-0.082840
H	6.484853	-6.483709	-5.497415	0.116546
C	4.618252	-7.481391	-8.174807	-0.069460
H	3.974417	-6.193408	-9.789556	0.097128
H	5.400599	-8.510160	-6.438005	0.101305
H	4.137714	-8.369357	-8.582784	0.103394
P	6.685415	-3.692389	-6.476054	0.884420
C	6.483589	-3.857228	-4.649326	-0.318844
C	7.531685	-3.536404	-3.770251	-0.050946
C	5.226567	-4.210230	-4.124189	-0.026507
C	7.324866	-3.566693	-2.384820	-0.083107
H	8.511189	-3.276230	-4.165920	0.117483
C	5.024746	-4.241070	-2.742395	-0.078731
H	4.409582	-4.460348	-4.796081	0.113681
C	6.072162	-3.917665	-1.867450	-0.094584
H	8.148615	-3.330051	-1.712770	0.096785
H	4.050266	-4.528645	-2.348841	0.083455
H	5.918187	-3.957443	-0.789441	0.089005
C	2.726553	-1.148461	-1.893206	0.010456
H	3.346910	-1.535665	-1.074876	0.160525
N	2.396336	0.279932	-1.512046	-0.327095
C	2.446749	1.375613	-2.353217	0.060189
C	1.995568	0.684097	-0.297437	0.283562
C	2.062474	2.463670	-1.614483	0.015211
H	2.762012	1.288988	-3.384385	0.222319
N	1.785159	2.012018	-0.334216	-0.307741
H	1.864258	0.051990	0.569337	0.164939
H	1.972078	3.506135	-1.883344	0.149352
C	1.344976	2.847245	0.796470	-0.162302
H	2.102206	3.613138	0.995665	0.171613
H	0.388443	3.318830	0.546629	0.172130
H	1.223238	2.211684	1.678188	0.148198
H	1.775899	-1.694429	-1.917778	0.163563

Energy = -1723058.59 kcal mol^{-1}

Py-Ph-I-Pd-(PPh_3)$_2$ *trans2* B3LYP

Cartesian Coordinates				Mulliken Atomic Charges
C	3.051730	-0.970970	-3.252767	-0.209452
C	2.557604	-1.772364	-4.284685	-0.048680
C	4.338354	-0.433439	-3.374755	-0.041123
C	3.328784	-2.018581	-5.420269	-0.090067
H	1.557679	-2.192077	-4.213175	0.084373
C	5.106792	-0.696572	-4.502418	-0.029179
H	4.737263	0.207838	-2.593234	0.077703
C	4.616231	-1.482810	-5.557201	-0.222508
H	2.905664	-2.626853	-6.212774	0.115440
H	6.092744	-0.250458	-4.570102	0.099886
Pd	5.710342	-1.779219	-7.255264	-0.405218
I	7.167998	-2.200595	-9.579262	-0.208163
P	4.934596	0.345063	-8.127882	0.918699
C	6.303285	1.361190	-8.825964	-0.337586
C	7.557517	1.307021	-8.206489	-0.031648
C	6.119935	2.208752	-9.922176	-0.034023
C	8.602430	2.105859	-8.659406	-0.077127
H	7.725175	0.617354	-7.387646	0.121534
C	7.172752	2.997072	-10.382220	-0.085135
H	5.166836	2.246269	-10.433420	0.114321
C	8.411963	2.952732	-9.749503	-0.080466
H	9.571079	2.049490	-8.176351	0.099602

H	7.022989	3.640520	-11.241520	0.105759
H	9.230038	3.564162	-10.112475	0.107696
C	4.142406	1.510379	-6.922211	-0.345119
C	2.828817	1.277910	-6.491246	-0.036385
C	4.835241	2.610034	-6.403741	-0.049852
C	2.221269	2.133258	-5.578164	-0.086667
H	2.269720	0.437841	-6.883590	0.113251
C	4.226916	3.460584	-5.480907	-0.091313
H	5.844802	2.821891	-6.731877	0.123287
C	2.918465	3.228412	-5.068599	-0.097206
H	1.195558	1.951601	-5.276148	0.093667
H	4.775060	4.315435	-5.101117	0.104080
H	2.439394	3.903521	-4.368130	0.099604
C	3.650709	0.203997	-9.445246	-0.377017
C	2.806575	1.281431	-9.755993	-0.063693
C	3.521239	-0.988814	-10.164977	-0.021538
C	1.858949	1.164234	-10.768712	-0.087819
H	2.880428	2.210576	-9.204816	0.125283
C	2.570300	-1.101429	-11.177035	-0.097591
H	4.183225	-1.817578	-9.952000	0.131842
C	1.738173	-0.027782	-11.480856	-0.077162
H	1.215621	2.005342	-11.000690	0.107032
H	2.486448	-2.029509	-11.730611	0.104873
H	0.999540	-0.116937	-12.269273	0.109788
C	8.451589	-3.795332	-6.462537	-0.323361
C	9.229340	-4.856465	-6.932137	-0.034248
C	9.086418	-2.624760	-6.026541	-0.046407
C	10.619045	-4.751612	-6.951337	-0.082927
H	8.760208	-5.756305	-7.306994	0.118740
C	10.473892	-2.528665	-6.034601	-0.082273
H	8.492744	-1.778515	-5.698653	0.110389
C	11.244179	-3.593888	-6.498245	-0.078904
H	11.211080	-5.575937	-7.331763	0.107929
H	10.952986	-1.616622	-5.697236	0.099488
H	12.324918	-3.514917	-6.519277	0.108577
C	6.070389	-5.387898	-7.260138	-0.381986
C	5.351210	-5.312198	-8.456665	-0.022108
C	6.357428	-6.650389	-6.716652	-0.053157
C	4.932467	-6.474417	-9.102078	-0.096148
H	5.143538	-4.346761	-8.897190	0.135801
C	5.944180	-7.807888	-7.368315	-0.087781
H	6.897588	-6.734301	-5.781304	0.120596
C	5.229860	-7.722091	-8.562844	-0.077358
H	4.380314	-6.399619	-10.031676	0.105941
H	6.178916	-8.776556	-6.942074	0.106682
H	4.907723	-8.625069	-9.068720	0.110720
P	6.611412	-3.848224	-6.399351	0.883886
C	6.268634	-4.325011	-4.632864	-0.332594
C	7.235326	-4.230094	-3.626576	-0.050619
C	5.007139	-4.842881	-4.305789	-0.017522
C	6.957844	-4.666063	-2.330525	-0.083750
H	8.221288	-3.846454	-3.854408	0.124560
C	4.734140	-5.289197	-3.016409	-0.132079
H	4.245707	-4.936906	-5.070044	0.115885
C	5.713003	-5.208121	-2.024075	-0.121431
H	7.730610	-4.608490	-1.572109	0.104330
H	3.767098	-5.729123	-2.796518	0.102846
H	5.516218	-5.595233	-1.029588	0.097884
C	2.204488	-0.670204	-2.052112	0.002359
H	1.171960	-0.983431	-2.214930	0.168398
H	2.211120	0.393832	-1.807271	0.160286
C	3.447077	-2.521940	-0.767417	0.057459
C	2.392197	-1.009486	0.439666	0.294065
C	3.612779	-2.840925	0.546431	0.016670
H	3.821137	-2.995202	-1.659918	0.217261
N	2.945576	-1.884362	1.287568	-0.320699
H	1.808443	-0.149654	0.722705	0.172227

H	4.148998	-3.651027	1.009275	0.159281
N	2.681956	-1.375676	-0.811303	-0.335692
C	2.873906	-1.827705	2.752764	-0.157958
H	2.419979	-2.743359	3.130629	0.171096
H	3.876394	-1.712295	3.164197	0.172058
H	2.263234	-0.976043	3.045382	0.147607

Energy = -1723783.14 kcal mol^{-1}

Py-Ph-I-Pd-$(PPh_3)_2$ *trans2* B97D

Cartesian Coordinates				Mulliken Atomic Charges
C	3.456172	-2.459275	-2.953461	-0.197266
C	2.783182	-2.636012	-4.170178	-0.034586
C	4.820590	-2.115797	-2.963510	-0.073805
C	3.469816	-2.486659	-5.381634	-0.092082
H	1.726689	-2.909614	-4.169140	0.077316
C	5.488376	-1.932049	-4.173445	-0.010712
H	5.360834	-2.008387	-2.021377	0.073941
C	4.828571	-2.126056	-5.404109	-0.218733
H	2.940303	-2.655433	-6.318489	0.115964
H	6.548517	-1.684885	-4.163106	0.104292
Pd	5.862657	-1.963919	-7.153178	-0.516251
I	7.275695	-1.742365	-9.543209	-0.206818
P	4.951218	0.178475	-7.489526	0.872456
C	6.255648	1.410853	-7.858039	-0.318371
C	7.503952	1.224856	-7.238135	-0.026484
C	6.045433	2.519158	-8.692082	-0.033530
C	8.528598	2.155600	-7.433061	-0.078681
H	7.673144	0.331140	-6.638734	0.133850
C	7.080427	3.440197	-8.897525	-0.080606
H	5.093558	2.650827	-9.200926	0.105404
C	8.317540	3.264539	-8.264390	-0.071388
H	9.497566	2.002375	-6.960655	0.093454
H	6.922002	4.289429	-9.560194	0.101085
H	9.120905	3.980015	-8.432117	0.103103
C	4.035366	0.957254	-6.077319	-0.308195
C	2.700543	0.580792	-5.832817	-0.018123
C	4.638183	1.917469	-5.246545	-0.033801
C	1.970402	1.177272	-4.801163	-0.092831
H	2.221642	-0.153784	-6.474425	0.118754
C	3.904786	2.517359	-4.212131	-0.115899
H	5.664722	2.227074	-5.432223	0.121021
C	2.566541	2.159024	-3.995932	-0.147665
H	0.928682	0.899064	-4.646593	0.095725
H	4.371313	3.297563	-3.610054	0.100663
H	1.976547	2.664710	-3.232180	0.100643
C	3.689365	0.226923	-8.819216	-0.352925
C	2.845033	1.343387	-8.984743	-0.060117
C	3.547265	-0.884129	-9.667660	-0.015951
C	1.886911	1.352361	-10.003621	-0.085666
H	2.927824	2.194648	-8.311850	0.113960
C	2.581721	-0.872380	-10.681744	-0.094592
H	4.208383	-1.737886	-9.542139	0.146351
C	1.755184	0.244822	-10.853982	-0.067524
H	1.243016	2.220950	-10.132616	0.101733
H	2.481873	-1.733955	-11.339791	0.098552
H	1.008223	0.253938	-11.646195	0.105494
C	8.583126	-4.126859	-6.980245	-0.312729
C	9.280424	-5.261112	-7.422993	-0.030356
C	9.287150	-2.962286	-6.627579	-0.022753
C	10.678167	-5.228113	-7.507386	-0.081779
H	8.737942	-6.155606	-7.720547	0.105934
C	10.683152	-2.939905	-6.696299	-0.081032
H	8.733089	-2.071838	-6.333316	0.129798

C	11.379958	-4.073312	-7.138447	-0.069964
H	11.217071	-6.103011	-7.867364	0.100594
H	11.225245	-2.033766	-6.430278	0.091066
H	12.466278	-4.051152	-7.208894	0.102034
C	6.041886	-5.412331	-7.835995	-0.349216
C	5.345633	-5.047937	-9.001188	-0.017382
C	6.178075	-6.773933	-7.499486	-0.060684
C	4.805896	-6.037627	-9.831323	-0.093785
H	5.254172	-3.996196	-9.261905	0.135131
C	5.638717	-7.758052	-8.334781	-0.082881
H	6.693555	-7.059696	-6.584602	0.116737
C	4.954163	-7.391046	-9.502308	-0.069297
H	4.274719	-5.749720	-10.737137	0.096853
H	5.751857	-8.809275	-8.074312	0.102174
H	4.536084	-8.159145	-10.151163	0.104105
P	6.763495	-4.109083	-6.772252	0.881367
C	6.515582	-4.764497	-5.066592	-0.322029
C	7.530579	-4.688073	-4.098331	-0.052891
C	5.245022	-5.245654	-4.698766	-0.025371
C	7.276195	-5.084203	-2.778215	-0.084052
H	8.518338	-4.326120	-4.375310	0.117974
C	4.995486	-5.639807	-3.382424	-0.075052
H	4.453723	-5.310870	-5.441658	0.112884
C	6.009771	-5.558407	-2.416560	-0.093650
H	8.073901	-5.033398	-2.038346	0.097181
H	4.010574	-6.019351	-3.112899	0.086583
H	5.818246	-5.878860	-1.392943	0.091572
C	2.736078	-2.623894	-1.648097	0.019921
H	3.287471	-3.271232	-0.953223	0.168301
H	1.727840	-3.029910	-1.791861	0.161652
C	2.060482	-1.180001	0.362761	0.045116
C	2.934455	-0.103731	-1.367776	0.300351
C	2.123646	0.147778	0.686032	0.036790
H	1.706474	-2.031288	0.926908	0.150437
N	2.674198	0.800194	-0.405581	-0.322818
H	3.355819	0.109273	-2.340836	0.228927
H	1.836670	0.676924	1.583982	0.154079
N	2.571542	-1.314156	-0.917105	-0.333431
C	2.959291	2.242684	-0.485217	-0.176317
H	2.017866	2.802440	-0.454158	0.167021
H	3.593989	2.527272	0.360807	0.166825
H	3.478304	2.438701	-1.426092	0.154906

Energy = -1723060.63 kcal mol^{-1}

Appendix 4 Relative energies (kcal mol-1), % Boltzmann, and theoretical Ω (Å2) values of species 3 and 3b at B3LYP/6-311G(d,p)

Compounds	Method B3LYP/6-311G**								
	Rel. E (kcal mol^{-1})	%	Default parameters			Campuzano par.	Siu parameters		
			PA	EHSS	TM	TM	PA	EHSS	TM
Imp=25; Inum=250000* standard deviation of CCS (percent)= 4.0									
Ph-Pd-$(PPh_3)_2$ (3b)									
Trans	0.0	100.0	181	206	198	193	169	185	186
Cis	6.1	0.0	178	203	193	188	166	182	181
%*Trans*+%*Cis*			181	206	198	193	169	185	186
Py-Ph-I-Pd-$(PPh_3)_2$ (3)									
Trans-1	0.7	19.0	206	235	213	208	194	212	201
Trans-2	0.8	16.6	205	235	225	219	194	212	212
Cis-1	0.0	64.3	204	234	210	206	193	210	197
Cis-2	3.9	0.1	203	232	225	219	192	209	212
%*Trans*+%*Cis*			205	235	213	208	193	211	201
Imp=1250; Inum=2500000* standard deviation of CCS (percent)= 0.7									
Ph-Pd-$(PPh_3)_2$ (3)									
Trans	0.0	100.0	180	206	195	190	169	185	183
Cis	6.1	0.0	177	202	192	187	166	181	180
%*Trans*+%*Cis*			180	206	195	190	169	185	183
Py-Ph-I-Pd-$(PPh_3)_2$ (3b)									
Trans-1	0.7	19.0	205	235	223	218	193	212	210
Trans-2	0.8	16.6	206	235	223	218	194	212	211
Cis-1	0.0	64.3	205	234	221	216	193	210	208
Cis-2	3.9	0.1	203	232	220	214	192	209	207
%*Trans*+%*Cis*			205	234	222	216	193	211	209

* Imp: Number of Montecarlo trajectories employed by TM; Inum: Number of random points employed in the EHSS trajectories

Appendix 5 Relative energies (kcal mol^{-1}), % Boltzmann, and theoretical Ω values of species 3 and 3b at B97D/6-311G(d,p)

Compounds	Method B97D/6-311G**								
	Rel. E (kcal mol^{-1})	%	Default parameters			Campuzano par.	Siu parameters		
			PA	EHSS	TM	TM	PA	EHSS	TM
Imp=25; Inum=250000* standard deviation of CCS (percent)= 4.0									
Ph-Pd-(PPh$_3$)$_2$ (3b)									
Trans	0.0	84.9	179	203	195	189	167	183	182
Cis	1.0	15.1	172	195	186	182	161	174	175
%*Trans*+%*Cis*			178	202	193	188	166	181	181
Py-Ph-I-Pd-(PPh$_3$)$_2$ (3)									
Trans-1	4.3	0.1	203	232	221	216	191	209	209
Trans-2	2.3	2.2	200	229	207	202	189	207	196
Cis-1	0.0	97.7	200	227	217	212	188	203	204
Cis-2	4.1	0.1	199	227	205	199	188	204	193
%*Trans*+%*Cis*			200	227	217	211	188	204	203
Imp=1250; Inum=2500000* standard deviation of CCS (percent)= 0.7									
Ph-Pd-(PPh$_3$)$_2$ (3b)									
Trans	0.0	84.9	179	204	194	189	167	183	182
Cis	1.0	15.1	172	195	186	181	161	174	174
%*Trans*+%*Cis*			178	202	193	188	166	181	181
Py-Ph-I-Pd-(PPh$_3$)$_2$ (3)									
Trans-1	4.3	0.1	203	232	219	214	191	209	207
Trans-2	2.3	2.2	200	228	217	211	188	206	205
Cis-1	0.0	97.7	200	228	215	210	188	204	203
Cis-2	4.1	0.1	199	226	214	208	188	203	202
%*Trans*+%*Cis*			200	228	215	210	188	204	203

* Imp: Number of Montecarlo trajectories employed by TM; Inum: Number of random points employed in the EHSS trajectories